APPROVAL SHEET

Title of Dissertation: Determining the role of phosphorylation of mouse melanopsin
in non-image forming vision

Name of Candidate: Preethi Somasundaram
                                  Doctor of Philosophy, 2017

Dissertation and Abstract Approved: _____
                                                      Dr. Phyllis R. Robinson
                                                      Professor
                                                      Department of Biological Sciences

Date Approved: _____

ABSTRACT

Title of Document:	DETERMINING THE ROLE OF PHOSPHORYLATION OF MOUSE MELANOPSIN IN NON-IMAGE FORMING VISION
	Preethi Somasaundaram, Doctor of Philosophy, 2017
Directed By:	Dr. Phyllis R. Robinson Professor Department of Biological Sciences

Purpose:

Melanopsin is a visual pigment, expressed in intrinsically photosensitive retinal ganglion cells (ipRGCs) of the mammalian retina, that plays a major role in non-image forming visual behaviors like the pupillary light reflex, circadian photoentrainment, and sleep. It is hypothesized that melanopsin-mediated phototransduction is terminated by the phosphorylation of melanopsin's C-terminus by a G-protein coupled receptor kinase, followed by β-arrestin activation and binding. Little is known about the contribution of melanopsin phosphorylation to ipRGC physiology and its influence on non-image forming behaviors. We investigated the role of melanopsin C-terminus phosphorylation on non-image forming behaviors by generating a phosphorylation deficient melanopsin mutant that lacks all putative C-terminal phosphorylation sites (C-phosphonull).

Method:

C-phosphonull mice were generated by expressing the C-terminal phosphorylation deficient melanopsin mutant in $Opn4^{Cre/Cre}$ mice by intravitreal delivery of an AAV2 construct for targeted expression of melanopsin in ipRGCs.

Results:

We found that C-terminal phosphorylation of melanopsin has a direct influence on the dilation kinetics of the pupillary light reflex, due to the observation that the C-phosphonull mice exhibit prolonged pupil constriction to a high intensity blue light stimulus, and have a half-time of dilation of 9.43min as compared to only 6s in wildtype animals. This phenotype is reflected in the physiology of ipRGCs as determined by both single cell and multielectrode recordings, where ipRGCs sustain action potentials for at least 15min to a 5s blue light stimulus. We also found that exogenous expression of melanopsin in melanopsin knockout animals enhances their ability to shift their activities to a delayed light dark cycle (a jet lag paradigm) and rescues a deficit in negative masking (reduction in activity exhibited by nocturnal animals in response to aberrant light during subjective night).

Conclusion:

Our results suggest that C-terminal phosphorylation of melanopsin influences the kinetics of some non-image forming behaviors and physiology, but does not completely explain deactivation of melanopsin and that there may be alternate mechanisms that play a role in its absence.

DETERMINING THE ROLE OF PHOSPHORYLATION OF MOUSE
MELANOPSIN IN NON-IMAGE FORMING VISION

By

Preethi Somasundaram

Dissertation submitted to the Faculty of the Graduate School of the
University of Maryland, Baltimore County, in partial fulfillment
of the requirements for the degree of
Doctor of Philosophy
2017

Dedication

I dedicate this dissertation to my parents- Somasundaram@Chandar and Vijaya

Somasundaram.

Acknowledgements

I thank my mentor Dr. Phyllis Robinson for her guidance, incredible support and for her confidence in me. Special thanks to Dr. Samer Hattar and Dr. Tudor.C.Badea, who apart from being part of my graduate committee, were equivalent to co-mentors during my graduate studies. I thank my graduate advisory committee for their direction and helpful comments. I thank my parents for giving me the freedom and motivation to pursue a career in research, and for always being there to encourage and support me. I thank my husband, Deepak, for the wonderful and fun conversations about the scientific world, and for being extremely patient and supportive.

Table of Contents

List of Figures

Abbreviations *(in alphabetical order)*

- **AAV2 –** Adeno associated virus serotype 2
- **CPΦ-** Melanopsin C-terminal phosphonull mutant (melanopsin with all 38 C-erminal phosphorylation sites mutated to alanines)
- **Cre-loxP –** The Cre-lox recombination is a genetic recombination technology that is used to create deletions, insertions, inversions or translocations in DNA. (Its components include loxp sequences and a cre-recombinase enzyme)
- **FLAG -** a synthetic hydrophilic epitope tag for proteins
- **Floxed -** Flanked by loxP sites
- **GPCR-** G protein coupled receptor
- **GRK –** G protein coupled receptor kinase
- **HEK293A –** Human embryonic kidney cell line
- **HEK293A-Cre -** Human embryonic kidney cell line expressing cre-recombinase
- **ipRGCs -** intrinsically photosensitive retinal ganglion cells
- **MKO -** Melanopsin knockout mouse (This term is interchangeably used with $Opn4^{cre/cre}$ in this document)
- **mRuby-** A monomeric variant of the red fluorescent protein with excitation and emission maxima at 558 nm and 605 nm respectively
- **PKA-TM-** Melanopsin PKA triple mutant (Melanopsin with all 3 putative PKA phosphorylation sites mutated to either alanines or glycines)
- **PLR** - Pupillary Light Reflex
- **OPN**- Olivary pretectal nucleus
- *opn4* **–** Melanopsin gene
- *$Opn4^{cre/cre}$* - Melanopsin knockout mouse expressing Cre recombinase driven by melanopsin promoter (This term is interchangeably used with MKO in this document)
- **pAAV -** Adeno-associated viral vector
- **PKA** – Protein kinase A
- **PLA –** Proximity dependent ligation assay (an assay to detect proximity between two epitopes)
- **P2A-** A viral derived self-cleaving peptide that can generate two individual peptides from a bi-cistronic transcript
- **RGCs –** Retinal ganglion cells
- **16:8 LD -** The light dark cycle used for circadian behavior analyses (Indicates 16 hours of 500 lux overhead white light and 8 hours of darkness)
- **SCN**- Suprachiasmatic nucleus

Chapter 1:

Background and introduction

Mammalian light detection and non-image forming vision

Light detection is the process by which an organism utilizes light from the environment for regulating a wide range of physiological processes (1). Light detection occurs through the mechanism of phototransduction, which takes place in a photoreceptor cell. Opsins, which are G-protein coupled receptors form functional visual pigments in the outer-segments of classical photoreceptor cells (rod and cone photoreceptors) and aid in the conversion of a photon of light into a change in the membrane potential of the cell (1, 2). This electrical signal results in a change in neurotransmitter release at the photoreceptor's synapse, resulting in the transmission of the signal through a tissue. In mammals, the light-sensitive tissue is the retina which lines the back of the eyecup. The mammalian retina serves to perform two different sets of functions - image forming vision and non-image forming vision (3). Image forming vision is the utilization of light to create an image of the scene in the field of view of the eye. This involves detection of color, contrast and motion of objects in the field. Non-image forming vision involves light driven accessory functions that aid image forming vision, but does not necessarily contribute to the generation of an image. This includes adaptive mechanisms like the pupillary light reflex, circadian photoentrainment, regulation of sleep, mood, etc. A complex network of pathways comprising the eye and the brain is involved in driving these physiological and behavioral functions. Some of these non-image forming functions are discussed in the following sections.

The pupillary light reflex (PLR)

The mammalian pupillary light reflex is an adaptation mechanism of the eye that allows adjustments in the size of the pupil to account for varying illumination levels in the environment. This reflex serves to protect the retina from very bright light and to maintain a stable visual representation of the environment in different illumination conditions. The PLR involves a simultaneous and identical constriction of both pupils in response to light shone on either of the eyes. The direct PLR is the constriction of the pupil of one eye in response to light directed at the same eye. Consensual PLR is defined as the constriction of one eye in response to light directed on the other eye. The afferent pathway of the PLR begins at the retina - the axons of the retinal ganglion cells converge onto the optic nerve which exits the eye at the back and forms the optic tract (see Fig 1.1) (4). Optic tracts from either eye intersect at the optic chiasm and enter the midbrain, where a subset of axons reach the olivary pretectal nucleus (OPN). The efferent pathway forms the fibers proceeding from the OPN and synapsing onto neurons in the Edinger Westphal (EW) nucleus. Pre-ganglionic parasympathetic fibers arise from the EW nucleus and exit the brain stem to synapse within the ciliary ganglion. Post-ganglionic fibers arise from the ciliary ganglion to innervate the sphincter muscle of the iris. The PLR serves to protect our light sensitive organ, while also fine tuning our ability to perceive images.
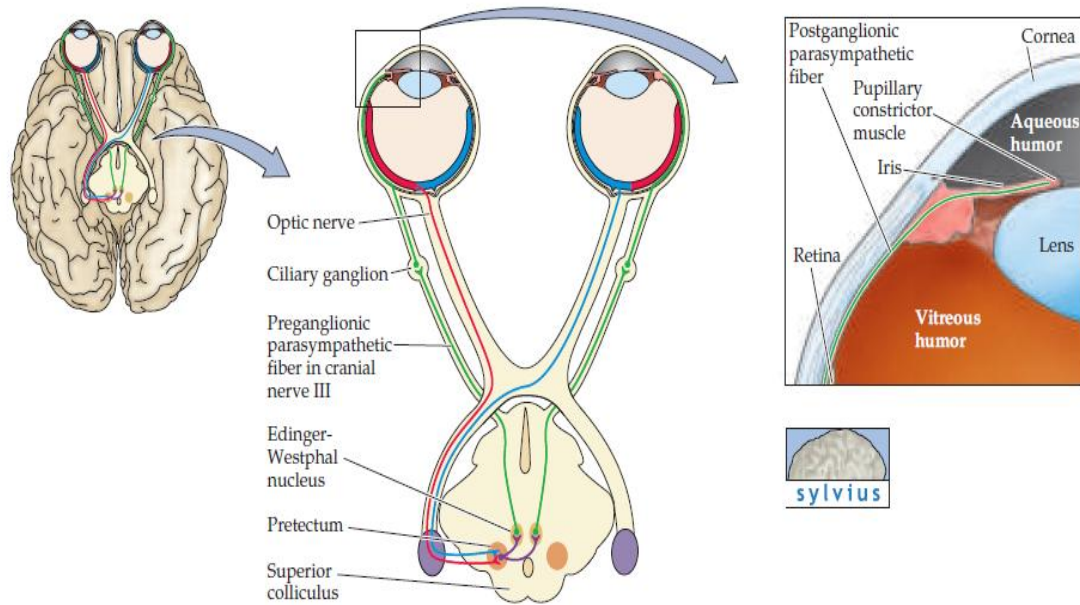
Figure 1.1: Pupillary light reflex pathway. *The afferent and efferent pathways of the pupillary light reflex starting from the retinal ganglion cells in the eye and ending in the sphincter muscle of the iris* (4)*.*

Circadian photoentrainment

Circadian photoentrainment is the adjustment of the inherent biological clock in organisms to external light-dark cycles. All animals have an internal biological clock based on the primary circadian pacemaker in the brain called the suprachiasmatic nucleus (SCN), which involves oscillations over a period of ~24 hours (5). Each single isolated neuron of the ~20,000 neurons in the master clock (SCN) exhibits neuronal activity that oscillates over ~24 hours. Although this rhythm is fairly close to 24 hours, there is a slight change in the period of this inherent oscillation everyday in the absence of an external signal. This change in period eventually leads the inherent clock to tick out of phase with the geological clock. Hence, environmental light cues are required to tune and maintain a precise 24 hour period of oscillation.

The machinery that provides the path for environmental light information to reach the SCN is the retinahypothalamic tract, which includes the axons of the retinal ganglion cells, directly projecting to the brain. This light information is then used by the SCN to tune its own inherent clock, which is then transmitted to other peripheral clocks located in almost every tissue throughout the body. The presence of peripheral oscillators is evident from the expression of molecular clock genes (that are also known to be present in SCN) in these clocks (6, 7).

At the heart of the molecular clock is a transcriptional-translational feedback loop that regulates the core clock components (8). In mammals, the core clock components involve *Clock*, *Bmal1*, *Period* and *Cryptochrome* genes. CLOCK and BMAL1 are transcription factors that heterodimerize and bind to E-box cis-regulatory enhancer elements (Figure 1.2). The transcription of *Period* and *Cryptochrome* are regulated by E-box enhancer sequences, and so CLOCK and BMAL1 are able to initiate transcription of *Period* and *Cryptochrome* genes. PER and CRY in turn heterodimerzie and translocate back to the nucleus to repress their own transcription by inhibiting CLOCK and BMAL1, thus forming a negative feedback loop. CLOCK and BMAL1 also activate transcription of *Rev-erbα* and *Rorα*, which are retinoic acid related orphan nuclear receptors. RORs activate transcription of *Bmal1* and REV-ERBs repress transcription of *Bmal1,* forming additional feedback loops. Furthermore, the clock components are also post-translationally controlled through phosphorylation and ubiquitination. These regulatory mechanisms together determine the 24 hour period of the clock and its timing precision.

How does light reset these clock components? It has been shown that light affects *Period* gene expression at both transcriptional and translational levels (9, 10). Light induces acute changes in *Per* mRNA transcript levels through several mechanisms (9) and affects *Per* translation through phosphorylation of elf4E (eukaryotic translation initiation factor) (10). Thus *Per* seems to be the primary switch in the resetting of the mammalian circadian clock.

At the cellular and molecular level, the mammalian circadian clock seems to have a complex but well-defined hierarchical network. The complexity of this network, however, is not yet been completely unraveled. Understanding the circadian clock and function can provide useful insights into situations where misregulation of the clock can lead to disorders such as seasonal affective disorder, and sleep and mood disorders. Circadian control of sleep and mood will be discussed in upcoming sections.
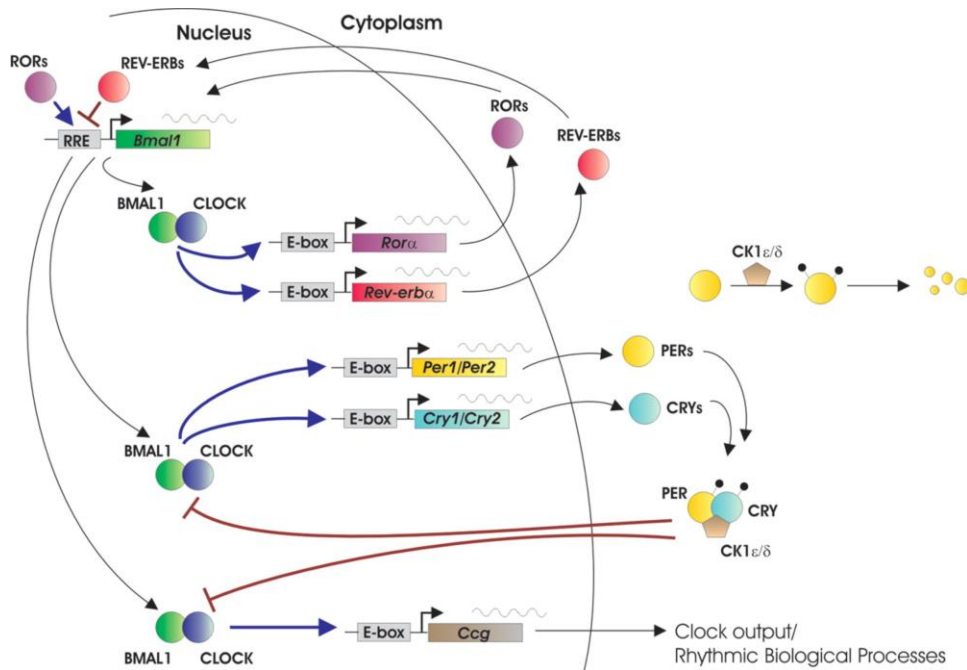
Figure 1.2: Mammalian circadian clock components. The transcriptional-translational feedback network surrounding CLOCK, BMAL1, PER and CRY proteins that forms the molecular basis of mammalian circadian clock (8).

Other non-image forming visual functions

Light has a profound influence on several other physiological and behavioral functions that do not involve the process of image formation. These include regulation of sleep, mood, hormonal changes, body temperature changes, metabolic processes, learning ability and so on (11). Animals require a cyclical process for regulating these functions to maintain homeostasis for healthy living. A simple example of the importance of circadian rhythms was demonstrated in cyanobacteria where competitive growth experiments showed that bacteria that had an internal rhythm synchronized to the external light-dark cycle had a reproductive fitness advantage as compared to those that had a mistuned circadian clock

Sleep is regulated by two different mechanisms - homeostatic and circadian (12). The homeostatic mechanism involves a drive to maintain balance between sleep duration and sleep intensity, and the circadian mechanism drives the synchronization of sleep/wake to day/light cycles. The inter-connection of the circadian pacemaker (SCN) with brain centers involved in sleep regulation such as the lateral habenula (LH) and ventral tegmental area (VTA) (see figure 1.5) suggest a strong circadian control of sleep (11). Thus there are direct and indirect pathways for light regulation of sleep. Light can directly influence sleep through light information from ipRGCs to their direct targets in the brain involved in sleep, as well as indirectly through the SCN mediated connection to these targets.

Melatonin is a hormone secreted by the pineal gland that has a strong association with sleep and circadian rhythms (13). There is two-way communication between pineal melatonin and the SCN. Melatonin secreted by the pineal gland influences circadian rhythms through melatonin receptors expressed in the neurons of SCN. Conversely, light information directed to the SCN alters melatonin secretion from the pineal gland. Melatonin is shown to be involved in resetting the phase of the circadian clock.

Sleep deprivation and circadian disorders are associated with mood and learning deficits (14). A recent study highlights how aberrant light can influence mood and learning indirectly by affecting sleep and circadian rhythms or directly without affecting them (14). Hence, light has quite a complex control of behavioral and physiological processes. However, light can influence these functions in mammals only through one point of entry, that is the retina.

The mammalian retina

The mammalian retina is a sheet of tissue that forms the inner lining of the eyecup (15). It is a concave structure inside the eye that is sandwiched between the vitreous, which is the jelly like substance that fills the eyeball, and the choroid. The retina is the sole photo-sensory part of the mammalian eye. Developmentally the retina is part of the forebrain that is extended out into a peripheral organ. Hence it is an excellent yet simplified model of the central nervous system.

Anatomically, the retina is composed of a non-photosensory outer layer called the retinal pigment epithelium (RPE) and the photosensory neural retina (Figure 1.3). The RPE is the recycling and housekeeping factory of the retina, playing important

roles such as phagocytosis of outer disk membranes of rods and cones, aid in visual cycle, etc (16). Immediately inner to the RPE is the photoreceptor layer (PRL), composed of the disc membranes of rods and cones (15). Rods are responsible for dim-light or scotopic vision, and cones are responsible for bright-light or photopic and color vision. The cell bodies of the rods and cones can be found in the outer nuclear layer (ONL). The outer plexiform layer (OPL) is a layer of nerve fibers, serving as the point of contact of photoreceptor axons with the dendrites of bipolar and horizontal cells. The bipolar cells are second in hierarchy in transmitting visual information through the retina. The inner nuclear layer (INL) contains the somata of bipolar cell neurons and constitutes the second major cellular layer in the retina. The inner plexiform layer (IPL) is the point of contact of bipolar cell axons and ganglion cell dendrites. The final major cellular layer is the ganglion cell layer (GCL) containing the ganglion cell bodies. The optic nerve fiber layer (ONFL) is a collection of all the ganglion cell axons that exit the eye at the back to the form the optic nerve. It is to be noted that the vertebrate retina is inverted i.e., light enters the eye and passes through the entire thickness of the retina starting from the ganglion cells, through the bipolar cells before reaching the photoreceptors (the primary mediators of light reception).
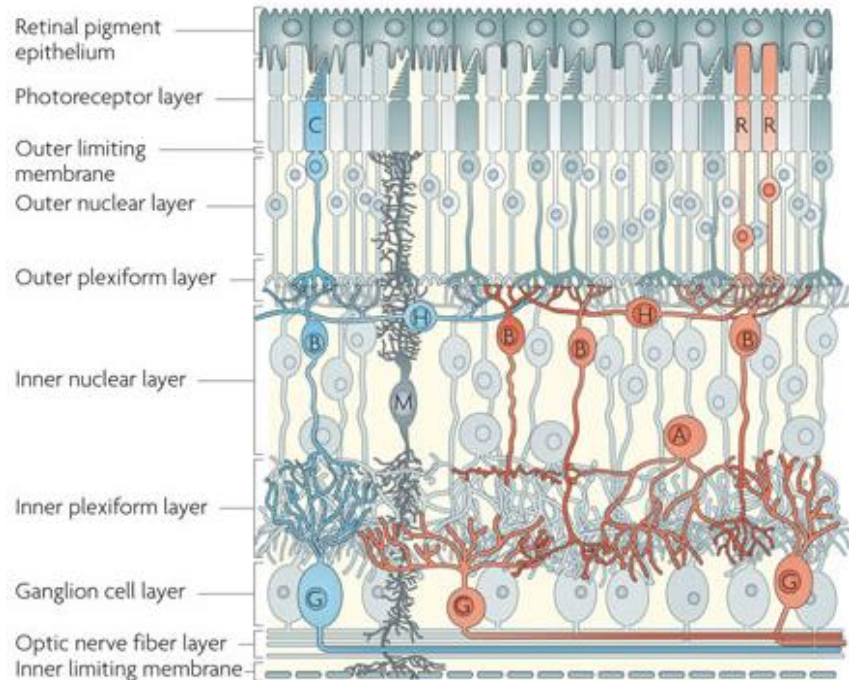
Figure 1.3 Anatomy of the mammalian retina. The three major cellular layers of the retina -ONL, INL and GCL can be seen interspersed between nerve fiber layers such as the OPL, IPL and ONFL. PRL and RPE form the outermost layers of the retina (17)

The visual pigment melanopsin

Visual pigments function as the principal mediators of light perception in animals by carrying out the first step in the light detection pathway. The primary visual pigments in mammals are rhodopsin and cone opsins, which are very well characterized in terms of their structure, biochemistry and function. A non-classical photopigment called melanopsin was first identified in 1998 in the dermal melanophores of Xenopus leavis and later found to exist in all vertebrates including mammals (18–20). Melanopsin expression was found to be widespread in Xenopus (18). It was detected in the iris and deep brain regions apart from the melanophores, suggesting a possible

role in non-visual photoreception. Melanopsin was first detected in mammals in 2000 (19), where its expression was found to be restricted to the retina (20).Unlike the classical visual pigments which are expressed in the photoreceptive layer in the mammalian retina, melanopsin is expressed in a small subset of cells in the ganglion cell layer deemed intrinsically photosensitive retinal ganglion cells (ipRGCS) (Figure 1.4). These ipRGCS represent about 2-3% of all the cells in the retinal ganglion cell layer (21). Adding to their complexity, a diverse range of ipRGC subtypes that differ in terms of location and morphology has been described (21, 22).

ipRGCs have been shown to project to the suprachiasmatic nucleus (SCN), the primary circadian pacemaker (21). Furthermore, Hattar et al showed that ablation of the melanopsin gene led to abnormal pupillary reflex and period lengthening in circadian photo-entrainment of mice (23). They also showed that melanopsin works in conjunction with the rods and cones to perform these complementary visual functions. This integrated response of the classical and non-classical visual pigments was also demonstrated in blind mice by Panda et al (24). Additionally, studies on mice where the melanopsin gene opn4 had been knocked out showed that the intrinsic pupillary light reflex of mice most likely involves melanopsin (25). These findings further confirm a non-visual role for melanopsin.
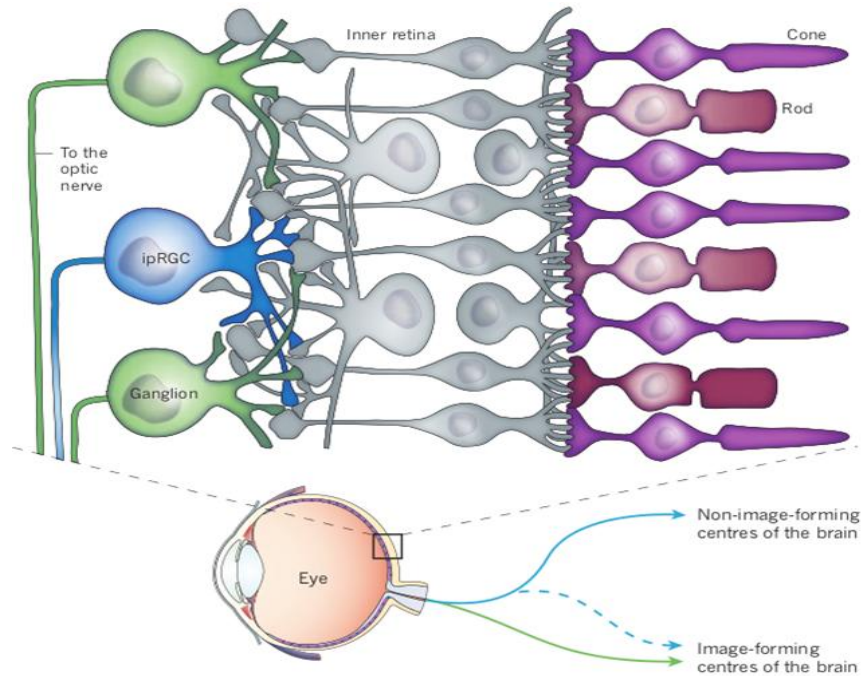
Figure 1.4: ipRGCs in the mammalian retina. A section of a mammalian eye showing the three major cell layers of the retina. The melanopsin expressing ipRGCs can be seen in blue in the ganglion cell layer (22).

Electrophysiological studies on isolated ipRGCs suggest that melanopsin activates a rhabdomeric phototransduction cascade involving activation of a Gq/G11 class G-proteins (26). Additionally, it was shown that the melanopsin generated response was lost upon ablating possible downstream signaling components in the melanopsin phototransduction cascade such as PLCβ, TRPC6 and TRPC7 (25, 27).

ipRGCs -diversity and targets in the brain

ipRGCs represent a small but diverse population of cells in the ganglion cell layer of the mammalian retina (11). There are now five known subtypes of ipRGCs (M1-M5), which are diverse in terms of their morphology, physiology, dendritic stratification and projections in the brain (22, 28–32) (Figure 1.5). The M1 subtype of ipRGCs is known to contribute to non-image forming visual functions such as the pupillary light

12

reflex and circadian photoentrainment. This is evident through the observation that M1 ipRGCs project to the SCN and OPN. Also implicated in circadian rhythms are the subparaventricular zone (SPZ) and intergeniculate leaflet (IGL) which are also direct targets of ipRGCs in the brain (22, 31). Interestingly, the M1 subtype is diverse within its own subclass through the presence or absence of a transcription factor called Brn3b (33). While Brn3b negative ipRGCs project to the SCN, Brn3b positive ipRGCs project to the OPN, which is involved in the pupillary light reflex. While 80% of ipRGCs projecting to the SCN are M1 cells, OPN is innervated by both M1 and M2 subpopulations, with M1s innervating the shell of the OPN and M2s innervating the core (28). In addition to non-image forming brain centers, non-M1 ipRGCs project to image-forming centers like the dorsal lateral geniculate nucleus (dLGN) and superior colliculus (SC) (32). Furthermore, ipRGCs show widespread innervation of regions involved in the regulation of sleep such as the ventrolateral preoptic area (VLPO) and lateral hypothalamus (LH), and regions involved in regulation of mood like the medial amygdala and lateral habenula, indicating a diverse functional role for this small group of cells (11).
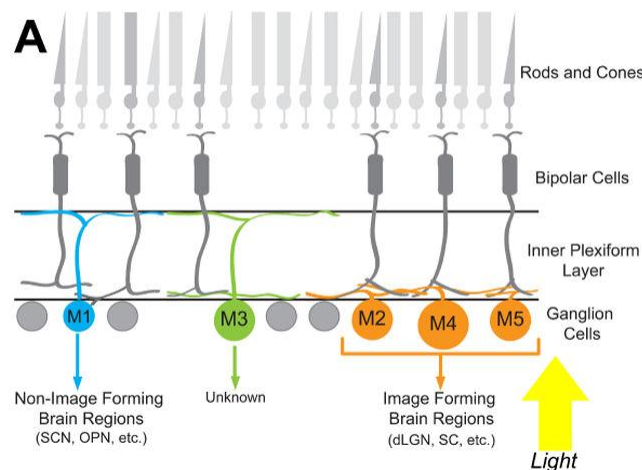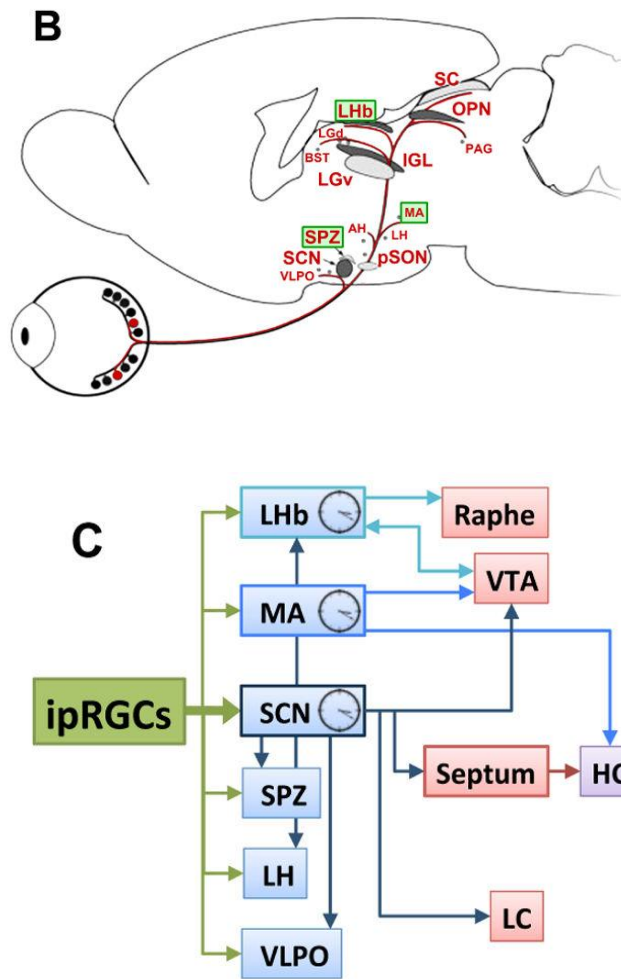
Figure 1.5 Diversity and targets of ipRGCs in the brain. *(A)The different subtypes of ipRGCs (M1-M5) are represented as colored cells within a schematic of the retina. Also indicated are the variety of roles played by the different known subtypes of ipRGCs (B)The direct axonal targets of ipRGCs in the brain are illustrated. (C) The direct ipRGC targets and the complex interplay and connectivity within these brain nuclei* (32).

Melanopsin structure and phototransduction cascade

Melanopsin is a G-protein coupled receptor, as are all other opsins in the visual pigment family (18). The secondary structure of frog melanopsin is predicted to have a short N-terminal extracellular region, seven transmembrane domains and an unusually long cytoplasmic tail (18). The presence of a long cytoplasmic tail suggests that the protein could be subjected to high levels of regulation. Supporting this hypothesis, mouse melanopsin is predicted to have 38 serines and threonines in its cytoplasmic tail that could undergo phosphorylation by a GRK (34, 35).

In its inactive state, the opsin (apo-protein) is bound to a chromophore, 11-*cis* retinal. Photopigment activation is caused by the photo-isomerization of the chromophore from an 11-*cis* retinal conformation to all-*trans* retinal form (36) . This in turn permits the photopigment to associate with a G-protein that initiates a signaling cascade. This binding and activation of the G-protein serves as a critical step in transducing and amplifying signals from melanopsin to downstream signaling components in the pathway. Expression and pharmacological studies suggest that the melanopsin signaling cascade involves the IP3/DAG pathway (27, 37). It is hypothesized that light-activated melanopsin activates a Gq/G11 G-protein, which in turn activates phospholipase C (PLC). PLC enzyme hydrolyzes phosphatidylinositol-4,5-bisphosphate (PIP2) to inositol triphosphosphate (IP3) and diacylglycerol (DAG). DAG remains bound to the membrane, whereas IP3 is soluble. This pathway is subsequently involved in gating open TRP channels, which results in the influx of sodium and calcium ions (26, 27). The exact mechanism underlying this cascade is still unclear.

Regulation of melanopsin activity

One way that melanopsin regulation occurs is by phosphorylation of the receptor by a G-protein coupled receptor kinase (GRK) in the presence of light, which has been shown to deactivate the receptor in cultured cells (34). Deactivation of melanopsin is thought to be a two-step process that involves the phosphorylation of melanopsin at specific amino acid residues followed by the binding of a protein called arrestin (34). Melanopsin phosphorylation serves as a signal for the activation and binding of arrestin. Arrestin association prevents the binding of a G-protein and blocks further activation of the signaling cascade (38). In order to identify the specific sites phosphorylated by GRK, Blasic et al constructed a series of truncation mutants of the C-terminal tail of melanopsin and tested their kinetic calcium responses. The results indicated that the kinase targets a set of six phosphorylation sites involving serines and threonines in the C-terminus of melanopsin (T388, S389, S391, S392, S394, S395) (34, 35) (Figure 1.6a).
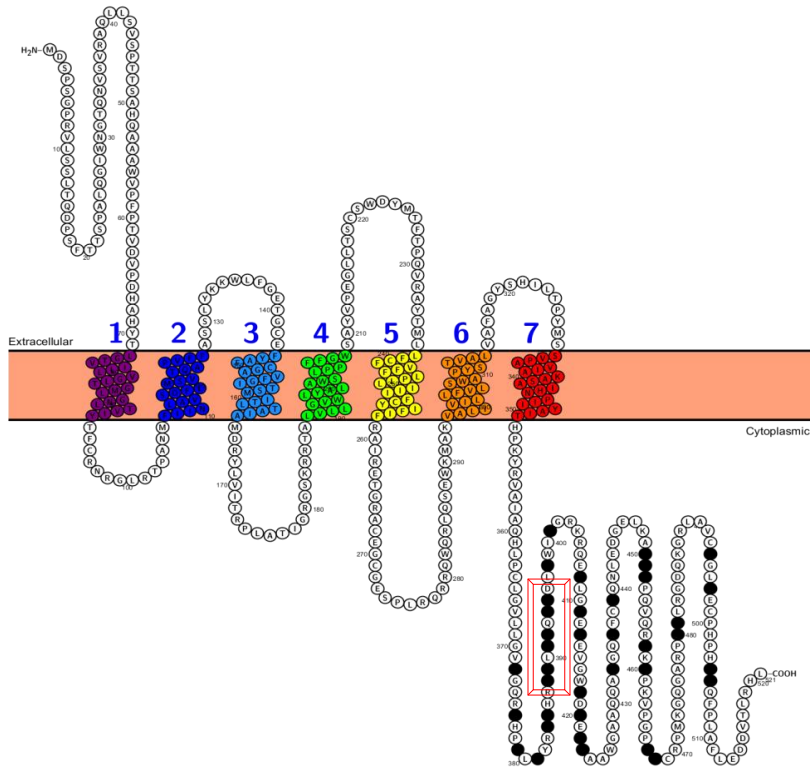
(a)
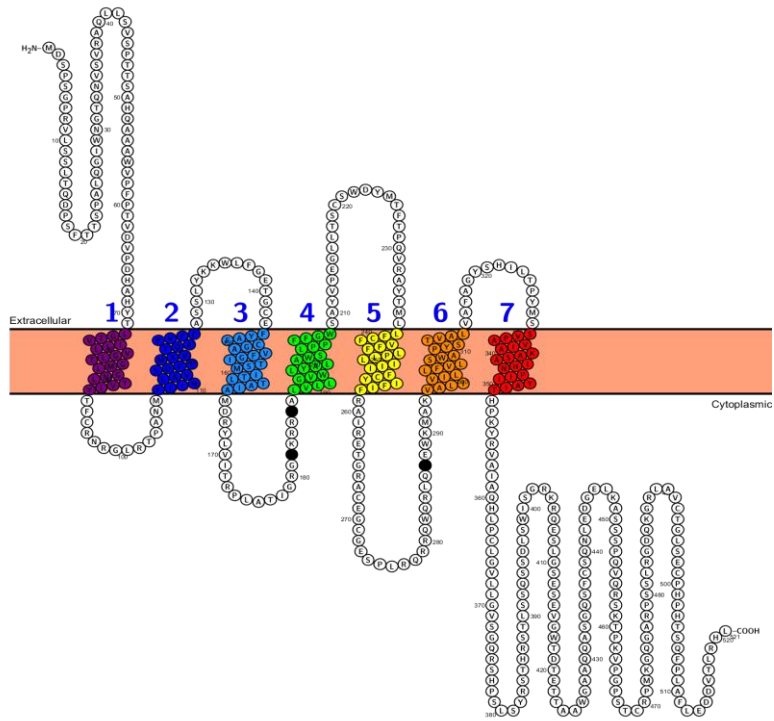
(b)

Figure 1.6: 2D representation of melanopsin. *The colored regions represent the transmembrane domains. Each open circle represents one amino acid residue. (a) The black filled circles represent the predicted GRK phosphorylation sites. Highlighted inside the red box are the 6 residues found to be primarily important for GRK-mediated phosphorylation. The predicted PKA phosphorylation sites can be seen as black circles in (b) (34, 35, 39)(Protter visualization platforms).*

A second mechanism of melanopsin regulation occurs by protein kinase A (PKA)-dependent phosphorylation. This phosphorylation has been shown to modulate or fine tune melanopsin activity in cultured cells (39). PKA targets three sites (S182, T186, S287) in the second and third intracellular loops of melanopsin, as seen in figure 1.6b (39). These modifications of melanopsin by phosphorylation are described in more detail in specific sections below.

G-protein coupled receptor kinases- structure, expression and role in opsin regulation

G-protein coupled receptor kinases (GRKs) make up a class of serine threonine protein kinases that are specifically involved in G-protein coupled receptor (GPCR) desensitization. GRKs are expressed ubiquitously in almost every animal cell type and are highly expressed in neurons. There are seven known GRKs in vertebrates – GRKs 1-7. GRKs 1 and 7 are cognate kinases for visual opsins (rod and cone opsins) (40). GRKs 2 through 6 are non visual GRKs. These seven GRKs phosphorylate the wide array of more than 800 GPCRs in vertebrates (41).

GRKs share structural similarity with respect to their domains (Figure 1.7). All seven GRKs have three common domains – N-terminal residues, regulator of G-protein signaling homology domain (RH) and serine threonine kinase domain (KD). Some GRKs contain a pleckstrin homology domain (PH) that allows them to bind Gβγ subunits (42, 43). GRKs 2 and 3 contain this domain. Based on this structural similarity, the GRKs have been grouped into three subclasses – GRK1 which contains GRKs 1 and 7; GRK2 which includes GRKs 2 and 3; GRK4 which includes GRKs 4, 5 and 6 (42).

The crystal structure of GRK2 complexed with Gβγ subunits was solved in 2006 by Lodowski et al (Figure 1.8, (44)). The structural studies revealed that GRKs are unique compared to other kinases in terms of the conformation of their kinase domain, which appears to be open. Additionally, the nucleotide gate in the C-terminus is disordered with or without the presence of ATP or Gβγ.
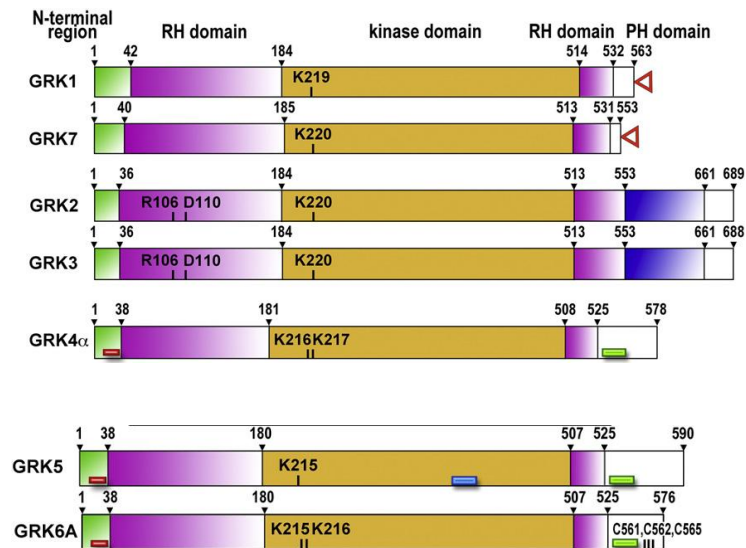
Figure 1.7: Comparison of the structural domains of GRKs 1-7. The N-terminal residues (green), RH (purple), PH (white) and kinase domains (mustard) are seen (45).
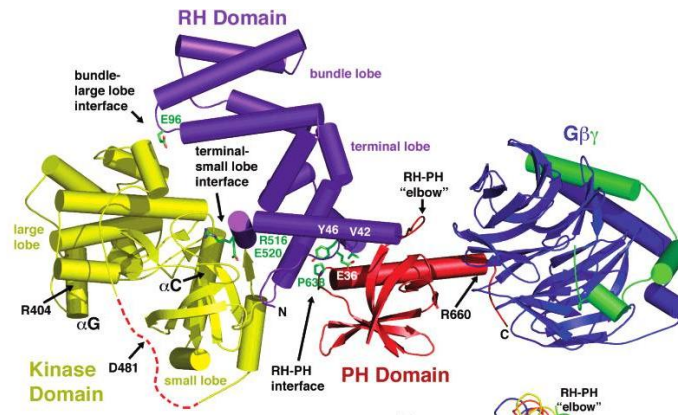
Figure 1.8: The crystal structure of GRK2 complexed with Gβγ. The RH domain has terminal and bundle lobes which interface with the small and large lobes of kinase domain respectively. The RH domain also forms a highly hydrophobic interface with the PH domain (45).

Each GRK is targeted to the membrane by a distinct mechanism. Membrane targeting of GRKs 2 and 3 is a receptor dependent mechanism (42). The activated receptor causes the Gα subunit to dissociate from the Gβγ, and the Gβγ recruits GRK2 to the membrane. GRK translocates to the membrane and phosphorylates the activated receptor.

GRKs play important roles in the function of opsins. GRK1 phosphorylation of rhodopsin was first described in 1972 (46). Phosphorylation by GRK1 is essential for the deactivation of rhodopsin. In mammals, there are six or seven potential phosphorylation sites for GRK in the C-terminus of rhodopsin (47). Blasic et al have

shown that six GRKs are expressed in mice retina (34). Single cell RT-PCR analysis and immunoblotting demonstrate that GRKs 1-6 are located in the retina (Figure 1.9). Further, melanopsin positive and rhodopsin negative cells (ipRGCs) predominantly expressed GRKs 2 and 3.
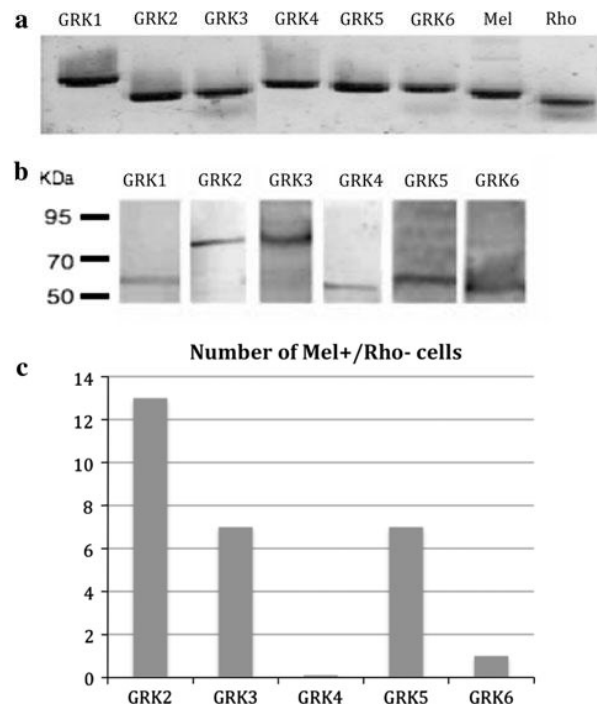
Figure 1.9: Expression of GRKs in the retina (a) (b) and specifically in ipRGCs (c). *RT-PCR analysis of GRKs in retina (a) and immunoblotting analysis(b) reveal expression of 6 GRKs. (c) Melanopsin positive and rhodopsin negative ipRGCs show predominant expression of GRKs 2 and 3 using single cell RT-PCR*(34)*.*

GRKs can themselves be phosphorylated by other kinases. Interestingly there is cross talk between GRKs and PKA, the two classes of kinases that are relevant to this study. GRK1 and GRK7 have been shown to be phosphorylated by PKA *in vitro* in cultured cells, and this regulation was shown to attenuate GRK-mediated rhodopsin

phosphorylation (48). *In vivo* experiments in mice lacking the adenylyl cyclase type 1 (an isoform of adenylyl cyclase) gene showed that GRK1 phosphorylation was greatly reduced in both light and dark (Figure 1.10) (49). Since adenylyl cyclase is the enzyme essential for cAMP synthesis (the second messenger involved in PKA activation), this suggests that GRK1 could be phosphorylated by PKA *in vivo* as well. These studies show the complexity of action and regulation of these kinases *in vivo*. It is unknown whether melanopsin kinase (GRK2/3) coould undergo such regulation by PKA. A complete understanding of the mode of action of these kinases on melanopsin can only be established by studying them in intact retina of mice.
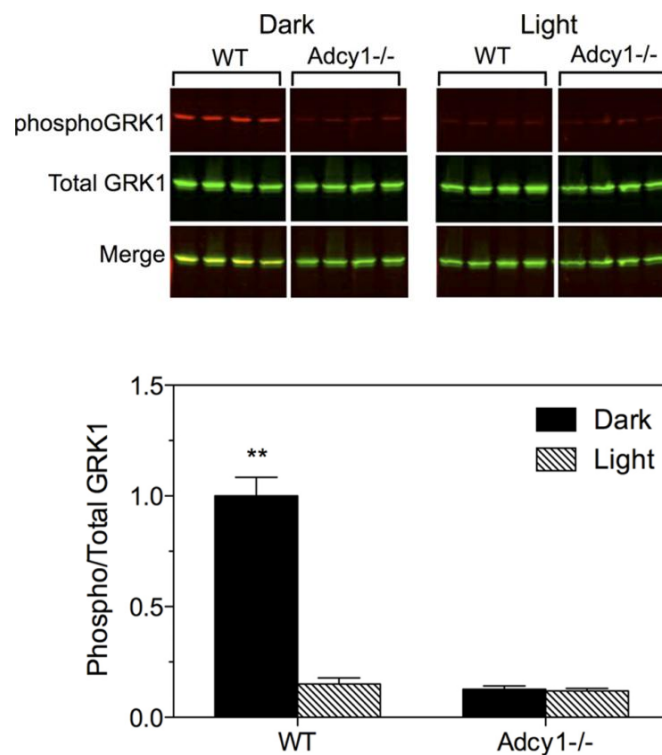
Figure 1.10: Adcy1 knockout mice show reduced phosphorylation of GRK1. GRK1 under wild type conditions undergoes phosphorylation in a light dependent manner. However, knockout of Adcy1 gene leads to attenuated phosphorylation (49)*.*

Light mediated deactivation of melanopsin via GRK

Recently Blasic et al demonstrated that melanopsin is phosphorylated both *in vitro* and *in vivo* in a light dependent manner (34). Using a proximity-dependent ligation assay (PLA), they showed that melanopsin that was expressed heterologously in HEK293A cells was phosphorylated in the presence of light (Figure 1.11). Additionally, they confirmed this result *in vivo* in murine retinal sections (Figure 1.12). PLA is a modern assay involving the use of antibodies to detect interaction or proximity between two epitopes *in situ* (Figure 1.12). Primary antibodies that target the two specific epitopes under consideration are followed by secondary antibodies attached to complementary oligonucleotide linkers. If the epitopes are <40nm apart, the oligonucleotides will hybridize to form a circular piece of DNA. The circular piece of DNA can then be amplified by rolling circle amplification and detected using fluorescent probes. The presence of red fluorescent spots indicates a positive result (Figures 1.12 and 1.13).
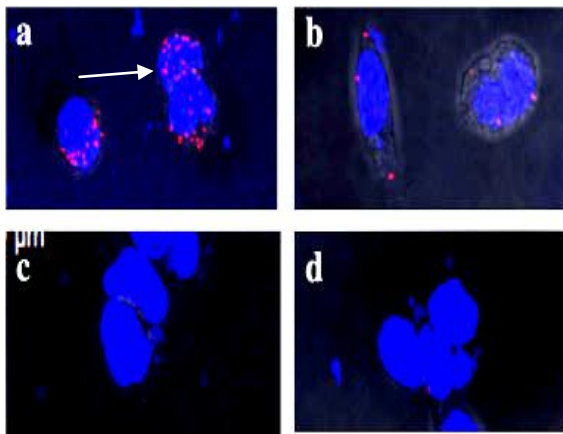
Figure 1.11: Light dependent phosphorylation of melanopsin in vitro. (a) HEK293A cells were transiently transfected with wild type melanopsin in light, (b) wild type melanopsin in dark, (c) phosphonull melanopsin in light (d) untransfected (a) cells in light. Red fluorescent spots(white arrow points to one red fluorescent spot) indicate interaction between anti-mel and anti-phosphoserine antibodies (34).
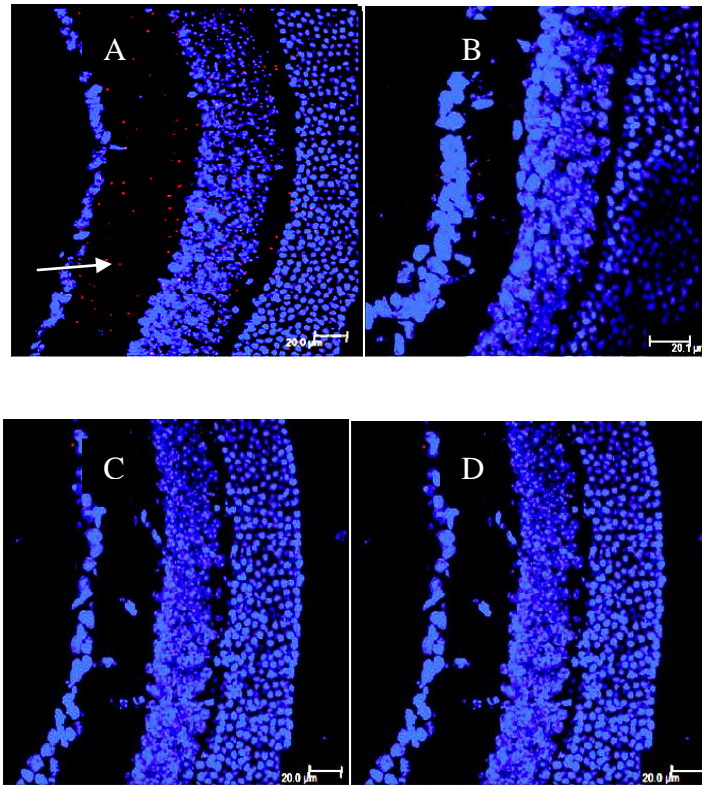
Figure 1.12: Light dependent phosphorylation of melanopsin in vivo. Sections from murine eyes were (a) light adapted and probed (b) dark adapted, (c) light adapted and probed with anti-phosphotyrosine in place of anti-phosphoserine, (d) sections from melanopsin knockout mouse light adapted. Red fluorescent spots (white arrow points to one red spot) indicate interaction between anti-mel and anti-phosphoserine antibodies (34).

1. Incubate with target primary antibodies
2. Add probes
3. Hybridize connector oligos
4. Ligation to form a complete DNA circle
5. Rolling circle amplification
6. Add fluorescent probes to reveal phosphorylation
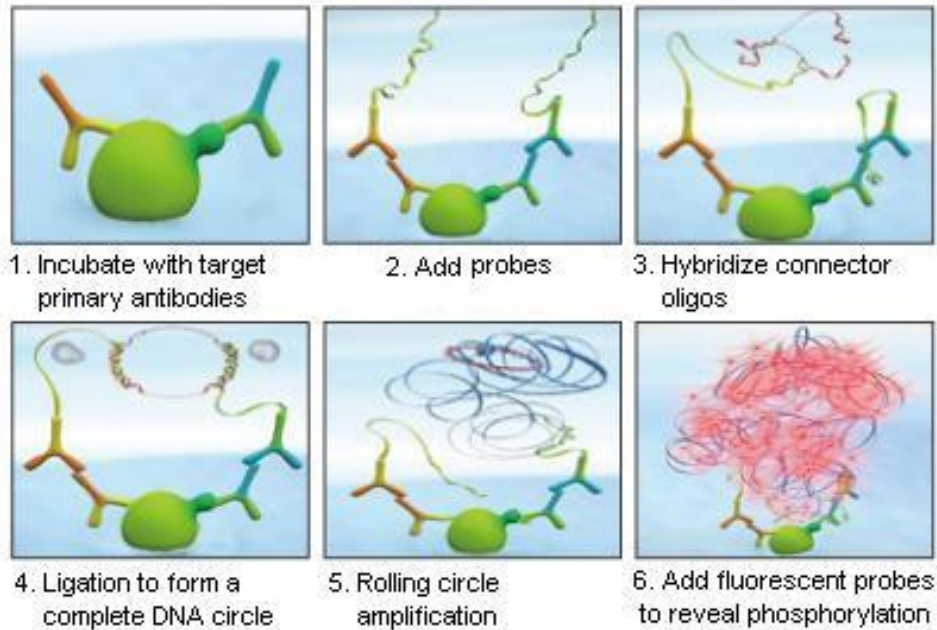
Figure 1.13: The sequential steps in PLA are indicated. Two epitopes <40 nm apart can be recognized by antibodies tagged with complimentary oligonucleotides that can be amplified and detected by fluorescent probes (50)*.*

Although all five GRKs are expressed in the retina, co-immunoprecipitation experiments revealed that the GRK2/3 family of kinases were most likely involved in deactivation of melanopsin, with GRK2 emerging as the stronger candidate (34).

Blasic et al also showed that mutation of the six essential GRK phosphorylation sites leads to delayed deactivation as seen by the calcium response curves in figure 1.14. This definitively confirms that GRK-mediated phosphorylation is vital for melanopsin deactivation *in vitro*. Recently, Mure et al demonstrated *in vivo* using multielelectrode array recordings and pupillary light reflex analyses that these 6 essential GRK phosphorylation sites as well as three additional serines and

threonines are crucial for melanopsin deactivation, further strengthening this result (51).
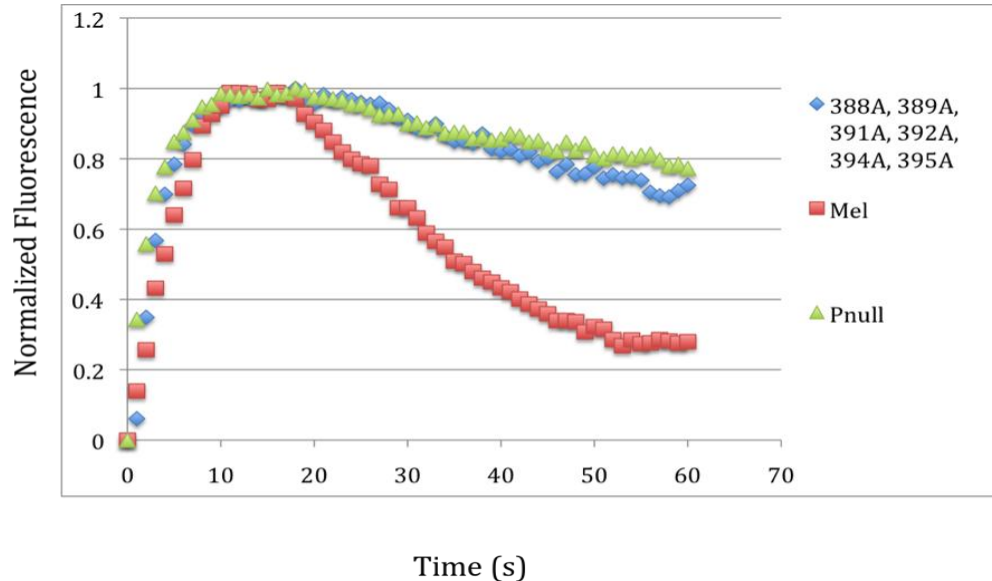
Figure 1.14: *In vitro calcium response curves for melanopsin wild type, PΦ and GRKphosphoΔ (melanopsin with all GRK phosphorylation sites removed). Red curve represents melanopsin wild type, green represents PΦ and blue represents GRK phosphoΔ. PΦ and GRK phosphoΔ show delayed deactivation kinetics (39).*

Studies on rhodopsin indicated that multiple phosphorylations in the C-terminus are required for complete quenching of the rhodopsin response (52). However, not all sites need to be phosphorylated to achieve this quenching. These experiments showed that a minimum of three phosphorylations were required to cause a conformational change in arrestin such that it could bind activated rhodopsin. I suggest that melanopsin could follow a similar pattern of deactivation, where multiple phosphorylation sites are available, but only a subset of them are needed at one point of time to achieve complete quenching of the melanopsin response.

Dopamine in the retina

Dopamine is a catecholamine that serves as neuroactive chemical in the central nervous system of animals. In the retina, dopamine is released by amacrine cells whose cell bodies are located in the inner lining of the inner nuclear layer (INL) of the retina (53). Dopaminergic amacrine cells (abbreviated as DA cells) (Figure 1.15) receive synaptic input from the inner plexiform layer and provide synaptic output to the outer plexiform layer. As these dopaminergic amacrine cells are spread out between multiple layers of the retina, they are also called interplexiform cells. These findings come from studies on dopaminergic amacrine cells in teleost fish and macaque monkeys (53).

Figure 1.15: Location of dopaminergic amacrine cells. The amacrine cells can be seen in yellow extending between the inner nuclear layer and the ganglion cell layer (54).
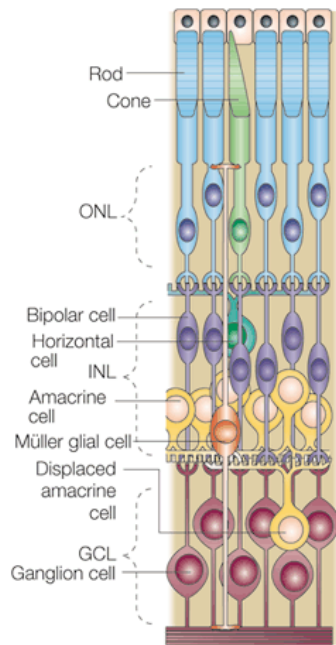
Nature Reviews | Neuroscience

Dopamine performs very diverse roles in the retina. It functions as a neuromodulator in the retina rather than just a neurotransmitter and hence exerts its effect on many cell types. Dopamine modulation of gap junction conductance in

horizontal cells of turtle retina was shown in 1984 (53). By intracellularly injecting Lucifer yellow dye in horizontal cells, Piccolino et al showed that dopamine was able to reduce the axonal diffusion of the dye in these cells (Figure 1.16). This indicated that dopamine attenuates signaling in horizontal cells by reducing the conductance at gap junctions. This effect was reproduced when the cells were treated with a stimulator of adenylate cyclase activity. These findings suggested that dopamine modulates signaling in the retina through a process that involves cAMP as a second messenger. However, these results have not been shown in mammalian retina.
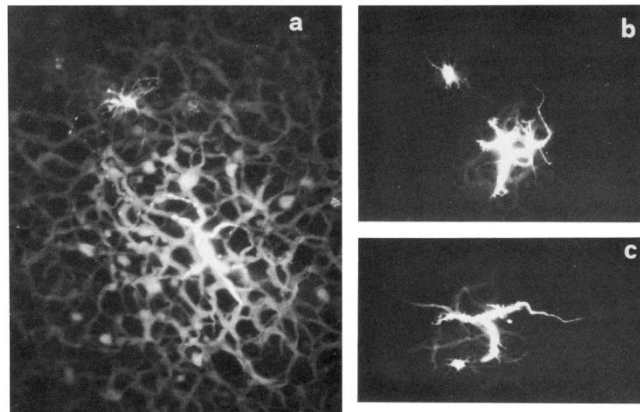
Figure 1.16: Effect of dopamine(c), and forskolin (b), on horizontal cell receptive fields for the diffusion of dye Lucifer yellow. Dopamine or forskolin treated cells show significantly less diffusion of the dye compared to control cells (a) (53).

Lasater et al. in 1987 demonstrated that horizontal cells isolated from white bass showed decreased coupling when injected with the catalytic subunit of cAMP-dependent protein kinase (PKA) (55) (Figure 1.17). They conducted whole cell voltage clamp experiments on pairs of horizontal cells isolated from white bass. Upon treatment with dopamine, the cell pairs showed decoupling for a significant period of

time and then returned to normal levels of firing. cAMP dependent protein kinase mimicked the effect of dopamine on cell coupling. Earlier studies had shown that dopamine attenuates ion flow across gap junctions in horizontal cells (53). These data and previous findings together suggest a mechanism by which dopamine could modulate horizontal cells. Dopamine activates an adenylate cyclase that causes increased intracellular levels of cAMP. This in turn activates a cAMP-dependent protein kinase that could phosphorylate gap junction channels and reduce ion flow between paired cells. Although it is not yet shown, it is possible that dopamine retains this role in the mammalian retina.
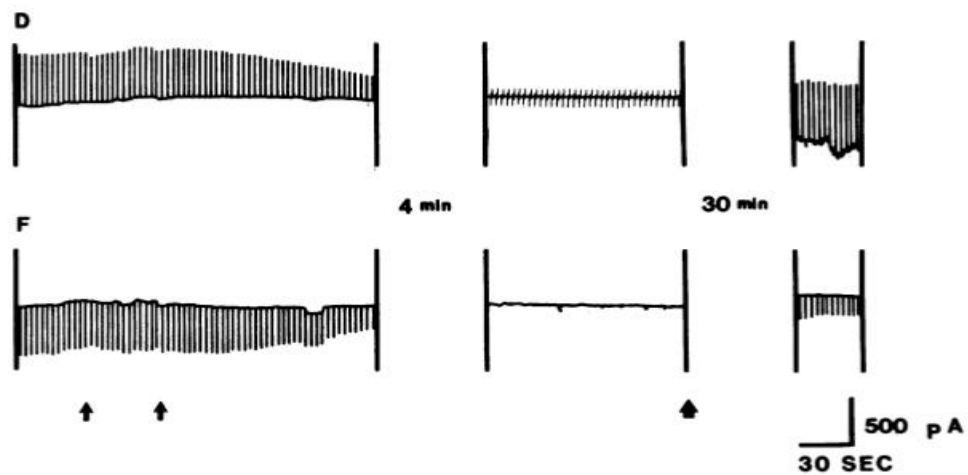
Figure 1.17: Effect of PKA on cell-cell decoupling observed in a pair of horizontal cells isolated from white bass. The thin arrows represent the time points at which PKA was applied and the thick arrow represents the time point at which negative pressure was applied to remove PKA. Decoupling began at 30 seconds, lasted over the next 4.5 min and was too low to be measured at later time points (Lasater et al., 1987).

We now know that dopamine exerts its effect not just on cells that dopaminergic amacrine cells synapse with, but also on cells that dopamine can access through diffusion (53). We also know that dopamine regulates ion flow in horizontal cells by activating PKA (55). There is evidence to suggest that dopamine follows a similar mechanism of neuromodulation via PKA in the retinal ganglion cells (39, 53, 55, 56). Further evidence that supports signal flow between DA neurons and ganglion cells comes from a study published in 2008 that showed that sustained light responses produced in dopaminergic amacrine cells (DA) are due to signaling from ipRGCs (57). DA neurons respond to different light levels ranging from a flicker or short pulse to a sustained light stimulus. ON-bipolar cells are the primary mediators of signaling from photoreceptors that detect light stimulus to the inner retina. By blocking ON-bipolar cells using L-AP4 in *in vitro* retinal mounts, Zhang et al. were able to demonstrate using whole cell voltage clamp that sustained light responses persisted in DA neurons even with the absence of firing from ON-bipolar cells (Figure 1.18). They further characterized this light response and determined that it was very similar to the light responses produced in ipRGCs, the melanopsin-containing retinal ganglion cells. The firing in DA neurons evoked by a sustained light stimulus had peak sensitivity at ~478nm, which is very close to the λ_{max} for melanopsin. The cells also exhibited long latencies and persistent responses even after the cessation of the light stimulus. These responses were produced in mice that had degenerate rods and cones. This further implies the involvement of ipRGCs, as melanopsin is the only other molecule known capable of photoreception apart from the classical visual pigments.
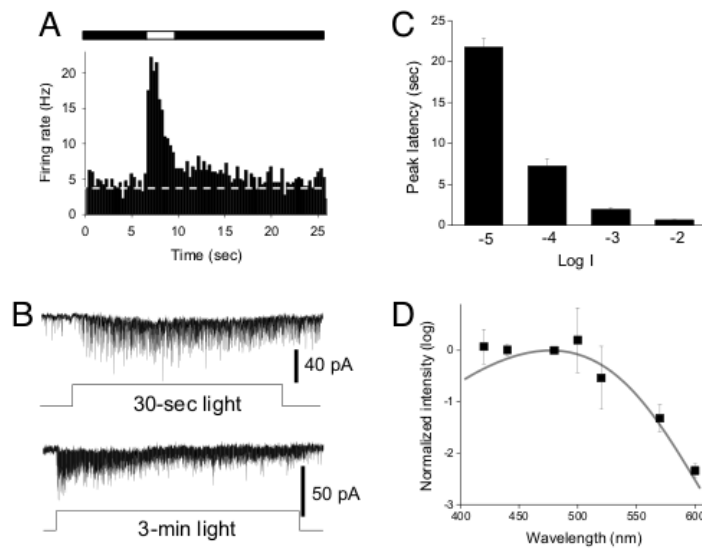
Figure 1.18: Sustained light responses produced in DA neurons upon application of L-AP4. (a) Firing seen before, during and after light stimulus. (b)Voltage clamp recording shows inward current in DA neurons in response to a 30 second pulse of light and 3 min sustained light. (c) Light responses have long latencies which decreased with increased light intensity. (d)DA light responses have a peak spectral sensitivity at 478nm (57).

The multiplicity of roles played by dopamine in the retina when correlated with the findings presented here, suggests that dopamine signaling from DA neurons to melanopsin-expressing ipRGCS could be a negative feedback mechanism to modulate melanopsin phototransduction. The role of dopamine in the retina can be better understood from the model presented in figure 1.19.
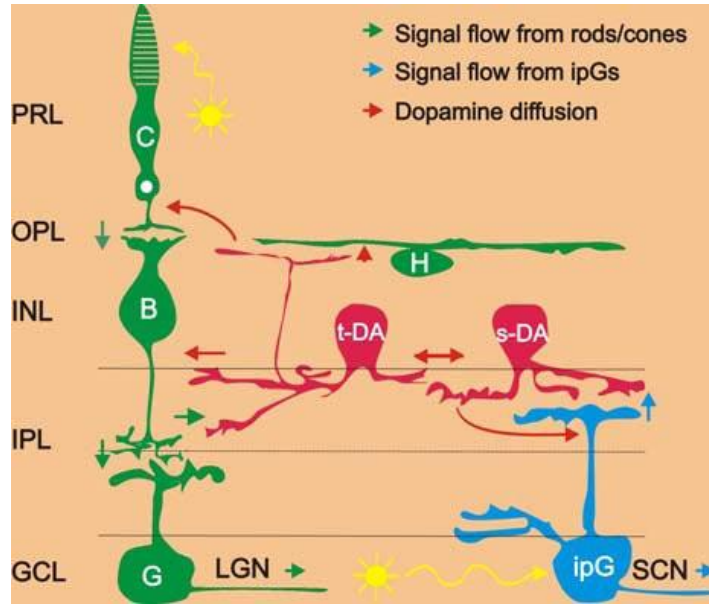
Figure 1.19: The role of dopamine in the retina. Dopamine affects cells that it synapses with such as the ipRGCs, ganglion, bipolar and horizontal cells. The red arrows indicate the diffusion of dopamine and the cells that it affects through diffusion (57) **.** *t-DA is transient dopaminergic amacrine cell and s-DA is sustained dopaminergic amacrine cell.*

Protein kinase A- structure, expression and role in opsin regulation

Protein kinase A (PKA) is a serine threonine kinase whose activity is entirely dependent on the levels of cAMP in cells (58). The PKA holoenzyme is generally a tetramer consisting of two regulatory and two catalytic subunits (59). PKA is extensively expressed in various eukaryotic cell types. The mammalian PKA is assembled from four types of regulatory and three types of catalytic subunits (RIα, RIβ, RIIα, RIIβ, Cα, Cβ, Cγ). Although three C-subunits have been identified, there are only two genes (Cα and Cβ) that code for these proteins. Cγ is described as a splice variant of the Cβ gene (60). The type I (RIα, RIβ) and type II (RIIα, RIIβ)

32

regulatory subunits differ in their elution profiles on ion exchange chromatography and in their binding affinities for cAMP (58). The α and β subunits differ in their expression patterns- α subunits show ubiquitous expression, whereas β subunits show a restricted pattern of expression (59). The γ subunit is restricted to the testis (60). Interestingly all PKA subunits except γ are expressed in neurons (59). However, PKA expression in the retina has not yet been established.

The PKA holoenzyme displays an activation mechanism that is commonly observed in many protein kinases (Figure 1.20). In its inactive form, the protein exists as a tetramer, with the regulatory subunits being bound to the catalytic subunits and blocking their activity (58). This inhibition is relieved when intracellular cAMP levels are elevated, allowing cAMP molecules to bind PKA regulatory subunits and induce a conformational change in the protein. This conformational change releases active catalytic subunits from the tetramer which are then free to act on substrates. Generally, the substrates of PKA may include ion channels, cellular proteins, receptors and transcription factors (58). cAMP levels in the cell are regulated by the enzymes adenylate cyclase and cAMP phosphodiesterase (PDE). One way to regulate intracellular cAMP levels is the activation of G-protein coupled receptors (GPCR). When a GPCR is activated by a neurotransmitter or a stimulus, it undergoes conformational change and binds a specific G-protein. GPCRs that use the cAMP/PKA signaling pathway bind the G-protein Gs. In subsequent steps, Gsα binds and stimulates the enzyme adenylate cyclase, which in turn triggers the conversion of ATP to cyclic-AMP (cAMP), causing elevation in the levels of intracellular cAMP.
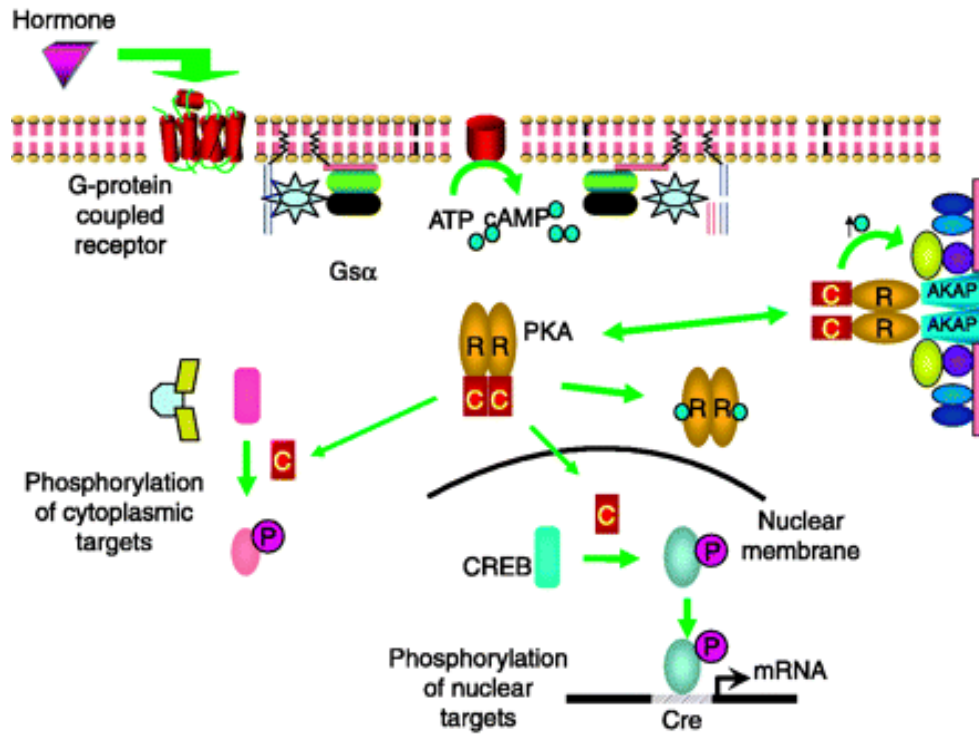
Figure 1.20: An overview of PKA signaling pathway. *GPCR activation by hormone triggers Gs pathway. Stimulation of adenylate cyclase causes increased cAMP levels and PKA activation. Active PKA catalytic subunits act on cytoplasmic and nuclear targets* (58)***.***

Activation of PKA is reversed by the hydrolysis of cAMP to 5'AMP by phoshphodiesterases (PDEs) (61). PKA is part of a negative feedback mechanism that causes a check on its own activation. By phosphorylating specific serine threonine residues on GPCRs, PKA may block efficient binding of G-protein to the receptor, thus inhibiting signal transduction (62). Decreased intracellular signaling leads to reduced cAMP levels and there is no further activation of PKA.

The crystal structure of PKA apoenzyme has been solved by Akamine et al. in 2003 (63). They discuss the structural conformations of the catalytic subunit which is

the active site bearing subunit. The active site cleft is flanked by two lobes which are oriented distinctly in each step of the catalytic cycle of the active enzyme (Figure 1.21). The C-terminal tail serves as a gate to the active site. In the unliganded state, the catalytic subunit shows an open conformation with the two lobes being far apart and the C-terminal tail being disordered. Upon binding ATP, the C subunit adopts an intermediate conformation with the two lobes being closer and the C-terminal tail gating the active site from solvent. When both ATP and substrate bind the active site, the lobes are seen tightly closed and hydrophobic residues surround the active site to eliminate water. Thus the C subunit apoenzyme, which represents the functional component of PKA, has a highly dynamic structure.
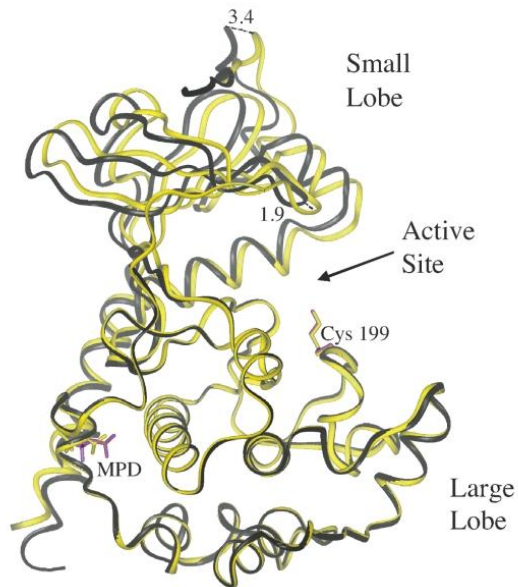
Figure 1.21: Apoenzyme crystal structure of PKA catalytic subunit with a resolution of 2.9 A°. The apoenzyme crystals consist of two molecules Apo A and Apo B which are superimposed in this figure. The active site cleft, and the lobes flanking the site can be seen (63)*.*

Cadd et al. have shown using *in situ* hybridization that the various subunits of PKA show distinct expression patterns in different areas of the mouse brain (61). They generated probes against the mRNA coding sequences of PKA isoforms and localized them to various regions of the mouse central nervous system. Their results indicated that the Cα, R1α and R1β subunits localize to forebrain regions like neocortex, hippocampus, hypothalamus and thalamus. The Cβ and RIIβ show moderate levels of expression in the above mentioned brain regions and relatively high expression in the dentate gyrus. The RIIα shows poor expression in the above mentioned brain regions but shows high expression in the media habenula. These results suggested that variation in the expression of PKA isoforms in different brain regions could translate into variability in cAMP responses in different tissues. Ventra et al. confirmed this hypothesis by correlating the differential expression of PKA subunits with cAMP responses in specific brain areas (64). They assessed cAMP responses in terms of dissociation of the hetero-tetrameric PKA and translocation of C-PKA to the nucleus. They observed two distinct patterns of cAMP responses – in the neocortex, PKA was mostly undissociated, and in the cerebellum PKA was almost completely dissociated. This variation in cAMP response coincides with a distinct variation in PKA isoform expression. RIIβ is expressed in high levels in the neocortex, but shows very poor expression in the cerebellum. Previous literature and work by Ventra et al. taken together show that isoform RIIβ may be the major determinant of the type of cAMP response observed in brain tissues. Ventra et al. have also demonstrated the presence of the catalytic subunit of PKA in cortical neurons derived from rat embryos by immuno-blotting with an anti C-PKA antibody.

Dunn et al. have used an innovative assay to indirectly measure PKA activity in retinal ganglion cells (RGCs) (65). In their experiment they simultaneously assayed calcium levels and PKA activity in RGCs in order to detect calcium induced PKA transients. Their dual imaging technique involved a FRET assay to measure PKA activity and a calcium imaging assay using a fluorescent fura-2AM dye to measure calcium influx into the cells. The FRET assay involved the use of a genetically encoded marker of PKA activity (AKAR3), which was composed of a cyan fluorescent protein, a phospho-amino acid-binding domain, a consensus substrate for PKA, and yellow fluorescent protein. In the un-phosphorylated state, this fusion protein adopts a structural conformation that holds the CFP and YFP far apart resulting in no FRET signal. When PKA phosphorylates the substrate, the phospho-amino acid binding domain binds the phosphate residue and brings the CFP and YFP closer, resulting in a positive FRET signal. The results of this experiment showed that spontaneous PKA transients in RGCs were always preceded by large calcium transients, but no detectable PKA transients were observed following smaller calcium currents. This result indicates that a threshold level of depolarization by calcium influx is required for a detectable PKA transient current.

Even though indirect assays of PKA activity indicate the presence of the protein in RGCs, there is still no direct evidence that PKA is expressed in these cells. In order to provide a clear understanding of the expression of PKA in the retina and specifically in RGCs, I attempted RT-PCR and immunofluorescence respectively as described in Appendix A.

Dopamine-mediated modulation of melanopsin via PKA

Light/GRK-dependent phosphorylation of melanopsin explains the deactivation mechanism of this receptor. However, the complexity of melanopsin's functional roles requires a more fine-tuned regulation of its activity. Blasic et al. showed that melanopsin activity is modulated *in vitro* in a cAMP dependent manner (39). In wild type and phosphonull melanopsin heterologously expressed in HEK cells and treated with an analog of cAMP, 8 Br-cAMP treated cells showed positive signal in PLA assay, suggesting that melanopsin could be phosphorylated in these cells (Figure 1.22). This phosphorylation was shown to modulate or significantly change the kinetics of melanopsin activity (Figure 1.23). The effect of a cAMP analog on melanopsin activity suggests that a cAMP-dependent protein kinase is most likely involved in melanopsin phosphorylation.
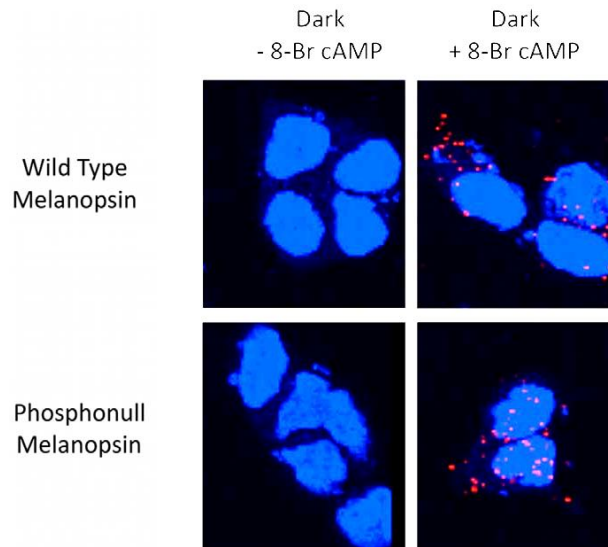
Figure 1.22: cAMP mediated melanopsin phosphorylation in vitro.
HEK293A cells transiently transfected with wild type melanopsin or phosphonull

melanopsin were dark adapted and untreated or treated with 8 Br-cAMP. Red fluorescent spots indicate melanopsin phosphorylation (66)*.*
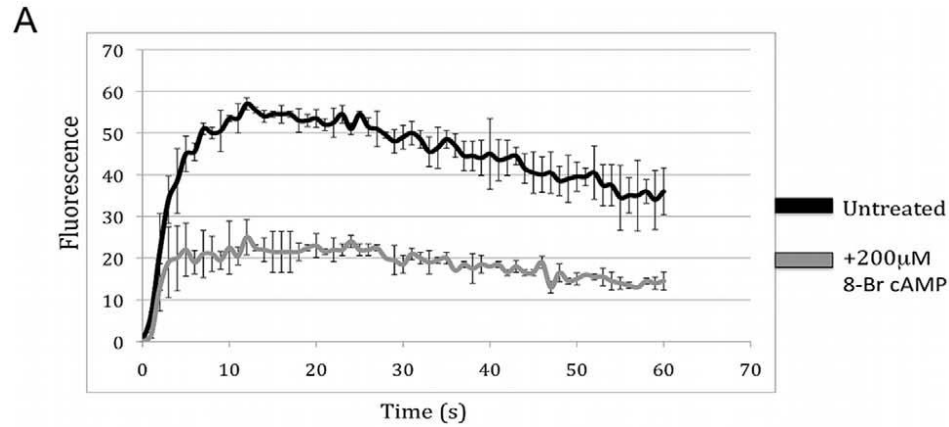
***Figure 1.23: cAMP mediated modulation of melanopsin activity.** Calcium response curves for HEK293A cells transiently transfected with melanopsin untreated or treated with 8 Br-cAMP (39).*

In order to confirm that the kinase involved is PKA, Blasic et al. treated the melanopsin transfected HEK cells with a PKA inhibitor Kt5720 prior to treatment with 8 Br-cAMP. The results showed that the cAMP response was abolished in cells treated with the PKA inhibitor (Figure 1.24). This suggests that melanopsin is phosphorylated by PKA *in vitro*. However, the expression and functioning of PKA in the retina is not yet clearly understood. The experiments discussed in Appendix A will help us get a better picture of PKA expression in the retina.
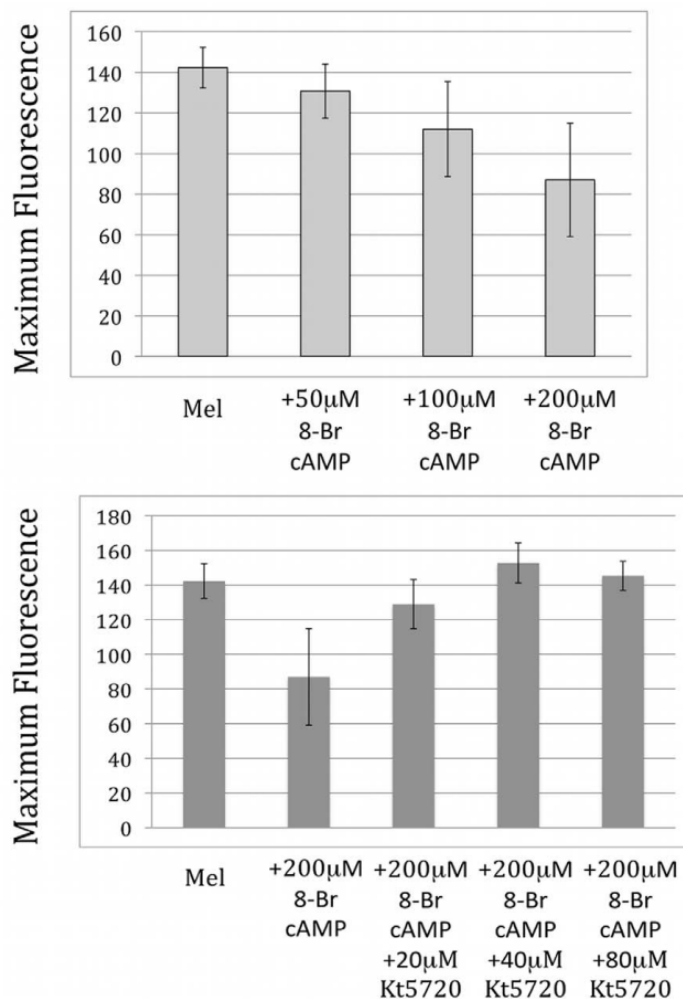
Figure 1.24: Effect of cAMP/PKA on melanopsin signaling in vitro. *(a)*
HEK 293A cells were transiently transfected with melanopsin and treated with
increasing concentrations of 8-Br cAMP. Calcium imaging showed an attenuation of
melanopsin activity upon treatment with 8 Br-cAMP. (b)HEK cells transfected with
melanopsin were treated with Kt5720 prior to treatment with 8 Br-cAMP . Kt5720
abolishes the cAMP response in a concentration-dependent manner (39)

Blasic et al. also showed the involvement of dopamine in melanopsin
regulation (39). Dopamine is a common neurotransmitter of the nervous system
which can indirectly control PKA activation in the cell. When dopamine levels go up,

it activates adenylyl cyclase (cAMP synthetic enzyme) through D1-like dopamine receptors. This allows for increased cAMP levels which in turn boost PKA activation. Blasic et al. treated murine retinal sections with a D1 agonist and conducted the PLA assay to test phosphorylation of melanopsin. The agonist-treated cells showed phosphorylation, while the untreated and melanopsin-knockout cells did not (Figure

1.25).
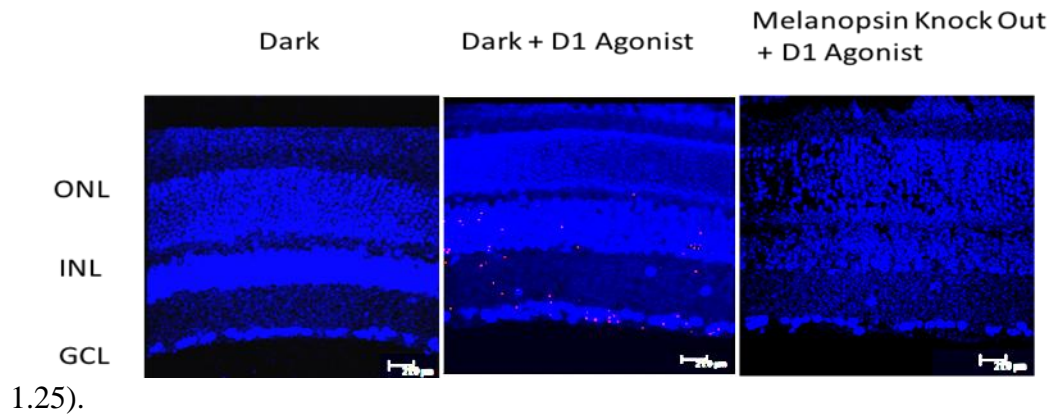
Figure 1.25: Dopamine-mediated melanopsin phosphorylation in vivo. PLA shows in vivo phosphorylation of melanopsin induced by dopamine agonists in retinal sections(White arrow points to a red fluorescent spot indicating proximity of melanopsin to a phosphorylated serine) (39)*.*

Further supporting this result, Van Hook et al. showed that dopamine in intact retina attenuates the melanopsin photocurrent. They conducted a whole-cell voltage clamp experiment on isolated ipRGCs and observed the effect of dopamine on the melanopsin photo-response. Dopamine-treated cells showed attenuation of melanopsin activity, and this response was abolished when dopamine was washed out (Figure 1.26).
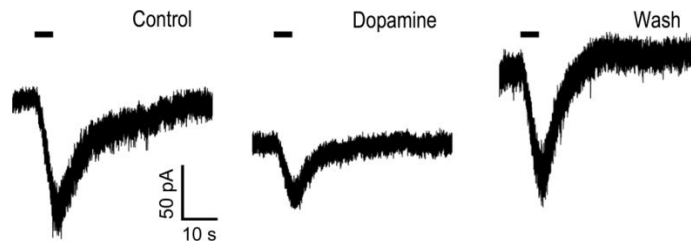
Figure 1.26: Dopamine-mediated attenuation of melanopsin photocurrent. *Whole cell voltage clamp recordings from isolated ipRGCs untreated, dopamine treated and dopamine washed out* (56)*.*

Dopamine-releasing amacrine cells of the retina have been shown to synapse with melanopsin-expressing ipRGCs, suggesting a possible role for dopamine in melanopsin regulation. Dopamine levels during subjective day are higher compared to subjective night (67). Moreover, signaling from ipRGCs to the suprachiasmatic nucleus (SCN) is lower during subjective day as compared to subjective night (68). As the primary target of melanopsin signaling in the brain is the SCN, these two results taken together suggest that melanopsin could be regulated by dopamine. However, the hypothesis that PKA is the downstream effecter of dopamine in controlling melanopsin activity still remains to be established *in vivo*. Exploring PKA phosphorylation of melanopsin in transgenic mice as described in Appendix A could provide confirmation of this pathway. Additionally, the experiments discussed in Appendix A will help us determine the role of dopamine on melanopsin regulation.

Synopsis and specific aims

Light detection is used by organisms to not only perceive the environment in the form of images but also to aid vision through accessory visual functions like the pupillary light reflex, and to regulate other physiological functions by synchronizing the

internal biological clock to external light and dark cycles through a process called circadian photoentrainment. These accessory visual functions and circadian regulations are collectively termed non-image forming vision. Melanopsin, in addition to rhodopsin and cone opsins in the retina, forms the first step in the light detection process for non-image forming vision, but melanopsin's role in non-image forming vision is much less appreciated compared to the classical visual pigments. Melanopsin's ability to consistently detect and transmit light information from the environment to internal physiological and behavioral centers largely depends on the reliable activation of the visual pigment and tight regulation of its deactivation. Previous work in tissue culture cells suggests that melanopsin is deactivated through a two-step process - phosphorylation of the carboxyl terminus of melanopsin through a GPCR kinase (GRK) and binding of arrestin to sterically block further G-protein activation. The goal of this project was to understand whether this proposed mechanism of deactivation that begins with phosphorylation of the C-terminus of melanopsin is important *in vivo* in a mouse model, and to uncover the implications of altering the phosphorylation target sites on the physiology of melanopsin expressing cells and the resulting non-image forming visual behaviors.

Specific aims

Specific aim 1: Develop a Cre-loxP dependent viral expression system for exogenously expressing melanopsin in melanopsin knockout animals.

The goal of this specific aim was to develop a system for easily generating targeted mutations of melanopsin in a mouse model. To achieve this, a combination of adeno-associated viral vectors, Cre-loxP recombination and melanopsin knockout mouse

(*Opn4$^{cre/cre}$*) models was used. The following objectives were outlined for this specific aim.

Objective 1: Construct floxed (flanked by loxP sites) melanopsin wild type and CPΦ fusion constructs with molecular markers in adeno-associated viral vectors

Objective 2: Test expression, functionality and localization of these constructs in HEK293 cells that express Cre recombinase

Objective 3: Package floxed viral constructs into suitable adeno-associated viral capsids and prepare titers

Specific aim 2: Analyze the physiological and behavioral effects caused by light dependent phosphorylation of mouse melanopsin *in vivo*

I hypothesize that C-terminal GRK-mediated phosphorylation determines the lifetime of active melanopsin *in vivo* and influences the kinetics of light evoked response of ipRGCs. In order to test this hypothesis, the following objectives were outlined.

Objective 1: Generate virally modified mice by ocular injections of AAV2 virus carrying either wild type melanopsin or CPΦ melanopsin mutant construct into *Opn4$^{cre/cre}$* mice.

Objective 2: Test pupillary light reflex, circadian photoentrainment and masking of virally modified mice to determine *in vivo* behavioral effects of absence of C-terminal melanopsin phosphorylation.

Objective 3: Perform multielectrode array recordings on retinal explants from virally modified mice to determine *in vivo* physiological effects of absence of C-terminal melanopsin phosphorylation.

Chapter 2:

Development of a Cre-loxP dependent viral expression system for restoration of melanopsin expression in melanopsin knockout mice

Introduction

Mice are a suitable system to study animal behavior and physiology as transgenic mice can be made and bred in large numbers. Transgenic mice have been used increasingly in the past few decades to study physiology, disease and development. They have proved to be excellent models for human diseases. Genetic techniques for knocking in and knocking out genes in mice have improved tremendously (69). The first transgenic mouse was generated by a technique involving pronuclear-microinjection of a plasmid carrying viral DNA into fertilized mouse oocytes, which were then implanted into the oviduct of female mice (70). This technique showed a transformation success rate of 2.7 % in the 78 viable animals produced out of several hundred microinjections. Nevertheless, the technique showed sufficient promise for it to be adapted in fields such as neuroscience, immunology and developmental biology. Since then numerous other techniques have emerged to facilitate the generation of genetically modified mice. A second common approach is the use of retroviral vectors to introduce DNA into mouse embryonic stems (ES) cells and injection of these ES cells into a blastocyst, which then develops into a viable animal. Unlike the former technique, the latter allows the manipulator to screen for successful clones containing the transgene construct very early on even before injection of ES cells into a blastocyst (71–73). This technique that was jointly pioneered by Capecchi, Evans and Smithsies in late 1980s earned them the Noble Prize in physiology and medicine for the year 2007. Both these techniques result in genomic integration of the transgene construct, with the former involving random

integration of foreign DNA into the genome and latter involving integration through homologous recombination. The disadvantages of these techniques are that they are time consuming and expensive because they require extensive screening of clones, culture of ES cells, and maintenance of offspring that have acquired the transgene through germ line transmission to name a few.

An efficient and highly successful technique for ocular gene delivery in mice is the use of viral vectors. Mammalian viruses are a preferred choice for gene delivery in mammalian tissues as they have naturally evolved to infect mammalian cells without damaging their own core nucleic acids. Viruses have been successfully used to transduce and label ipRGCs in the past (32). Recently, adeno-associated viruses have been used for gene delivery due to their non-pathogenicity in humans. Adeno-associated virus (AAV) is a small non-enveloped virus that belongs to the *Dependovirus* genus of the *Parvoviridae* family (33). It consists of a single stranded DNA genome which is about 4.7kb in size. AAV serotype 2 has been extensively examined and exhibits tropism for neuronal cells in addition to a few other cell types (34). Several studies have shown that recombinant AAV can be intravitreally injected to transduce RGCs (35, 36). More specifically, Gooley et al. have used rAAV-GFP fusion virus to transduce RGCs for anterograde labeling of ipRGC projections. Hence, these recombinant viral vectors have been chosen for our research, because of their ability to show persistent and stable transgene expression, low immunogenicity and broad tropism. Use of AAV greatly reduces the time and cost of generating genetically modified mice due to the following: - 1. Mice can be sequentially injected with the virus in batches based on the requirements and timing

of the experiments, eliminating the need to maintain a lineage of mice carrying a specific mutation. 2. The time taken for viral transduction to occur in AAV injected mice is ~ four weeks as compared to conventional knock-in/knock-out strategies which may require several generations of breeding.   3. It does not require the expertise or resources needed to obtain and culture ES cells and embryos. In addition to the above advantages, AAV in combination with Cre-loxP (discussed below) recombination system allows conditional expression of transgenes in tissue specific and/or developmental stage specific manner.

The Cre-loxP recombination system is an enzyme-DNA sequence combination system that allows a molecular biologist to create additions, deletions or inversions of a specific sequence of DNA (74) . The Cre recombinase, which stands for "**C**auses **re**combination", is a 38kDa enzyme that belongs to the integrase superfamily of enzymes in the P1 bacteriophage (74). loxP, which stands for "**l**ocus **o**f crossover(**x**)", is a sequence of DNA in P1 bacteriophage that resembles a restriction enzyme sequence in that it contains two 13bp palindromic sequences separated by an 8bp non-palindromic spacer. Two loxP sequences are recognized, excised and re-ligated by Cre based on the order in which the sequences are oriented allowing either deletion, addition or inversion of the piece of DNA that lies between the loxP sequences (see Fig. 2.3). This recombination occurs at an optimal temperature of 37°C without the need for any additional co-factors, making it a perfect tool for molecular biologists to create genetic modifications. Cre-loxP exchange systems have been used to target the melanopsin locus for knocking in reporter genes downstream of the melanopsin promoter in mouse lines (6, 8). Such systems have shown

48

successful expression of reporter genes in melanopsin cells. A combinatorial approach utilizing the AAV vectors that preferentially transduce RGCs and the Cre-loxP exchange cassette was used in our study to ensure efficient and cell specific transduction of target genes. This method was chosen due to its relative ease, flexibility and speed in generating genetically modified mice.

Materials and methods

Protein immunoblot or western blot analysis

Cloned viral vectors were tested for expression in HEK-Cre cells by western blot analysis. pAAV/(mRuby-P2A-Melanopsin-FLAG) and pAAV/(mRuby-P2A-CPΦ-FLAG) were transiently transfected into HEK293-Cre cells. 48 hours post transfection, total cell proteins were solubilized and separated on a SDS-PAGE gel (Biorad-4561081). Protein was transferred onto a PVDF membrane and probed with a rabbit anti-FLAG antibody (ABCAM-ab1162;1:200). Anti-rabbit IgG-alkaline phosphatase (AP) conjugate secondary antibody (1:1000) was used and protein was visualized by fluorescence observed after application of Attophos AP-fluorescent substrate.

In vitro calcium imaging

In vitro calcium imaging protocol was conducted as described in Blasic et al. (34, 35). Viral vectors were transiently transfected into HEK293 and HEK293-cre cells, and mammalian expression vectors were transiently transfected into HEK293 (Figure 2.2 and 2.5). Four hours post transfection cells were split into a 96 well dish at a density of ~80,000 cells per well and dark-adapted. 48 hours after transfection,

cells were treated with Fluo-4AM (calcium sensitive fluorescent dye) and incubated for 60 min. Following incubation, fluorescent measurements were made at excitation and emission wavelengths of 485nm and 520nm respectively using a fluorescent plate reader (Tecan Infinite M200 microplate reader) (Figure 2.2 and 2.5).

Animals

All animals used for behavior were male $Opn4^{Cre/Cre}$ on a mixed BL/6;129SvJ background and were between one and two months of age at the start of the behavioral experiments. All protocols were in accordance with Johns Hopkins University Animal Care and Use Committee (IACUC) guidelines. Animals were individually housed in plastic cages with steel wheels and were kept in light-tight boxes on a light-dark protocol of 16 hours of light and 8 hours of dark (16:8 LD) with 500 lux overhead white light. Food and water were made available *ad libitum*. Behavioral experiments were initially conducted for ~ 30 days, followed by viral injection, four weeks of post-injection recovery for expression of virally-encoded proteins (75), and ~ 30 days of post-injection behavioral studies. Animals were euthanized then by intraperitoneal injection with overdose of avertin (1ml of 20 mg/ml) followed by cervical dislocation to obtain retinas for immunofluorescent verification of melanopsin expression.

Virus

AAV2 (mRuby-P2A-Melanopsin-FLAG) with a viral titer = 5×10^{12} vg/ml was prepared by the Wu lab, Ocular Gene Therapy Core, National Eye Institute, NIH (75) (see figure 2.3 for the viral vector map showing critical components of the vector).

Intravitreal viral injections

Mice were anesthetized by intraperitoneal injection with 0.5 ml avertin (20 mg/ml; volume was adjusted based on body weight of the mice). 1 µl of AAV2(mRuby-P2A-Melanopsin-FLAG) or AAV2(mRuby-P2A-C-terminus phosphonull-FLAG) was dispensed onto a strip of parafilm. The viral preparation was then drawn up into a micropipette (Sigma, P0674) connected to the hose of a pico-injector (Harvard apparatus, Model PLI-90), which in turn was connected to a compressed nitrogen gas tank. Injection pressure was maintained at 30 psi using a regulator. The anesthetized animal was placed under a dissection microscope and forceps was used to open the eyelids and expose the eye. The eye was punctured by the injection needle near the ora serrata, aiming the tip towards the center of the eyeball. Depression of the footswitch created a surge of pressure to deliver the viral preparation from the microcapillary tube into the vitreous. After injection, the animals were kept warm to allow them to recover from the injection and wake up. They were then returned to their cages in the same setting.

Immunofluorescence

Mice were euthanized by cervical dislocation after intraperitoneal injection with 1 ml avertin (20 mg/ml). The eyes were removed and initially fixed whole in 4% paraformaldehyde for 30 min. The cornea was then removed, and the eyecup with exposed retina was fixed in 4% paraformaldehyde for an additional hour. The eyecups were washed thrice with 1X PBS for each of the wash steps before application of blocking buffer (0.3% triton, 4% goat serum), primary antibody, and secondary antibody. Immunofluorescence was performed by using rabbit anti-

melanopsin (1:1000; Advanced Targeting Systems AB-N38) as primary antibody with a 2 day incubation period, followed by goat anti-rabbit – IgG 488 (1:1000; Life Technologies A11008) as secondary. After immunostaining, the retinas were mounted and imaged using Zeiss Axioimager M1 microscope. The images were processed in ImageJ (NIH).

Results

In order to develop a Cre-loxP-dependent viral expression system for exogenously expressing melanopsin in ipRGCs, the initial approach was to generate a transgene cassette with the gene of interest (melanopsin wild type or CPΦ), a fusion tag (FLAG), and a reporter gene (mRuby) in an adeno-associated viral vector (See Figure 2.3). This transgene cassette (Figure 2.3) was constructed in multiple cloning steps as outlined below.

Addition of a FLAG fusion tag to melanopsin coding sequence

Initially melanopsin wild-type coding sequence including a FLAG tag at the C-terminus was cloned in a mammalian expression vector (pMT3). FLAG is a synthetic hydrophilic tag that can be used for melanopsin protein purification from the virally modified mice for future biochemical assays. Its hydrophilic nature makes it less likely to denature or inactivate the protein attached to it (Schmidt et al., 2012). Additionally, its small size and flexibility make it an excellent choice for tagging target proteins. Initially, FLAG was added to the N-terminus of melanopsin, but it greatly affected protein expression. Hence, it was moved to the C-terminus. Once the mammalian expression vector (pMT3 (MelanopsinWT-FLAG)) was constructed,

protein expression and functionality were assayed *in vitro* in human embryonic kidney (HEK293) cells by western blotting, and calcium imaging techniques respectively (Figures 2.1 and 2.2). More specifically, calcium imaging was used to test melanopsin's ability to signal by measuring the light dependent increase in intracellular calcium in cells that heterologously express melanopsin (Figure 2.2). Once the melanopsin-FLAG fusion construct was determined to be fully functional, it was then cloned into an adeno-associated viral vector.
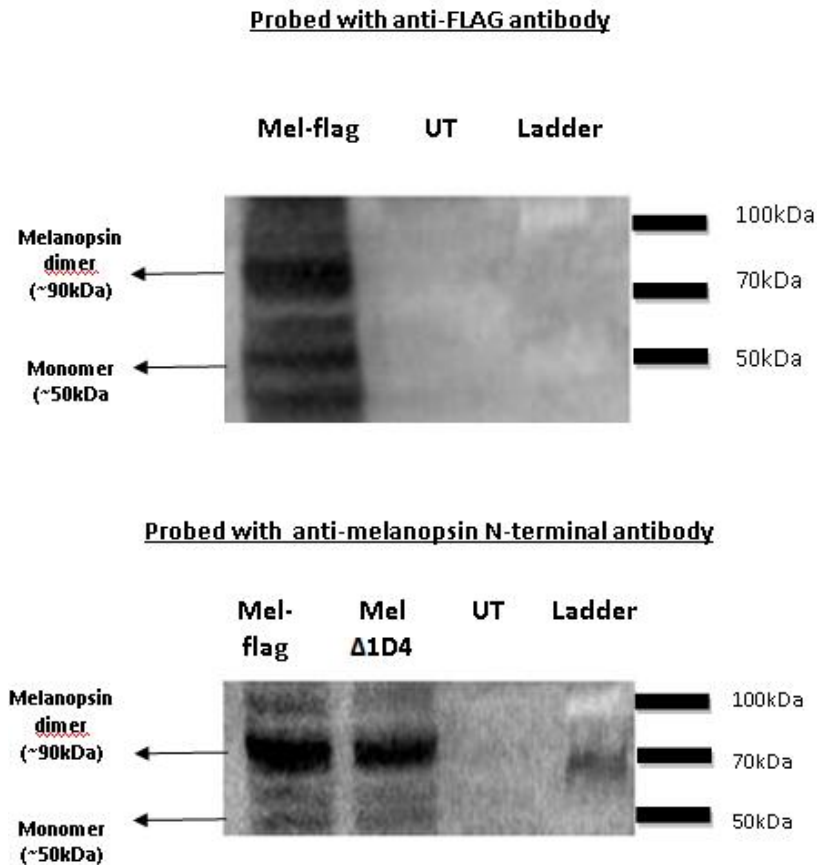
***Figure 2.1: Expression of MelanopsinWT-FLAG demonstrated by western blotting.** HEK293A cells were transiently transfected with pMT3 (MelanopsinWT-FLAG) construct. 48 hours post transfection, total cell protein was solubilized and*

run on a SDS-PAGE gel. Protein was transferred onto PVDF membrane and probed with anti-FLAG and anti-melanopsin N-terminal antibodies. Expression of melanopsin-FLAG can be seen as two bands corresponding to the predicted monomer and dimer of melanopsin (~45kDa and ~90kDa respectively). Mel-Δ1D4 served as a positive control for the anti-melanopsin N-terminal antibody.
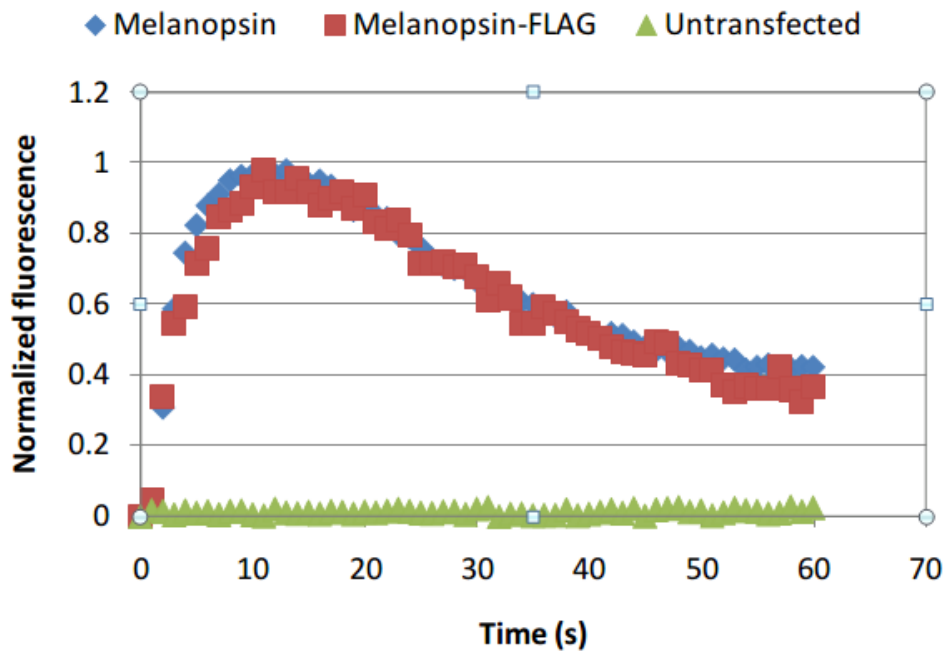
Figure 2.2: Functionality of melanopsinWT-FLAG fusion protein demonstrated by calcium imaging. *pMT3(MelanopsinWT-FLAG) construct was transiently transfected into HEK293A cells and in vitro calcium imaging was performed using calcium sensitive Fluo-4AM dye to indirectly measure activity of melanopsin. MelanopsinWT-FLAG calcium response kinetics was identical to melanopsin wild type.*

Generation of adeno-associated viral vector transgene cassettes

Floxed (flanked by loxP sites) melanopsin wild type and CPΦ (melanopsin mutant with all C-terminal serines and threonines mutated to alanines- discussed in Chapter

3) constructs with a C-terminal FLAG tag and N-terminal mRuby-P2A tag were cloned into pAAV (adeno-associated viral vector) (Figure 2.3). mRuby is a red fluorescent protein (~25kDa) that acts as a quantitative visual marker of cells expressing melanopsin in the virally modified mice (37). mRuby will help track single cells expressing melanopsin for patch clamp electrophysiology and for visualizing viral infectivity. P2A is a viral peptide that will allow the expression of melanopsin fusion construct into a bi-cistronic transcript and will self-cleave during translation to generate two peptides (Melanopsin-FLAG and mRuby) of equimolar proportions (38). After self-cleavage, the P2A site will leave a proline attached to the N-terminus of melanopsin. The single proline attached to the N-terminus of melanopsin coding sequence did not affect melanopsin's expression or activity (fig 2.5). The melanopsin-FLAG and CPɸ-FLAG fusion proteins expressed from pAAV(mRuby-P2A-MelanopsinWT-FLAG) and pAAV(mRuby-P2A-CPɸ-FLAG) were detected using anti-FLAG antibody in western blots (Figure 2.4). The vectors were further tested for melanopsin activity in HEK and HEK-Cre cells by calcium imaging assay. The pAAV vectors were found to show a calcium response curve in HEK-Cre cells, but no activity in HEK cells (Figure 2.5). This confirms the occurrence of Cre-loxP recombination in the vectors in the presence of Cre recombinase and the selective functionality of the viral constructs only in the presence of Cre.
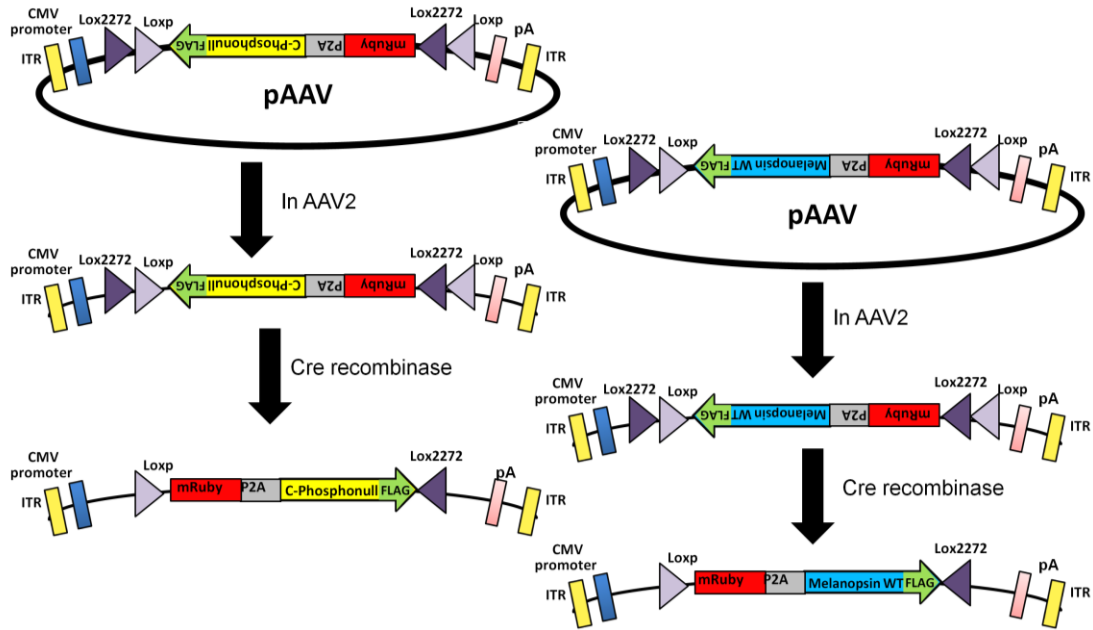
Figure 2.3: Critical components of the adeno-associated viral vectors expressing wild type melanopsin. (Left) *Melanopsin wild type coding sequence and (**Right**)* *CPΦ coding sequence in pAAV with C-terminal FLAG tag and N-terminal mRuby-P2A tag in reverse complement orientation flanked by loxP and lox2272 sequences (floxed). CMV promoter drives expression of the transgenes in these viral vectors in the presence of Cre recombinase. Inverted terminal repeats (ITRs) are viral derived sequences that are recognized by viral proteins for packaging into AAV2 capsids. The first step indicates the final construct that gets packaged into AAV2 capsids and the second step indicates the functional construct after cre-loxP recombination that is expected to be expressed in ipRGCs after viral transduction.*
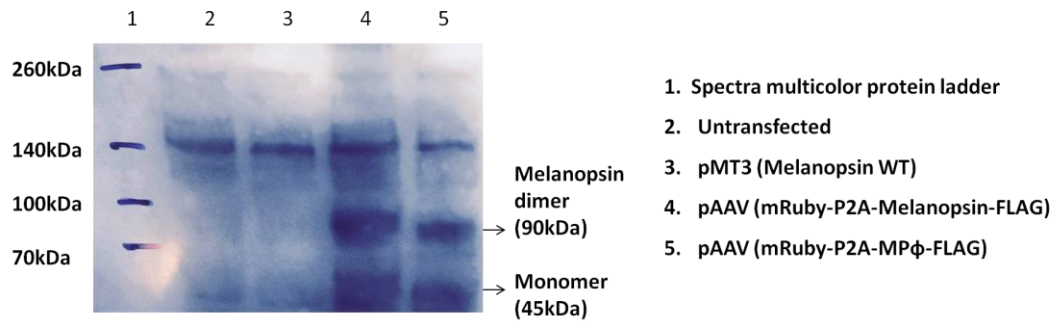
Figure 2.4: Expression of melanopsin-FLAG and CPφ-FLAG fusion proteins demonstrated by western blotting. *HEK293-Cre cells were transiently transfected with* pAAV(mRuby-P2A-MelanopsinWT-FLAG) *and* pAAV(mRuby-P2A-CPφ-FLAG) *constructs. 48 hours post transfection, total protein was extracted from the cells and run on SDS-PAGE gel. Protein was transferred onto PVDF membrane and probed with anti-FLAG antibody. Expression of melanopsin-FLAG and CPφ-FLAG fusion proteins can be seen as two bands corresponding in molecular weights to the predicted monomer and dimer of melanopsin. pMT3(MelanopsinWT) served as a negative control for the anti-FLAG antibody.*

A
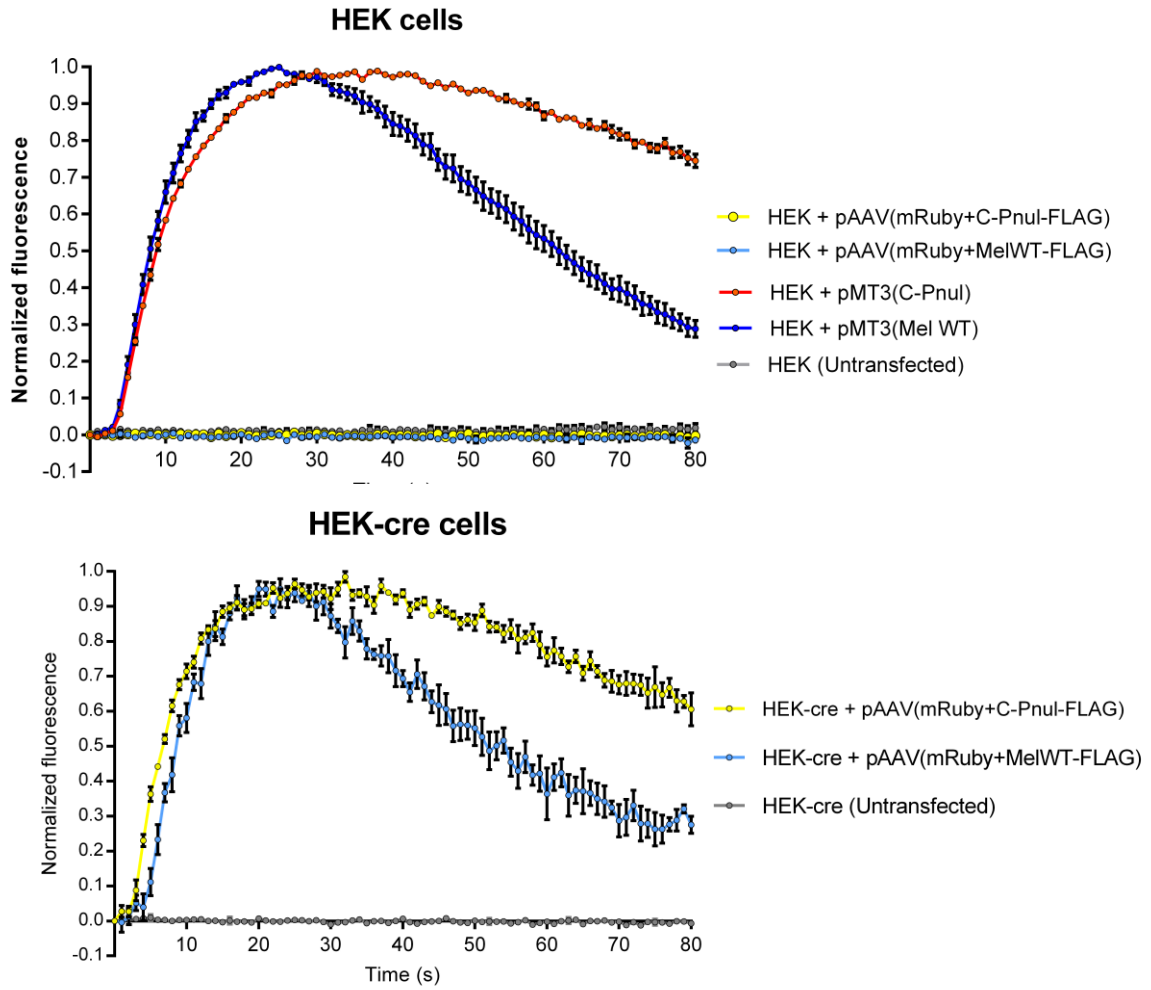
B

| pAAV/ (*mRuby*-P2A-Melanopsin-FLAG) | pAAV/(*mRuby*-P2A-CPΦ-FLAG) |
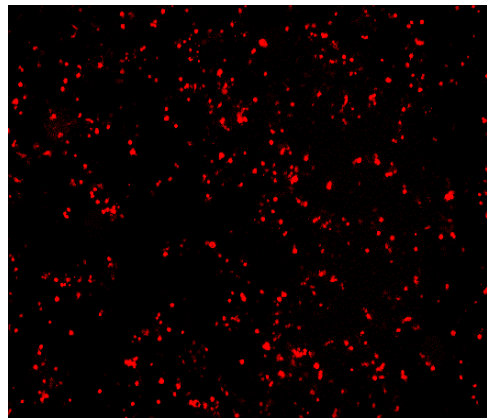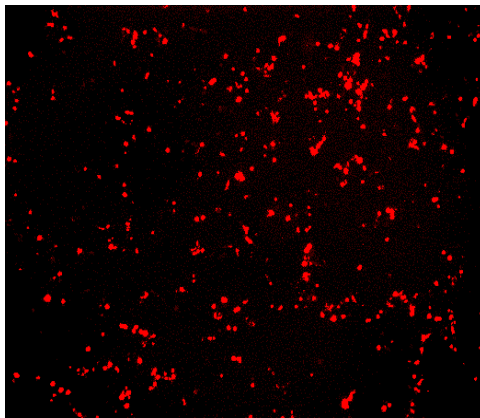
Figure 2.5: Expression and function of pAAV vectors with melanopsin wild type and CPϕ through Cre-loxP recombination. (A) Activity of Melanopsin-FLAG and CPϕ-FLAG under the control of Cre-loxP recombination demonstrated using calcium imaging (B) Expression of mRuby marker from the viral vectors in HEK293-Cre cells visualized by fluorescence microscopy. Each red fluorescent puncta represents a cell expressing mRuby.

Preparation and verification of AAV2 viruses carrying melanopsin transgene cassettes

Once the pAAV constructs were found to be functional, they were sent to Dr. Zhijian Wu's lab at NEI for preparation of viral titers. Viral titers were produced in cultured cells by co-transfection of viral vectors carrying the target genes, helper plasmids carrying the replication and packaging genes (for viral assembly), and helper adenoviruses (to improve infectivity). Viral titers were then injected bilaterally into the vitreal compartment of melanopsin (*opn4*) knockout Cre dependent mice. *Opn4$^{Cre/Cre}$* is a knock-in mouse line generated by Ecker et al. that expresses Cre recombinase in the melanopsin open reading frame (43). *Opn4$^{-/-}$* knockout mice were used in order to ensure that the melanopsin protein expressed in the animals is only derived from the heterologous source. The Cre-loxP system was used to conditionally express the trangenes in ipRGCS at the *Opn4$^{-/-}$* locus. The strategy for cloning and expressing melanopsin cassette in ipRGCs is shown in Figure 2.3. Viral vector based gene delivery methods and required materials are a kind gift from Dr. Tudor Badea at the National Institute of Health.

The viruses obtained (34) were first tested for infectivity in HEK-Cre cells. Two days post infection, HEK293-Cre cells showed mRuby expression when observed under a fluorescent microscope (Figure 2.6). HEK293 cells infected with the same viruses did not show any mRuby fluorescence. This indicates viral infectivity and specificity of transgene expression in Cre expressing cells.

AAV2(mRuby-P2A-**Melanopsin**-FLAG)   AAV2(mRuby-P2A-**MPφ**-FLAG)

HEK-cre

HEK
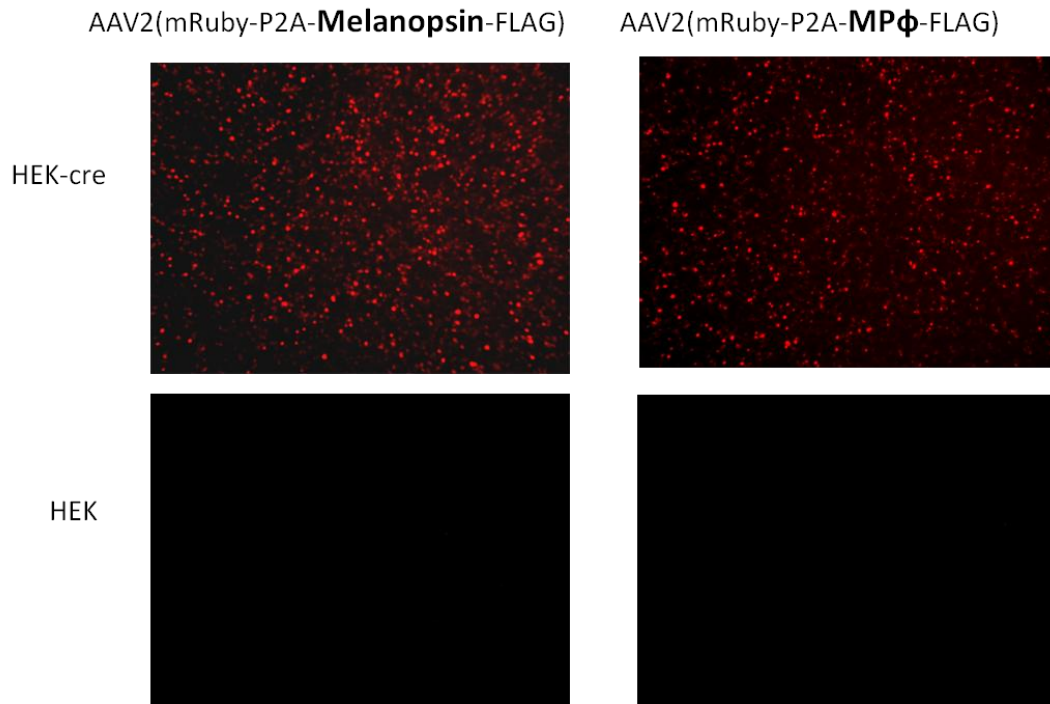
Figure 2.6: AAV2 infectivity observed in HEK-Cre cells. HEK293-Cre and HEK293 cells were infected with AAV2(mRuby-P2A-Melanopsin-FLAG) and AAV2(mRuby-P2A-CPΦ-FLAG) (5.7X10^8 vg/ml). Two days post infection, the cells were visualized using a fluorescent microscope. mRuby expression was observed in HEK-Cre cells infected with the viruses, but not in HEK cells infected with the same viruses.

The viruses were used for intravitreal injections into *Opn4$^{Cre/Cre}$* mice. Initially, both *Opn4$^{Cre/Cre}$* and *Opn4$^{Cre/+}$* mice were used for testing the infectivity of the virus. mRuby expression was used as an indicator of viral infectivity. Red

fluorescent cells expressing mRuby were observed four and five weeks after injection in the retinas of these mice with no apparent difference in infectivity between the two time points (Figure 2.7a). Four weeks after viral infection was chosen to be a suitable time point for behavioral assays (42).

Five weeks post viral infection, the mice were sacrificed and cross sections from their brain were visualized under fluorescence to observe viral infectivity in the brain targets of ipRGCs. As expected, mRuby fluorescence was observed in the Suprachiasmatic nucleus (SCN-the master circadian pacemaker) and Olivary pretectal nucleus (OPN-the center for pupillary light reflex) of the hypothalamus (Figure 2.7b). This suggests that M1 subtype of ipRGCs are transduced by the virus, as M1 is the primary subtype that innervates SCN and OPN (28).

A

B
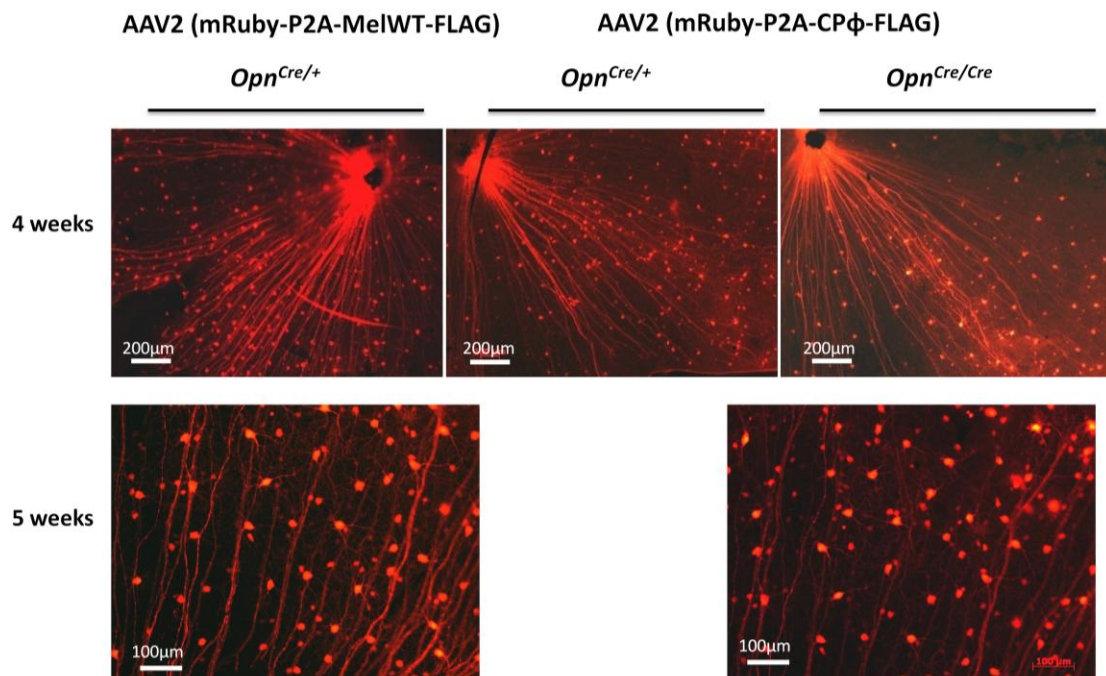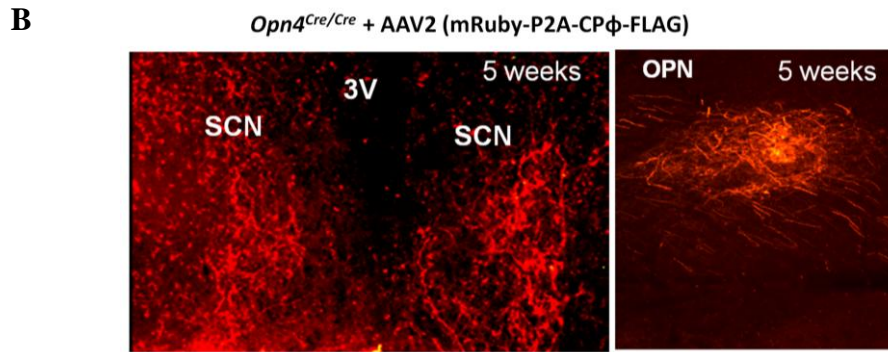
Figure 2.7: mRuby reporter gene expression in transgenic mice retinas and brain visualized by fluorescence microscopy. (A) Bilateral intravitreal injections were performed on Opn4$^{Cre/Cre}$ or Opn4$^{Cre/+}$ mice with 1μl virus per eye (titer ~10^{12} vg/ml). Animals were sacrificed 4 and 5 weeks after injection. Their retinas were dissected and whole mounts were used for fluorescence microscopy. mRuby expression was visualized at both 4 (top row) and 5 weeks (middle row) after injection with no apparent difference in infectivity between the two time points.(B) Brain sections were prepared from one of the transgenic mice to visualize infectivity in the brain at 5 weeks post injection. mRuby expression was observed in both SCN and OPN (bottom row- left and right respectively).

In order to determine if the viral infected cells express melanopsin, immunostaining was carried out using anti-melanopsin N-terminus antibody. Immunostained retinas from both AAV2(mRuby-P2A-Melanopsin-FLAG) and AAV2(mRuby-P2A-CPΦ-FLAG) infected mice showed colocalization of melanopsin and reporter gene mRuby in the same cells, with melanopsin expression visible on the plasma membrane and mRuby in the cytoplasm of ipRGCs (Figure 2.8A-E).
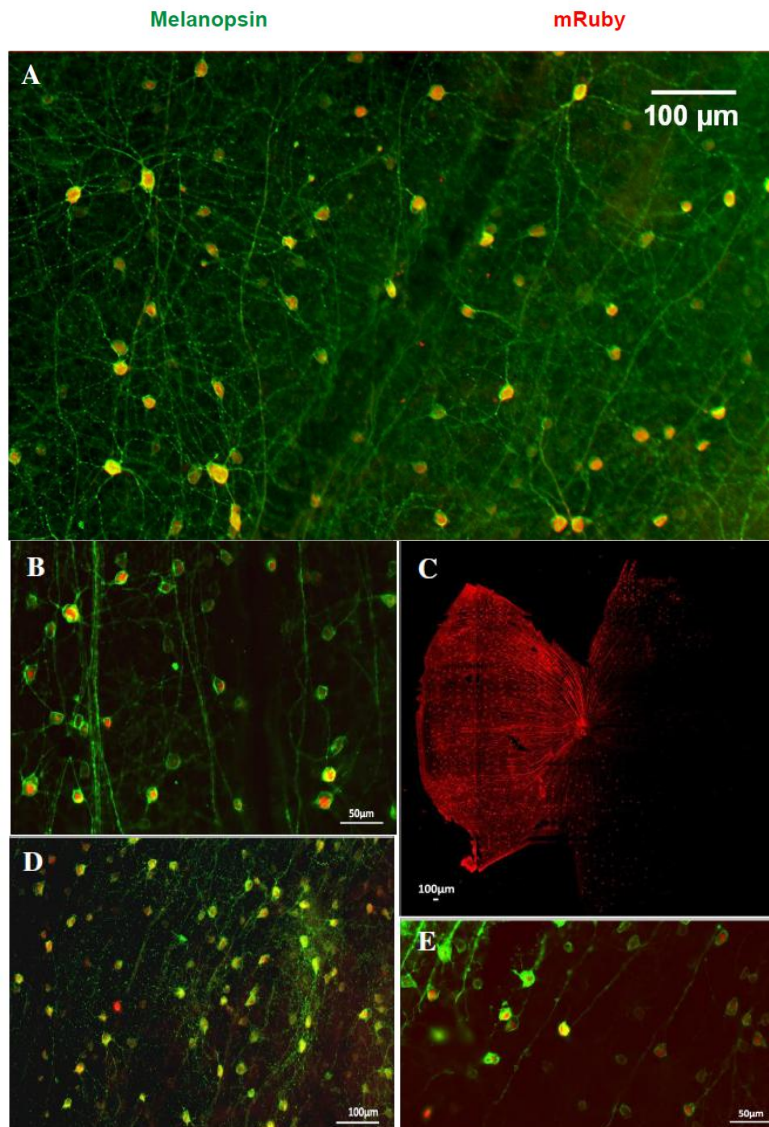
Figure 2.8: Viral infectivity and co-localization of mRuby and melanopsin in the retina. *4 weeks after intravitreal injection with either AAV2(mRuby-P2A-Melanopsin-FLAG) (A)(C) or AAV2(mRuby-P2A-C-Phosphonull melanopsin-FLAG) (B)(D)(E), the retinas were harvested and immunostained with rabbit anti-melanopsin antibody or imaged directly without immunostaining. Fluorescent images from 5 different retinas depict anti-melanopsin staining on the plasma membrane of ipRGCs in (A)(B)(D) and (D) and mRuby in the cytoplasm (A-E). All infected cells in the field showed co-localization of mRuby and melanopsin in the same cells.*

Discussion

Described here is an AAV2 mediated transduction approach to easily express wildtype melanopsin or its mutant form in mouse models, which is a far more facile approach to studying genetic mutations in whole organisms compared to conventional generation of transgenic mouse models due to its speed and flexibility as discussed earlier. In our system, AAV2 transduces ipRGCs efficiently, and the presence of a quantitative visual marker mRuby facilitates easy visualization of viral infectivity. This strategy in combination with the $Opn4^{Cre/Cre}$ transgenic mouse line opens up opportunities to create mutations in other ipRGC specific genes to study their physiological and behavioral roles. Despite the convenience of this approach, there are certain shortcomings to this strategy- 1. Intravitreal delivery of the virus allows little control over the spread of viral infectivity in the retina. Through the intravitreal route, the first cells encountered by the virus are the ganglion cells, which are the target cell type. However, the reach or spread of infectivity over the retina can differ between injections, possibly leading to variation in expression levels of transgenes between animals. Further experiments are needed to determine efficiency of transduction in each animal and to correlate percentage of transduction with observed behavioral phenotype 2. It is unknown whether AAV2 preferentially transduces certain ipRGC subtypes. From data shown in figure 2.7, it is likely that M1 subtype of ipRGCs are transduced. However, incomplete innervation of the SCN in this data suggests that not all M1cells may have been transduced by the virus. Subtype-specific markers may be needed to determine whether each known subtype of ipRGC has been transduced. 3. It is not evident whether the level of expression of exogenously

expressed melanopsin (mutant or wildtype) reflects endogenous wild type like expression levels. Western blot analysis may be needed to determine melanopsin protein expression levels in retinas of virally modified mice. The caveat to this experiment is the difficulty to determine melanopsin expression level from a single retina using a western blot. Since ipRGCs represent only about 1-2% of the ganglion cell population, the level of expression of melanopsin protein in one retina is expected to be low.

Regardless of these shortcomings, AAV2 viral approach of generating genetically modified mice offers a low cost, time efficient and easy technique to quickly create mutations in a gene of interest. This may be especially useful when one intends to screen a series of mutations individually in a gene of interest. Generating and screening a transgenic mouse for each mutant can be very laborious and time intensive as compared to generating viral vectors for each of these mutants and quickly injecting a batch of mice. This approach can also be useful for a preliminary screen of putative mutants, before moving onto further analysis using a conventional transgenic approach.

Chapter 3:

C-terminal phosphorylation of melanopsin regulates the kinetics of a subset of melanopsin-mediated behaviors in mice

(Work described in this chapter was recently published in the Proceedings of National Academy of Sciences -

Somasundaram, P., Wyrick, G.R., Fernandez, D., Ghahari, A., Pinhal, C.M., Simmonds-Richardson, M., Rupp, A.C., Cui, L., Wu, Z., Brown, R.L., Badea, T.C., Hattar, S Robinson, P.R. (2017) C-terminal phosphorylation regulates the kinetics of a subset of melanopsin-mediated behaviors in mice. *Proc Natl Acad Sci U S A. 114, 2741-2746.)*

Introduction

The mammalian retina uses light for both image forming and non-image forming vision. Non-image forming vision involves the conversion of ambient light into chemical and electrical signals that regulate physiological functions such as the entrainment of the circadian clock, regulation of pupil size, sleep and mood. Melanopsin is a visual pigment, expressed in intrinsically photosensitive retinal ganglion cells (ipRGCs) of the mammalian retina and plays a major role in non-image forming vision (8, 9). Like all other opsins, melanopsin belongs to the G-protein Coupled Receptor (GPCR) super-family of membrane proteins (3, 11).

Melanopsin-expressing ipRGCs show a sluggish and sustained response to light, unlike the light response of rods and cones which show a rapid onset and decay of light evoked responses (39) . This sluggish response of ipRGCs could be attributed to the low level of expression of melanopsin in these photoreceptors compared to the expression of rhodopsin and cone opsins in traditional photoreceptors. Melanopsin's activity and the phototransduction cascade have a direct influence on ipRGCs' photoresponse.

Recent studies indicate that melanopsin activity can be regulated through phosphorylation by kinases, one of which is a G-protein coupled receptor kinase (GRK) (14, 17). The predicted structure of melanopsin also suggests that it is regulated by GRK activity. The secondary structure of melanopsin is predicted to have a short N-terminal extracellular region, seven transmembrane domains and a characteristically long cytoplasmic tail (3). The presence of a long cytoplasmic tail suggests that the protein is subjected to high levels of regulation. Supporting this idea,

mouse melanopsin is predicted to have 38 serines and threonines in its long cytoplasmic tail that are potential sites for phosphorylation by a GRK (19). GRK-mediated phosphorylation has been implicated in the deactivation of melanopsin signaling *in vitro* (17). Blasic et al. also showed that a light dependent phosphorylation of melanopsin by GRK occurs in the mouse retina *in vitro*. Although GRK-mediated regulation has been demonstrated *in vitro*, the physiological role played by this protein modification *in vivo* is not well characterized.

Recently, Sexton et al. investigated the role of GRK2 in regulation of melanopsin activity and found that the contribution of GRK2 to deactivation of melanopsin was minor . However, their study did not probe other GRKs expressed in ipRGCs (40). Another recent work by Mure et al. explored the role of melanopsin C-terminal phosphorylation on physiology and behavior, but their study was limited to specific subsets of putative phosphorylation sites on the C-terminus (41).

We hypothesized that GRK-mediated melanopsin phosphorylation *in vivo* is crucial in controlling the lifetime of the active protein and contributes to termination of the light-evoked ipRGC response. In order to understand and establish the *in vivo* implications of this regulation we generated melanopsin C-terminal phosphorylation-deficient transgenic mice using an AAV2-mediated transduction approach. Here we utilized a phosphorylation mutant of melanopsin called CPΦ (C-terminal phosphonull mutant -mutation of all serines and threonines in C-tail to alanines, (Figure 2.8)**,** which completely lacks any C-terminal phosphorylatable residues, to test the role of C-tail phosphorylation in three melanopsin-mediated behaviors in mice. *In vitro* data suggest that a set of six

phosphorylation sites involving serines and threonines in the C-terminus of melanopsin (T388, S389, S391, S392, S394, S395) are necessary for phosphorylation dependent deactivation(19). This region was characterized as an important phosphorylation domain for melanopsin deactivation. However, there is no evidence to eliminate the possibility that other sites may be phosphorylated *in vivo*. We do not know the number and identity of the residues that are actually phosphorylated *in vivo* in a light-dependent manner. Hence, in our *in vivo* experiments we used the CPΦ mutant, which completely lacks all possible GRK phosphorylation sites on the C-terminus.

Here we show that eliminating all the C-terminal GRK putative phosphorylation sites results in a sustained pupil constriction following a high-intensity light stimulation, indicating that C-terminal phosphorylation sites are crucial for a normal pupillary light reflex. This effect is also observed at the physiological level of ipRGCs, where CPΦ ipRGCs fire action potentials for an extended period of time to a 5s blue light stimulus in both single cell and multielectrode array recordings. In addition, we provide evidence that deactivation of melanopsin directly influences the adaptation to phase-delay. Finally, we demonstrate that exogenous expression of either wild type or CPΦ melanopsin in melanopsin knockout mice (MKOs) ipRGCs results in the rescue of the negative masking deficit that is characteristic of MKOs.

Materials and methods

Animals

All animal used for behavior were male $Opn4^{Cre/Cre}$ on a mixed BL/6;129SvJ background and were between one and two months of age at the start of the behavioral experiments. All protocols were in accordance with Johns Hopkins University Animal Care and Use Committee (IACUC) guidelines. Animals were individually housed in plastic cages with steel wheels and were kept in light-tight boxes on a light-dark protocol of 16 hours of light and 8 hours of dark (16:8 LD) with 500 lux overhead white light. Food and water were made available *ad libitum*. Behavioral experiments were initially conducted for ~ 30 days, followed by viral injection, four weeks of post-injection recovery for expression of virally-encoded proteins (42), and ~ 30 days of post-injection behavioral studies. Animals were euthanized after post-injection behavioral studies to obtain retinas for immunofluorescent verification of melanopsin expression.

Virus

AAV2 (mRuby-P2A-Melanopsin-FLAG) with a viral titer = $5x10^{12}$vg/ml and AAV2 (mRuby-P2A-C-terminus phosphonull-FLAG) with a viral titer=$2.5x10^{12}$vg/ml were prepared by the Wu lab, Ocular Gene Therapy Core, National Eye Institute, NIH (42) (see Fig 2.3).

Intravitreal viral injections

Mice were anesthetized by intraperitoneal injection with 0.5 ml avertin (20 mg/ml; volume was adjusted based on body weight of the mice). 1 µl of AAV2(mRuby-P2A-

Melanopsin-FLAG) or AAV2(mRuby-P2A-C-terminus phosphonull-FLAG) was dispensed onto a strip of parafilm. The viral preparation was then drawn up into a micropipette (Sigma, P0674) connected to the hose of a pico-injector (Harvard apparatus, Model PLI-90), which in turn was connected to a compressed-nitrogen gas tank. Injection pressure was maintained at 30 psi using a regulator. The anesthetized animal was placed under a dissection microscope and forceps was used to open the eyelids and expose the eye. The eye was punctured by the injection needle near the ora serrata, aiming the tip towards the center of the eyeball. Depression of the footswitch created a surge of pressure to deliver the viral preparation from the microcapillary tube into the vitreous. After injection, the animals were kept warm to allow them to recover from the injection and wake up. They were then returned to their cages in the same setting.

Immunofluorescence

Mice were euthanized by cervical dislocation after intraperitoneal injection with 1 ml avertin (20 mg/ml). The eyes were removed and initially fixed whole in 4% paraformaldehyde for 30 min. The cornea was then removed, and the eyecup with exposed retina was fixed in 4% paraformaldehyde for an additional hour. The eyecups were washed thrice with 1X PBS for each of the wash steps before application of blocking buffer (0.3% triton, 4% goat serum), primary antibody, and secondary antibody. Immunofluorescence was performed by using rabbit anti-melanopsin (1:1000; Advanced Targeting Systems AB-N38) as primary antibody with a two day incubation period, followed by goat anti-rabbit – IgG 488 (1:1000; Life Technologies A11008) as secondary. After immunostaining, the retinas were

mounted and imaged using Zeiss Axioimager M1 microscope. The images were processed in ImageJ (NIH).

Pupillometry

All animals used for all PLR experiments were dark adapted for 1 hour prior to the experiment. Animals were manually restrained, and the left eye was exposed to a 30 s stimulus of high-intensity blue light using an LED bulb (Superbright LEDs). Light intensity was attenuated using neutral density filters (474 nm; Intensities used were ~$1x10^9$, ~$5.5x10^{11}$, ~$2.8x10^{12}$, ~10^{15} and ~$1.4x10^{15}$ photons cm^{-2} s^{-1}). The consensual PLR was recorded from the contralateral eye using a SONY Handycam (DCR-HC96). Video recordings were analyzed by generating screenshots of the video in Windows Media Player every 5 seconds. The pupil area was measured using the circular selection and measure tools in ImageJ software (NIH). PLR recordings and measurements were conducted identically for pre- and post-injection measurements. The length of each recording from this type of measurement was ~2 min.

A second type of PLR recording was conducted by restraining the mice using a headpost as described in Cahill et al., 2008 (32). In this method, all experimental procedures involving the stimulus protocol and video recording were similar to the method using manual restrainment. The variations were the use of the headpost, the duration of the recording and the method of analyses. In the headmount PLR experiment, the duration of each recording was 45 min. To analyze each recording, screenshots were generated every 5s for the first ~2 minutes of the video recordings and for every 1 minute for the remainder of the recordings (to reduce data points for easier handling of data).

PLR decay half-times were calculated by fitting a single exponential curve to the dilation phase of the PLR data from the headmount restraint PLR experiments and extracting half-times using the in-built function in GraphPad Prism 6 software (Figure 3.4D). The Y_o value (Y-axis initial value) was constrained to the mean pupil size in each group at T33(time of light OFF) and K-value was constrained to >0.

Wheel running activity

Animals were single housed in 16:8 LD (500 lux white) in cages with 4.5-inch steel running wheels. The wheel running activity was continuously monitored in 10 min bins using the VitalView software (Mini Mitter). The light-dark cycle was controlled using a timer connected to the light-tight box in which the cages were kept.

Jet-lag paradigm

$Opn4^{Cre/Cre}$ mice were kept in 16:8 LD cycle (light-dark cycle) for ~ 2 weeks, followed by a 6 hours phase-delay, mimicking the jet-lag experienced in a West-bound trans-Atlantic flight. The animals were allowed to photo-entrain to this shifted light cycle. The average activity offset of the animals during the stable part of their actograms (after phase-delay) was calculated. The number of days taken to reach that average offset was noted and this yielded the value for number of days to entrain to phase-delay. This procedure was repeated in the same mice 4 weeks after viral injection for comparison and a before and after comparison analysis was drawn. Percent reduction in number of days taken to shift activity to delayed light cycle was calculated as

$$\left(\left(\frac{\# \, days \, taken \, to \, shift \, activity \, before \, injection - \# \, days \, taken \, to \, shift \, activity \, after \, injection}{\# \, days \, taken \, to \, shift \, activity \, before \, injection}\right) * 100\right)$$

Masking

Opn4$^{Cre/Cre}$ mice kept in 16:8 LD cycle after the phase-delay analysis were subjected to a three hour light pulse (500 lux white) two hours after the onset of subjective night (ZT 14) on one specific day. The wheel running activities recorded in 10-min bouts on the day before and day of three hour light pulse was calculated. The normalized activity before, during and after this three hour light pulse was calculated over a time window of 5 hours (ZT13 to ZT18). This experiment was repeated in the same mice four weeks after viral injection, and a before-after comparison analysis was made.

Phase angle of entrainment

The average onset of activity of each group of animals was measured over a period of ten days in the stable part of their actograms. The deviation of average onset from the time of dark onset was calculated and plotted for each animal in a 12-hour clock format.

Results

Carboxy -terminal serines and threonines of mouse melanopsin play a crucial role in PLR kinetics

We hypothesized that G-protein coupled receptor kinase (GRK)-mediated C-terminal phosphorylation of mouse melanopsin is involved in deactivation of the receptor *in vivo,* and this deactivation determines the lifetime of active melanopsin. In order to test this hypothesis, we utilized a mutant melanopsin (CPφ or C-phosphonull, Figure 3.1) with all 38 putative C-terminal GRK phosphorylation sites (serines and threonines) mutated to alanines. This mutant was generated earlier by Blasic et al. and

shown to exhibit delayed deactivation kinetics in an *in vitro* calcium imaging assay (17, 19). A floxed melanopsin wild type gene and the CPΦ constructs, both with a C-terminal FLAG tag and N-terminal mRuby-P2A tag were cloned into pAAV (adeno-associated viral vector) (Figure 2.7, Chapter 2). mRuby is a red fluorescent protein that acts as a quantitative visual marker of cells expressing melanopsin (37). P2A is a viral peptide that will allow the expression of melanopsin fusion construct into a bi-cistronic transcript and will self-cleave during translation to generate two peptides (Melanopsin-FLAG and mRuby) of equimolar proportions (38). The viral vectors were tested for functionality and then packaged into AAV2 capsids (as discussed in Chapter 2). AAV serotype 2 has been extensively examined and exhibits tropism for neuronal cells in addition to a few other cell types (34).

After functionality tests, our construct in AAV2 was then used for bilateral intravitreal injections into $Opn4^{Cre/Cre}$ mice. $Opn4^{Cre/Cre}$ is a knock-in mouse line generated by Ecker et al. that expresses Cre recombinase in the melanopsin open reading frame (43). mRuby expression was used as an indicator of viral infectivity. Red fluorescent ganglion cells expressing mRuby in their axons and soma were observed four weeks after injection in the retinas of the mice, colocalized with melanopsin. four weeks after viral infection was chosen to be a suitable time point for behavioral assays (42). $Opn4^{Cre/Cre}$ mice aged between one and two months at the start of the experiments were used. The mice were tested for behavior before and after viral injections. Initially, the pupillary light reflex (PLR) of the mice in response to a high intensity blue light stimulus was tested, and then the mice were individually housed in cages with wheels. The circadian behavior of these mice were tested by

75

monitoring their wheel running activity in 16:8 LD cycle for ~30 days, before they were subjected to viral injection. The 16:8 LD cycle was chosen because unpublished data from Dr. Hattar's lab suggest that $Opn4^{Cre/Cre}$ mice exhibit phenotypic changes in circadian behavior in this lighting condition (Personal communication from Melissa Simmonds). Bilateral intravitreal injections were performed with either AAV2(mRuby-P2A-Melanopsin-FLAG) or AAV2(mRuby-P2A-CPΦ-FLAG).. The animals were returned to the same cages with wheels after injection. Four weeks post injection, PLR and circadian behavior analyses were repeated in the same conditions as done before injections.
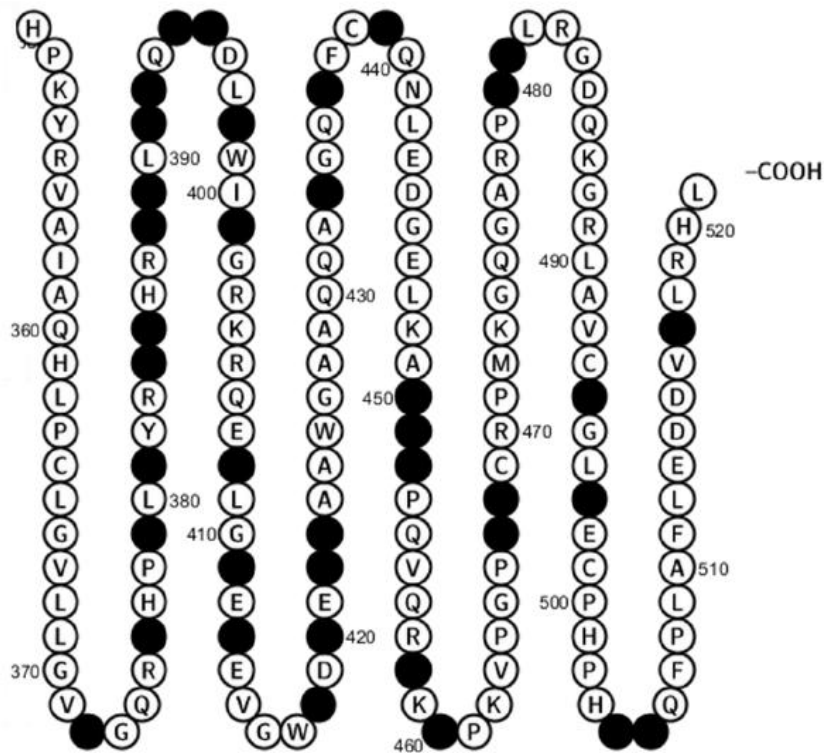
Figure 3.1: Melanopsin CPϕ construct used for the generation of Cre-dependent cell type specific viral expression system. *Graphic representation of the C-terminus*

of CPϕ mouse melanopsin indicating all the serines and threonines that were mutated to alanines (black solid circles), generated using Protter visualization platforms software.

$Opn4^{Cre/Cre}$ mice were tested for behavior (pupillary light reflex, phase-delay, and masking) before injection and four weeks post viral injection, and a comparison of pre and post injection behaviors was drawn. The PLR for mice injected with AAV2(WT melanopsin) showed no difference in kinetics before and after injections (Figure 3.2B). $Opn4^{Cre/Cre}$ mice before injection with AAV2(WT melanopsin) or AAV2(CPΦ) exhibited a mean maximum pupil constriction of 21.1% and 20.6% of the baseline pupil area respectively in response to a high-intensity blue light stimulus placed close to the contralateral eye (Figure 3.2A and 9B). $Opn4^{Cre/Cre}$ mice after injection individually with AAV2(WT melanopsin) or AAV2(CPΦ) exhibited a mean maximum relative pupil constriction of 22.6% and 19.5% respectively. After the stimulus was turned OFF, $Opn4^{Cre/Cre}$ and $Opn4^{Cre/Cre}$ +AAV2(WT melanopsin) showed dilation of pupils almost immediately, whereas $Opn4^{Cre/Cre}$ +AAV2(CPΦ) mice sustained constriction of their pupils until the recording was terminated at 90s (Figure 3.2B). The PLR for mice injected with AAV2(CPΦ) showed a distinct difference in kinetics before and after injections. The CPΦ mice showed no dilation of their pupils in the first 1 min recorded after the stimulus was turned OFF (Figure 3.2A). This phenotypic difference in PLR before and after injections was observable in each mice injected with AAV2(CPΦ) (Figure 3.3). This result suggests that melanopsin is active for a longer duration in these animals than wild type and is driving this prolonged constriction.

In order to determine the time duration for CPΦ mice to dilate their pupils after a bright light exposure, a second PLR experiment was conducted where the mice were manually restrained for a longer duration (two minutes; the longest that they could be held steadily for recording). After the 30s light stimulus, the CPΦ mice sustained constriction of their pupils for as long as the recording was done (120s) and did not start dilating their pupils (Figure 3.2A top and bottom). The mean relative pupil area between 33s and 118s (time frame between stimulus OFF and the end of initial recording) was between 27.7% and 44.3%. Within this time frame, no individual pupil size at any specific time point exceeded 56%.
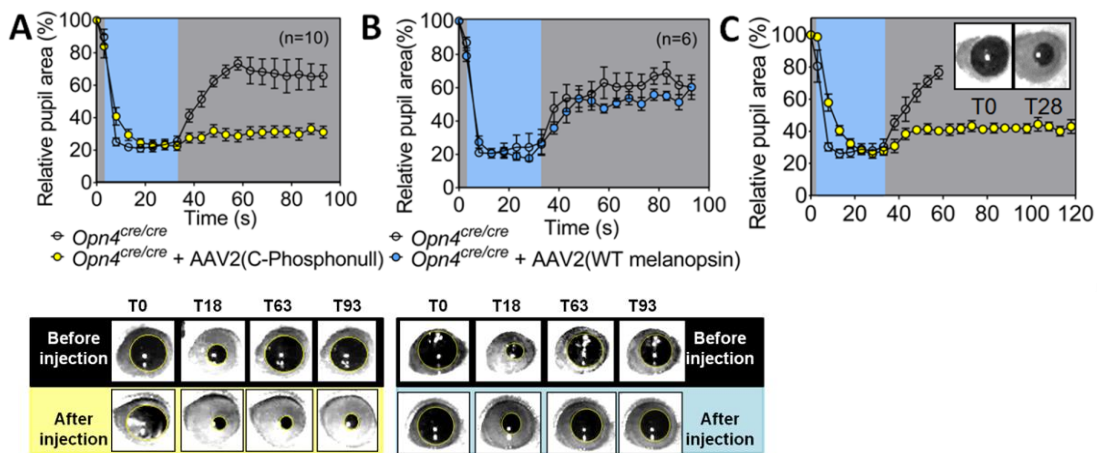
Figure 3.2: Expression of phosphonull melanopsin in MKO (Opn4Cre/Cre) mice causes prolonged pupillary constriction. A comparison of the relative pupil area vs time after light exposure between (A-Top) MKO (Opn4$^{Cre/Cre}$) mice and MKO (Opn4$^{Cre/Cre}$) mice injected with an AAV virus with the gene for mouse melanopsin where all the serines and threonines in the Carboxy tail have been mutated to alanines (C-phosphonull; AAV2(mRuby-P2A-CPφ-FLAG), and B-Top) MKO (Opn4$^{Cre/Cre}$) mice and MKO (Opn4$^{Cre/Cre}$) mice injected with a virus containing a

*gene for the wild type long form of mouse melanopsin (AAV2(mRuby-P2A-Melanopsin-FLAG); reveals that phosphonull mice (yellow circles; n=10) exhibit prolonged pupil constriction to a high intensity blue light stimulus (~10^{15} photons cm^{-2} s^{-1}), while MKO mice (open circles; n=10+6) and MKO mice injected with a virus expressing wild type melanopsin (blue circles; n=6) dilate their pupils normally after the light stimulus is turned OFF. PLR images at four specific time points during the experiment from a representative mouse (**A-Bottom**) before and after injection with the viral phosphonull melanopsin construct , and (**B-Bottom**) before and after injection with the viral wild type melanopsin construct. (**C**) Time course for mice injected with the phosphonull viral construct (yellow circles; n=4) to dilate their pupils in comparison to MKOs mice (open circles; n=4) after 30s of a high intensity blue light stimulus (~1.4×10^{15} photons cm^{-2} s^{-1}), recorded by manually restraining the mice. Statistical analyses conducted for before-after comparisons in (**A**) and (**B**) were linear mixed effect models. Statistical comparisons were conducted between Opn4$^{Cre/Cre}$ and Opn4$^{Cre/Cre}$+AAV2(mRuby-P2A-Melanopsin-FLAG) (ns,p=0.209) , and between Opn4$^{Cre/Cre}$ and Opn4$^{Cre/Cre}$+AAV2(mRuby-P2A-C-terminus phosphonull-FLAG) (****, p≤0.0001). (Mice were manually restrained)*
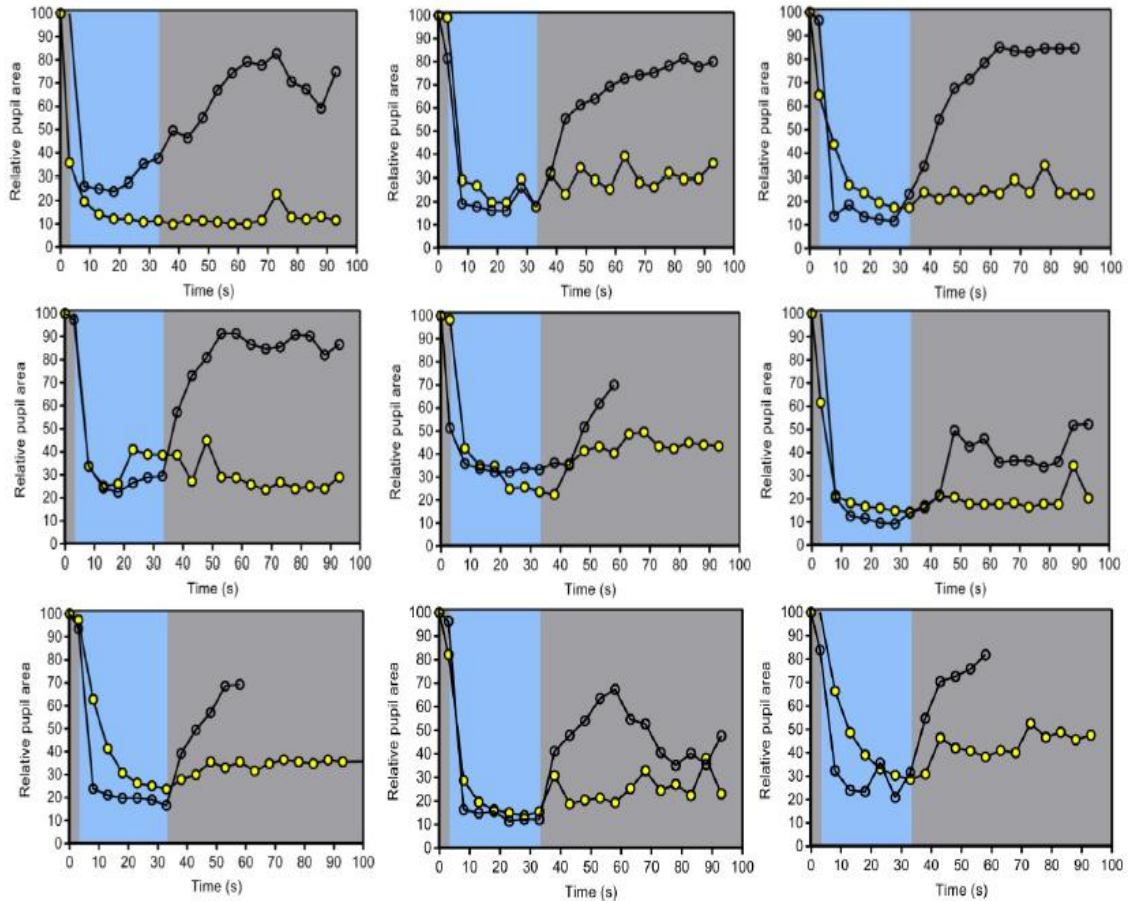
Figure 3.3: CPϕ animals show prolonged pupil constriction to high intensity blue stimulus. *Individual PLR responses from 9 animals before injection (Opn4^{cre/cre}-open circles) and after injection (Opn4^{cre/cre} +AAV2(CPΦ) - yellow circles) demonstrate that individual animals show a prolonged pupil constriction to a high intensity blue light stimulus.(Mice were manually restrained)*

In order to examine the full time-course of pupil dilation in mice expressing the C-terminus phosphonull melanopsin, we used a head mount setup to record the PLR for up to 45 minutes. The maximum constriction of melanopsin knockout animals was attenuated compared to WT as shown previously (19), whereas the C-terminal phosphonull animals showed similar maximum response to those observed

in WT animals (Figure 3.4A). Differences in these animals, however, were observed in the pupil dilation phase. Specifically, melanopsin KO mice and those expressing WT melanopsin exhibited pupil dilation half-time of approximately 6 and 4.6 seconds respectively (Figure 3.4A, C and D). In contrast, the pupil of the C-terminus phosphonull mice remained constricted 100-times longer, with a dilation half-time of ~9.4 minutes (Figure 3.4A, C and D). This reveals that C-terminal phosphorylation of mouse melanopsin is important for its deactivation on a timescale of seconds, and other deactivation mechanisms come into play at later times.

Group	PLR decay half time ($T_{1/2}$)	~T0.55	~T0.63	~T0.65	~T9.98
		(From graph above)			
$Opn4^{cre/cre}$	4.6s				----
$Opn4^{+/+}$	6s				----
$Opn4^{cre/cre}$ +AAV2 (C-Pφ)	565.6s (9.43min)				

81
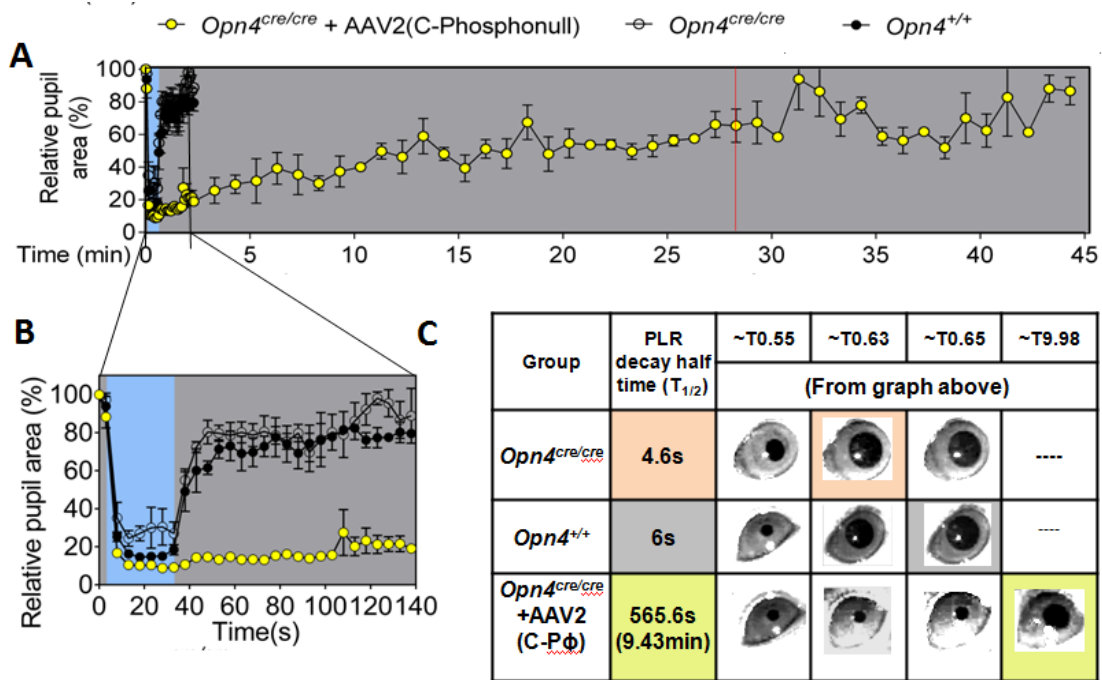
D
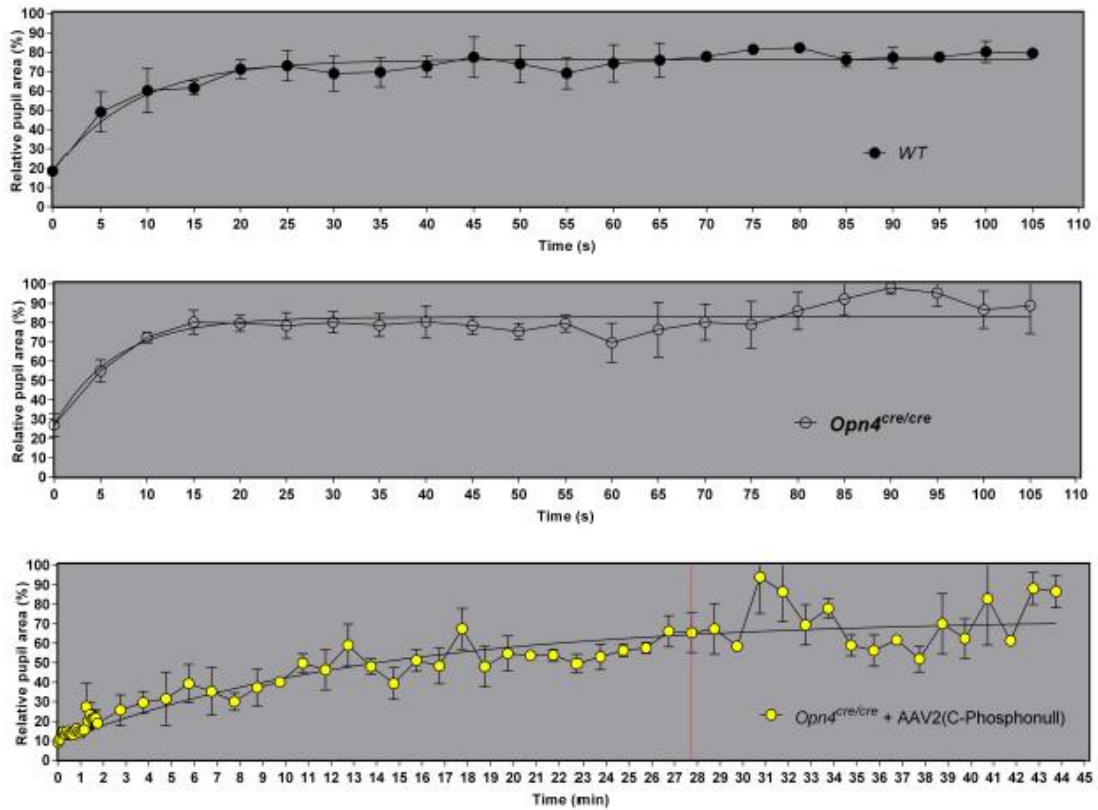
Figure 3.4:Viral phosphonull melanopsin causes prolonged pupil constriction (A)(B)Time course for mice injected with the phosphonull viral construct (yellow circles; n=3) to dilate their pupils in comparison to MKOs mice (open circles; n=3) and wildtype Opn4$^{+/+}$ mice (black solid circles; n=3) after 30s of a high intensity blue light stimulus (~1.4x10^{15} photons cm^{-2} s^{-1}), recorded by restraining the mice using a headmount. The red line indicates time point until which data are means from three animals. Beyond red line data shown are from two animals. (C) Table showing half-time calculations for PLR decay of three genotypes - MKO(top), Wildtype(middle) and Opn4$^{Cre/Cre}$+AAV2(mRuby-P2A-C-terminus phosphonull-FLAG)(bottom). Representative pupil images for each of the indicated time points are shown.

Statistical analyses conducted in (A) and (B) was Krustal-Wallis test with Dunn's multiple comparisons. Statistical comparisons were conducted between Opn4^{+/+} and Opn4^{Cre/Cre}+AAV2(mRuby-P2A-C-terminus phosphonull-FLAG) (**), between Opn4^{Cre/Cre} and Opn4^{Cre/Cre}+AAV2(mRuby-P2A-C-terminus phosphonull-FLAG) (****) and between Opn4^{+/+} and Opn4^{Cre/Cre} (ns). (D) Single exponential curve fits of the dilation phases of the PLR for Opn4^{+//+} (top) , Opn4^{cre/cre} (middle) and Opn4^{cre/cre} +AAV2(CPΦ) (bottom) for the extraction of PLR decay half-times.

Melanopsin knockout mice are known to exhibit a deficit in the pupillary light reflex behavior at high irradiance levels of >12.5 log photons cm^{-2} s^{-1} (9, 44). We hypothesized that the CPΦ PLR deficit will be specific to high light intensities. To determine if the longer pupil dilation times are specific to melanopsin-based phototransduction and not rod/cone input (76, 77), we measured the PLR at 4 different light intensities to generate intensity response curves. As predicted, the dilation phase of the PLR did not show any difference between *Opn4^{Cre/Cre}* +AAV2(C-terminus phosphonull) and *Opn4^{Cre/Cre}* at low light intensities where the PLR is driven by rod/cone input (Figure 3.5) (76, 77). At intensities > 15 log (photons cm^{-2} s^{-1}), however, which is known to activate melanopsin-based phototransduction (77, 78), the curve for *Opn4^{Cre/Cre}* +AAV2(C-terminus phosphonull) deviated from *Opn4^{Cre/Cre}* and WT animals (Figure 3.5). This result strongly suggests that GRK-based shutoff of melanopsin-based phototransduction through C-terminal phosphorylation is important for the proper kinetic regulation of the PLR.

A — *Opn4$^{cre/cre}$* + AAV2(C-Phosphonull)

Legend:
- 1.07E+09 photons cm^{-2} s^{-1}
- 5.47E+11 photons cm^{-2} s^{-1}
- 2.8E+12 photons cm^{-2} s^{-1}
- 1.43E+15 photons cm^{-2} s^{-1}

B — *Opn4$^{+/+}$*

Legend:
- 1.07E+09 photons cm^{-2} s^{-1}
- 5.47E+11 photons cm^{-2} s^{-1}
- 2.8E+12 photons cm^{-2} s^{-1}
- 1.43E+15 photons cm^{-2} s^{-1}

C Opn4$^{cre/cre}$
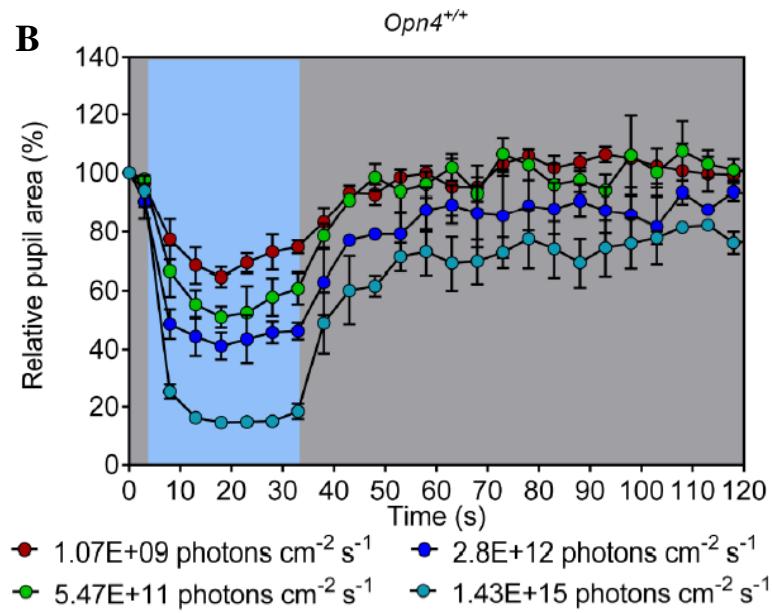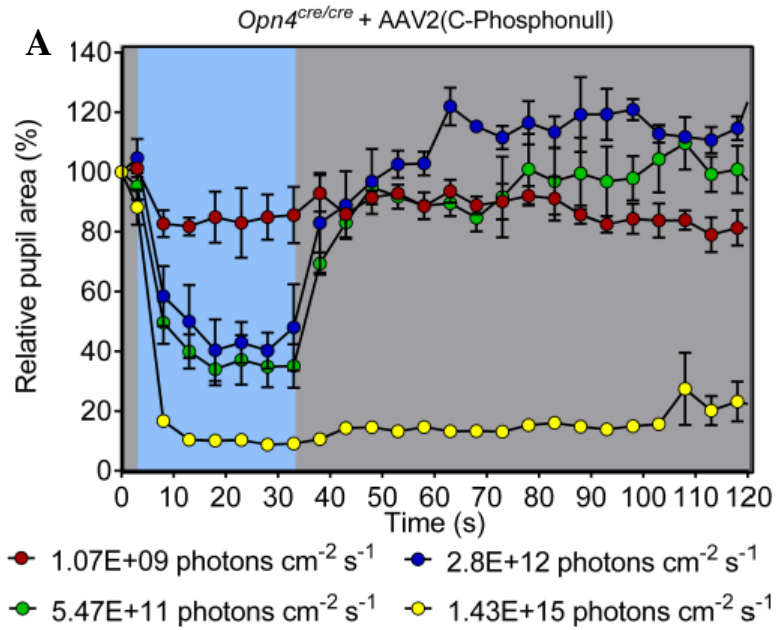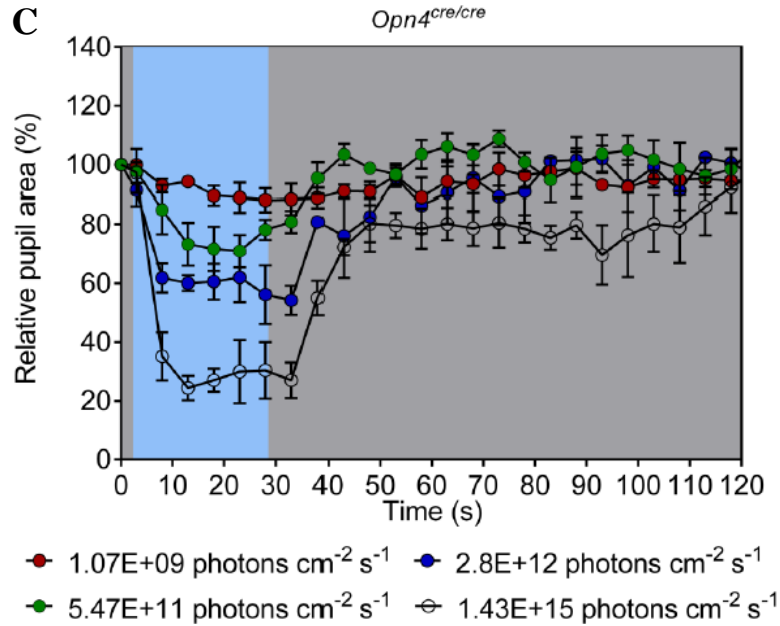
Figure 3.5: CPφ PLR dilation deficit is due to melanopsin phototransduction and not rod/cone input. Intensity response curves for (**A**) MKO mice injected with the C-terminal phosphonull construct (n=3), (**B**) wildtype, and (**C**) MKO recorded using four different blue light intensities by restraining the mice using a headmount. (Mice were restrained using a headpost)

C-terminal phosphorylation of mouse melanopsin is crucial for the proper shutoff of ipRGC photoresponse

To determine if the longer constriction of the PLR is due to a prolonged light response in the ipRGCs, single cell (conducted by Dr. Lane Brown) and multielectrode array (MEA) recordings were carried out from ipRGCs expressing WT and virally-encoded phosphonull melanopsin. The sensitivity and duration of the WT melanopsin-based light response was consistent with light responses previously reported for endogenous melanopsin (78, 79). A 5-sec stimulus of 480 nm light (1 x

10^{15} photons cm^{-1} sec^{-1}) elicited a light-dependent increase in spiking activity (up to 25 Hz) in 18 out of 21 mRuby-expressing cells, which typically terminated in < 1 min ($t_{1/2}$ = 22 sec post-peak, with 90 % recovery in 52 sec) (Figure 3.7A-B). In contrast, light responses were much more difficult to detect in ipRGCs expressing the melanopsin C-terminus phosphonull. In all, only five cells of > 50 cells that were recorded exhibited a detectable intrinsic light response. The light response in these cells, however, was dramatically prolonged compared to those expressing WT melanopsin, showing robust spiking activity persisting for at least for 15 minutes after the cessation of the light stimulus (Figure 3.7A-B). In a single cell that remained viable for an extended duration, the firing rate eventually returned to near baseline after more than 20 min. For all of these cells, the light response onset was more sluggish than that seen in ipRGCs expressing WT melanopsin, often taking > 5 min to reach peak firing rate (Figure 3.7B). The peakfiring rate was also depressed compared to the peak firing rate of ipRGCs expressing WT melanopsin (Figure 3.7B).

In the MEA recordings, ipRGCs expressing WT and phosphonull melanopsin were detected in approximately equal numbers (about 5 % of all identified cells), and typically several ipRGCs were detected in each retinal preparation. For the MEA from wild type animals, the majority of ipRGCs shut off within 50 sec after the light stimulation (Figure 3.6A, C and E). In contrast, for the phosphonull, ipRGC responses persist for at least 4.5 mins, the longest recording time achieved (Figure 3.6B, D and E). Together, these results show that the persistent light response in ipRGCs is consistent with the persistent response of the PLR in darkness.
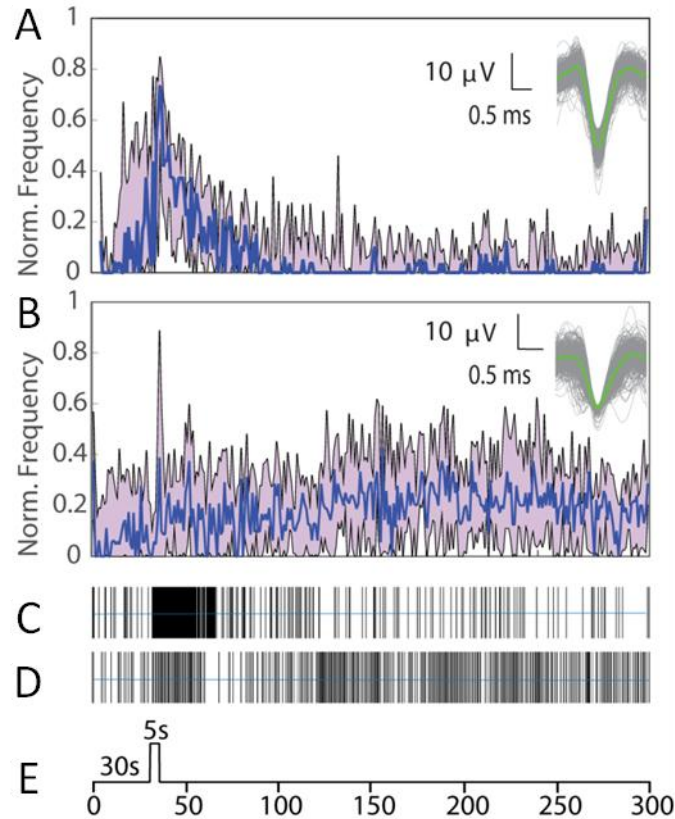
Figure 3.6: Light responses of ipRGCs expressing phosphonull melanopsin are dramatically prolonged. (A-E) MEA recordings of retinas from WT (A,C) or Opn4$^{Cre/Cre}$+AAV2(mRuby-P2A-C-terminus phosphonull-FLAG) (B,D) mice, under conditions of complete synaptic block (methods). (A, C) Normalized frequency response curves to a 5 second blue light pulse (digitized trace in I) of 9 (A, WT) and 11 (B, Pnull) ipRGCs which preserved light responsiveness under pharmacologic synaptic block. Data is represented as median (blue curve), and 25 % - 75 % interquartile interval (purple area). Data was binned to 1 second bins and normalized to the maximum firing frequency for each cell (maximum frequency ranged from 8 to 39 Hz for WT and 10 – 48 Hz for ipRGCs). Note that both WT and Pnull ipRGCs respond to light stimulation with increased firing. However WT ipRGCs return to baseline at about 60 seconds after the 5 s light pulse, while PNull

ipRGCs continue to fire at a reduced and inconsistent rate for the whole length of this recording (4 minutes 25 seconds after light off). (C, D) Example spike raster plots for individual light responsive units, for WT (C) and PNull (H) ipRGCs. Registered, overlayed spikes for the individual cells in C and D are shown as insets in A, and B, (gray curves) together with their respective average spike shapes (green line). (I) Digital sync signal outlining the experimental protocol. After 30s in the dark a 5s blue flash is applied, followed by complete darkness. For WT retinas, 9 ipRGCs were identified amongst 191 distinct cells detected in 5 retinal pieces from 4 different mice. For PNull, 11 ipRGCs were diagnosed from 187 units (5 retinal pieces from 3 different mice).
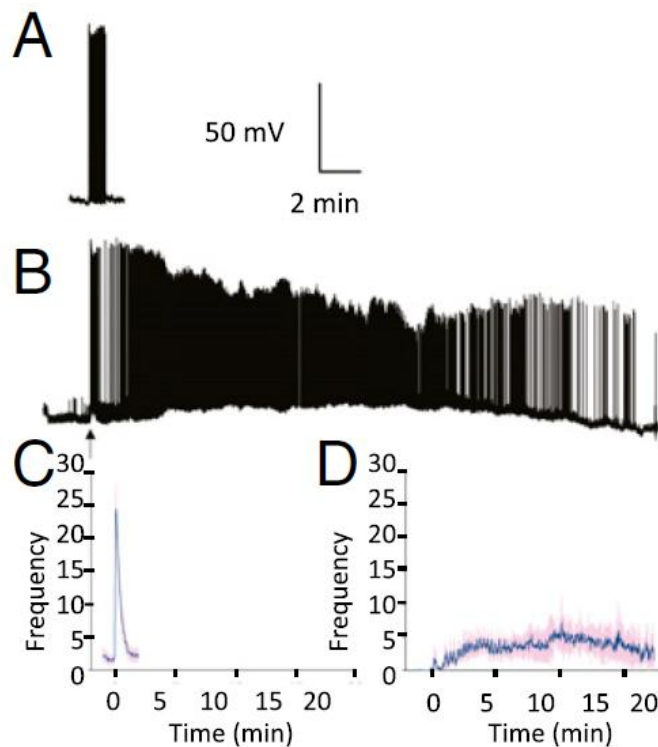
Figure 3.7: Phosphonull melanopsin-expressing ipRGCs show a prolonged light response. *(A–D) Current-clamp recordings from ipRGCs expressing WT (A) and*

phosphonull melanopsin (B). Cells were initially maintained at −60 mV. Light stimulation (arrow; 480 nm, 5 s, 1 × 1015 photons per cm−2·s−1) increased action potential frequency, which terminated within 1 min in WT but was prolonged (>20 min) for phosphonull melanopsin. Spike frequency (averaged over 2-s bins) is shown as a function of time in ipRGCs expressing WT (C; n = 10) and phosphonull (D; n = 4); error bars are SEM. (Data from Dr. Lane Brown).

The delayed shutoff properties of the C-terminus melanopsin phosphonull mutant renders** phase-delay**s more efficient, but surprisingly does not affect the phase angle of entrainment

In order to determine if C-terminal phosphorylation plays a role in tuning circadian behaviors, an experiment was conducted where a 6-hour phase-delay jet lag was introduced to $Opn4^{Cre/Cre}$ mice in 16:8 LD before and after injections with AAV2(WT melanopsin) and AAV2(CPΦ). The number of days taken by the animals to shift their activities to the new delayed light-dark cycle was noted. $Opn4^{Cre/Cre}$ mice before and after injections with the virus were able to photoentrain to 16:8 LD due to the presence of intact rods and cones in these animals (Figure 3.8A and 3.8B). $Opn4^{Cre/Cre}$ mice before injections individually with AAV2(WT melanopsin) and AAV2(CPΦ) took an average of 8.6 and 9.3 days respectively to shift their activities and entrain to the delayed light-dark cycle (Figure 3.8A and B[top],3.8C and D[left]). $Opn4^{Cre/Cre}$ +AAV2(WT melanopsin) on an average needed 5.6 days to shift their activities (Figure 3.8A[bottom], C[right]), whereas $Opn4^{Cre/Cre}$ +AAV2(CPΦ) needed only an average of 2.8 days (Figure 3.8B[bottom] D[right]). The number of days needed to photoentrain for the injected animals were significantly smaller from their uninjected

counterparts. In general, the presence of melanopsin (WT or mutant melanopsin) renders $Opn4^{Cre/Cre}$ mice more efficient in adapting to phase-delay jet lag.

$Opn4^{Cre/Cre}$ +AAV2(CPΦ) mice exhibited a 65.3% reduction in the number of days taken to entrain to phase-delay in comparison with $Opn4^{Cre/Cre}$ mice before injection (Figure 3.8E). Similarly, $Opn4^{Cre/Cre}$ +AAV2(WT melanopsin) mice exhibited a 34.6% reduction in the number of days taken to entrain to phase-delay in comparison with $Opn4^{Cre/Cre}$ mice. The former was significantly different from the latter, thus suggesting that exogenous CPΦ melanopsin is more efficient in rescuing a phase-delay deficit than exogenous WT melanopsin (Figure 3.8E).

In addition to phase-delay, these animals were also tested for their phase angle of entrainment, which is the alignment of the onset of their activity to the onset of subjective night (in nocturnal animals) (80). Surprisingly, there were no changes in the phase angle of entrainment of the virally modified animals as compared to melanopsin knockouts (Figure 3.9). This result indicates that after prolonged light stimulation shutoff mechanisms independent of GRK-mediated C-terminal phosphorylation contribute to melanopsin phototransduction termination even in the presence of light input.
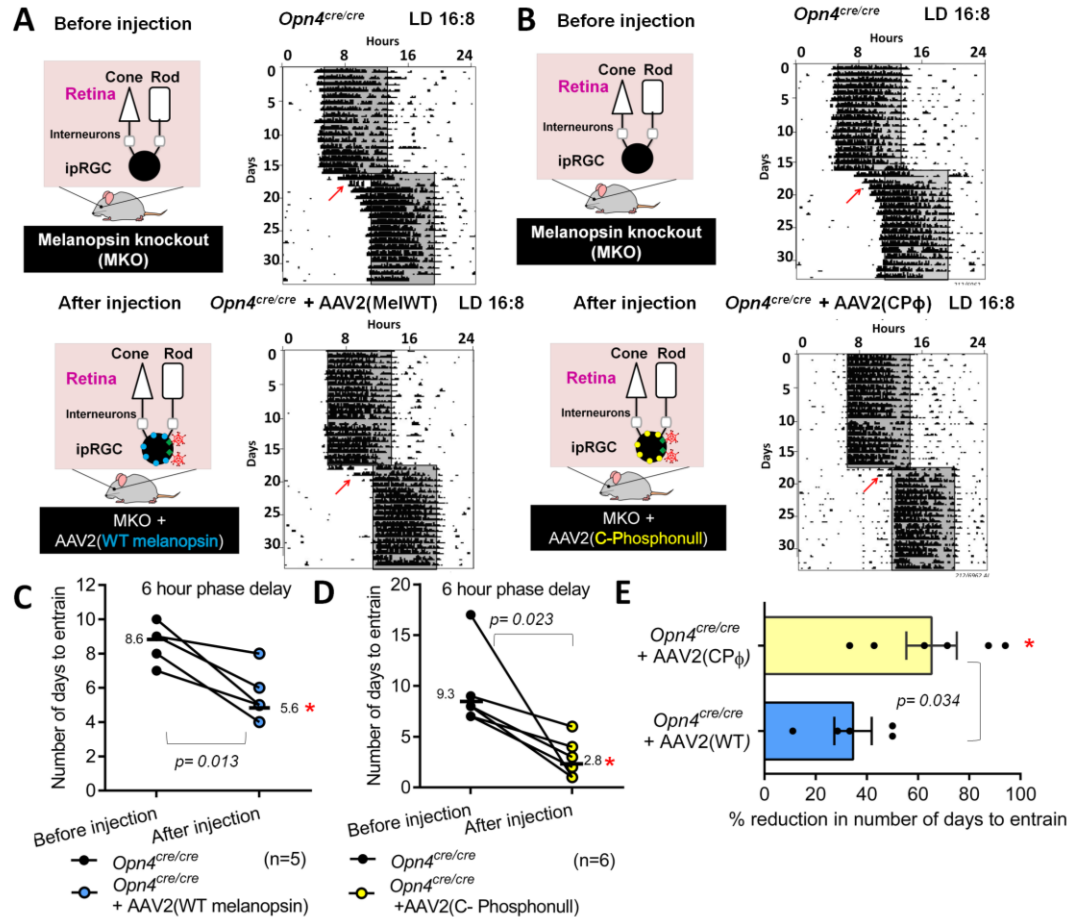
Figure 3.8: Phosphonull melanopsin and wild type melanopsin rescue the jet lag deficit observed in MKO(Opn4Cre/Cre) mice. (**A**) *Representative actograms using a paradigm of 16 hours of light and 8 hours of darkness (16:8 LD) of one MKO Opn4$^{Cre/Cre}$ mouse before [top] and after [bottom] injection with AAV2(mRuby-P2A-Melanopsin-FLAG).* (**B**) *Representative actograms of one MKO Opn4$^{Cre/Cre}$ mouse before [top] and after [bottom] injection with AAV2(mRuby-P2A-C-terminus phosphonull-FLAG) [bottom] in 16:8 LD. Red arrows indicate the 6 hour phase shift jet lag introduced at ~2weeks.(A)(B) Graphic illustrations of mice used or generated in this study ((A)-top and (B)-top)- Melanopsin knockout (Opn4$^{Cre/Cre}$), MKO mice injected with a viral vector containing the wild type melanopsin gene (blue; (A)-*

bottom) , or a viral vector containing the phosphonull melanopsin gene (yellow; **(B)-bottom)**. The red structures represent AAV2 **(c)** The number of days taken by MKO $Opn4^{Cre/Cre}$ mice (n=6) before and after injection with AAV2(mRuby-P2A-CPϕ-FLAG) and **(D)** MKO $Opn4^{Cre/Cre}$ mice (n=5) before and after injection with AAV2(mRuby-P2A-Melanopsin-FLAG) to phase shift their activities to the 6 hour jet lag. {open circles- $Opn4^{Cre/Cre}$; blue filled circles- $Opn4^{Cre/Cre}$+AAV2(mRuby-P2A-Melanopsin-FLAG); yellow filled circles- $Opn4^{Cre/Cre}$ + AAV2(mRuby-P2A-C-terminus phosphonull-FLAG)}. **(E)** Comparison of percent reduction in number of days taken by MKOs to phase shift their activities to 6 hour jet lag after injection with either AAV2(mRuby-P2A-Melanopsin-FLAG) (blue) or AAV2(mRuby-P2A-C-terminus phosphonull-FLAG) (yellow). The black dots represent the percent reduction in number of days values for each individual mouse. Statistical analyses performed for **(C)** and **(D)** were paired two tailed t-tests (*=p≤0.05), and for **(E)** was unpaired two tailed t-test with Welch's correction (*=p≤0.05) . Statistical

analyses conducted in **(C)** and **(D)** for before-after comparisons were paired two tailed t-tests, comparing $Opn4^{Cre/Cre}$ before and after injection with AAV2(mRuby-P2A-Melanopsin-FLAG) (*,p=0.013), and $Opn4^{Cre/Cre}$ before and after injection with AAV2(mRuby-P2A-C-terminus phosphonull-FLAG), (*,p=0.023). Comparison between $Opn4^{Cre/Cre}$+AAV2(mRuby-P2A-Melanopsin-FLAG) and $Opn4^{Cre/Cre}$+AAV2(mRuby-P2A-C-terminus phosphonull-FLAG) in **(e)** was conducted by unpaired t-test with Welch's correction test , (ns,p=0..34).
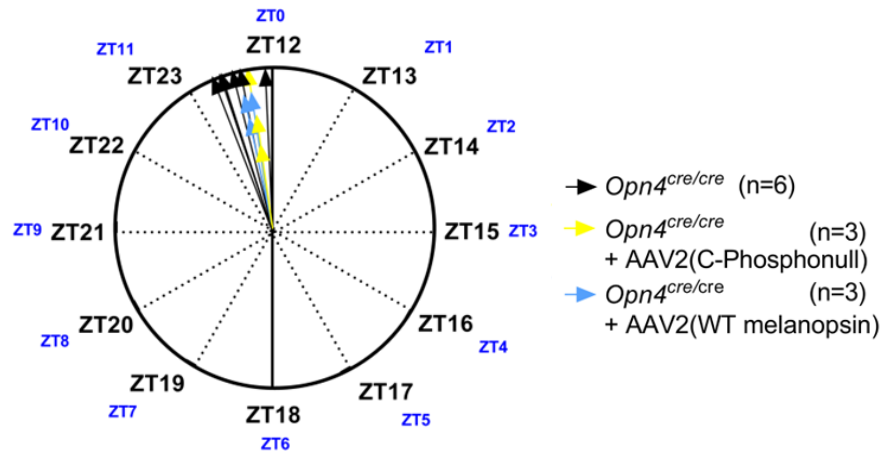
Figure 3.9: Phosphonull and wildtype melanopsin do not affect phase angle of entrainment. Comparison of phase angle of entrainment to 16:8 LD paradigm between $Opn4^{Cre/Cre}$(black, n=6), $Opn4^{Cre/Cre}$ + AAV2(mRuby-P2A-Melanopsin-FLAG) (blue, n=3), and $Opn4^{Cre/Cre}$ + AAV2(mRuby-P2A-C-terminus phosphonull -FLAG) (yellow, n=3). Statistical analyses conducted for before-after comparisons were paired two tailed t-tests, comparing $Opn4^{Cre/Cre}$ before and after injection with AAV2(mRuby-P2A-Melanopsin-FLAG) (ns, p=0.388), and $Opn4^{Cre/Cre}$ before and after injection with AAV2(mRuby-P2A-C-terminus phosphonull-FLAG) (ns,p=0.47). Comparison between $Opn4^{Cre/Cre}$+AAV2(mRuby-P2A-Melanopsin-FLAG) and $Opn4^{Cre/Cre}$+AAV2(mRuby-P2A-C-terminus phosphonull-FLAG) was conducted by Kruskal-Wallis test (ns,p=0.150).

Exogenous CPΦ melanopsin rescues negative masking deficit in MKO

In addition to circadian photoentrainment, masking is another mechanism by which animals exhibit light mediated changes in behavior . Nocturnal animals reduce their activity during their subjective night when given a light stimulus of high intensity (negative masking) and increase their activity when given a light stimulus of low

intensity (positive masking). Melanopsin knockout animals exhibit a deficit in negative masking under 16:8 LD at light intensities of 10lux or higher ((45), personal communication Melissa Simmonds). $Opn4^{Cre/Cre}$ mice were housed in 16:8 LD and given a 3 hour light pulse (500lux) at ZT14 (2 hours after the onset of darkness). When $Opn4^{Cre/Cre}$ mice were injected with either AAV2(mRuby-P2A-Melanopsin-FLAG) or AAV2(mRuby-P2A-CPΦ-FLAG), a rescue of this deficit was observed (Figure 3.10). Both melanopsin WT and CPΦ virus were able to restore negative masking in $Opn4^{Cre/Cre}$ mice for the entire 3 hour duration of light stimulus. There was no apparent difference between the ability of either melanopsin construct to restore this deficit.
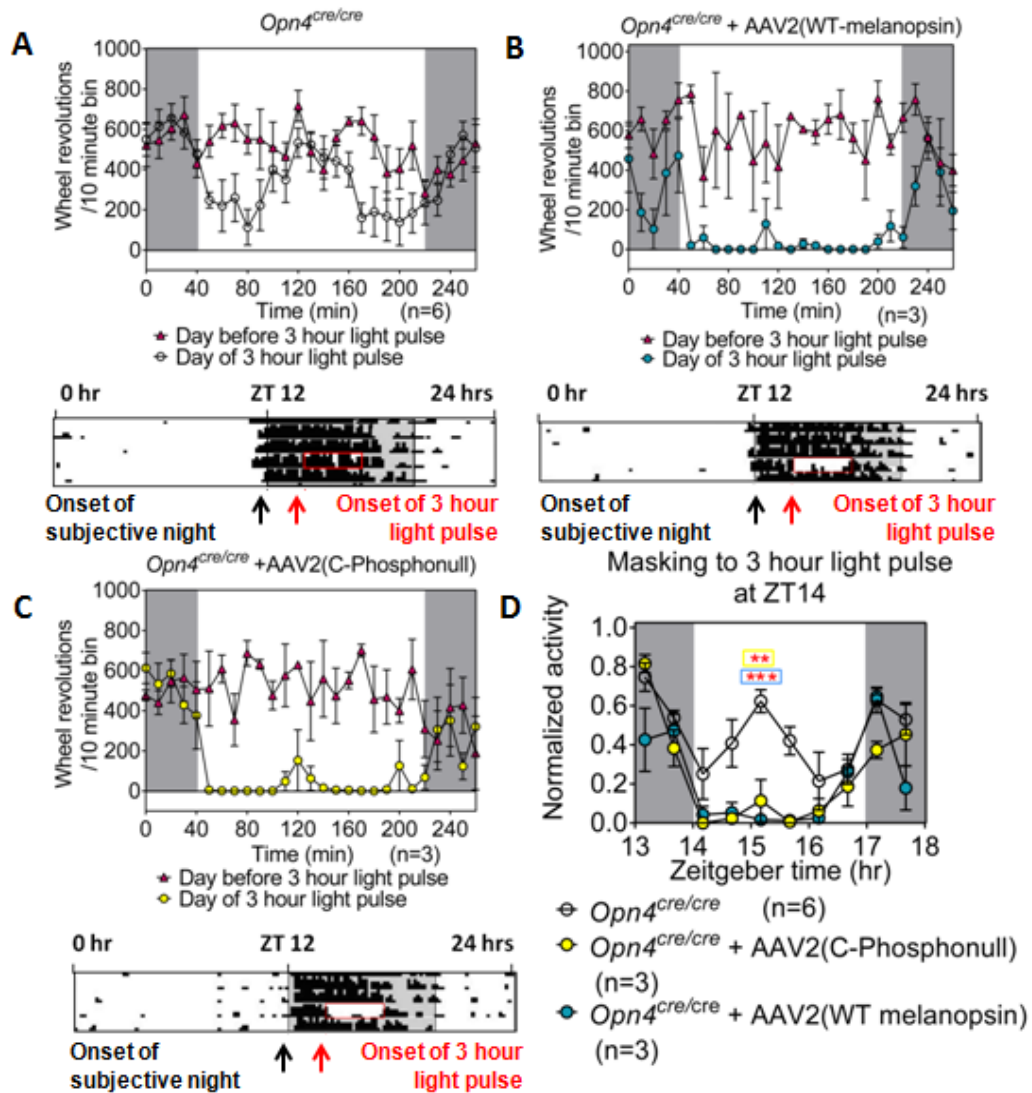
Figure 3.10: Both melanopsin and C-terminus phosphonull melanopsin rescue masking deficit in MKO. *Comparison of wheel running activities recorded in 10 min bouts between day before and day of 3 hour light pulse in (**A**) Opn4$^{Cre/Cre}$, (**B**)Opn4$^{Cre/Cre}$ injected with AAV2(mRuby-P2A-Melanopsin-FLAG) and (**C**) Opn4$^{Cre/Cre}$ injected with AAV2(mRuby-P2A-C-terminus phosphonull-FLAG). Representative actograms from one mouse in each group are shown below the graphs in (**A**), (**B**) and (**C**) . The 3 hour light pulse is indicated by the red box. (**D**) Comparison of the normalized activities of Opn4$^{Cre/Cre}$, Opn4$^{Cre/Cre}$ + AAV2(mRuby-*

P2A-Melanopsin-FLAG), and Opn4$^{Cre/Cre}$ + AAV2(mRuby-P2A-C-terminus phosphonull -FLAG) represented in 20 min bins from ZT13 to ZT18. 3 hour light pulse was initiated at ZT14. Wheel running activities were normalized to the highest activity bout in the day for each group (Highest activity bout occurs outside of the window of time shown here). Statistical analyses conducted in (A), (B) and (C) for before-after comparisons were linear mixed effect models, comparing activities on the day before and day of 3 hour light pulse in Opn4$^{Cre/Cre}$ (p=0.042), Opn4$^{Cre/Cre}$+AAV2(mRuby-P2A-Melanopsin-FLAG) (p=0.009) and Opn4$^{Cre/Cre}$+AAV2(mRuby-P2A-C-terminus phosphonull-FLAG) (p=0.045). Comparison of Opn4$^{Cre/Cre}$ with Opn4$^{Cre/Cre}$+AAV2(mRuby-P2A-Melanopsin-FLAG) and Opn4$^{Cre/Cre}$+AAV2(mRuby-P2A-C-terminus phosphonull-FLAG) in (D) was conducted by 2 way ANOVA with multiple comparisons.

Discussion

The utilization of wild type melanopsin in our construct has enabled us to study the effect of restoration of wild type melanopsin to melanopsin knockouts. We saw that transduction of *Opn4$^{Cre/Cre}$* with AAV2(WT melanopsin) exhibits a strong effect on circadian behaviors such as the 6 hour phase-delay jetlag and negative masking. MKOs or *Opn4$^{Cre/Cre}$* show a partial deficit in negative masking under 16:8 LD and a longer duration to phase shift to a 6 hour phase-delay jetlag. These deficits are abolished upon expression of exogenous melanopsin. These results are essentially proof of principle to this approach of making transgenic like mouse models.

GPCRs commonly undergo desensitization through phosphorylations by GRKs and subsequent arrestin mediated termination of receptor signaling. We

propose that melanopsin, a non-traditional visual pigment also follows this mechanism of deactivation. Melanopsin undergoes phosphorylation by GRK at specific residues on the C-terminus and this phosphorylation plays a critical role in melanopsin's influence on ipRGC photoresponse and kinetics of associated non-image forming behaviors. We provide evidence for this by demonstrating that eliminating all possible phosphorylation sites on the C-terminus of melanopsin results in prolongation of contralateral pupillary constriction in response to a high intensity light stimulus. Interestingly, we found that this prolongation is short lived (half-time of ~10 min), implying that melanopsin phosphorylation influences PLR kinetics only for a short duration after the receptor is activated. This opens up interesting questions about alternative mechanisms that could be deactivating the receptor in the absence of phosphorylation. One possibility is that the chromophore disassociates from the opsin and is regenerated, allowing the visual pigment to switch back to its inactive state.

Although C-terminal phosphorylation sites seem crucial for normal deactivation of melanopsin, we do not know precisely the candidate GRK involved in this function. GRKs 1-6 are expressed in the retina, and GRK 2,3 and 5 are particularly well expressed in ipRGCs (7). Blasic et al. showed that GRK 2 and 3 are co-expressed with melanopsin in ipRGCs in a light dependent manner. Despite this evidence that suggest an interaction between GRKs and melanopsin, it has been shown that GRK2 only minimally regulates melanopsin activity and only in very young animals (10). Sexton showed that specifically knocking out GRK2 does not significantly impact melanopsin activity or ipRGC function (81). We propose that this could be explained by the presence of other GRKs in ipRGCs. In the absence of

97

GRK2, GRK3 could be phosphorylating melanopsin and compensating for the loss of GRK2. Further studies that completely ablate all GRKs in a conditional manner may shed light on the identity of the GRK primarily phosphorylating melanopsin in native conditions. Melanopsin is a promiscuous GPCR in terms of its interaction partners. It associates with more than one type of G-protein (22,23,24). Similarly, it is likely that melanopsin is non-selective towards the type of GRK that it associates with.

Studies on rhodopsin indicate that multiple phosphorylations in the C-terminus are required for complete quenching of the rhodopsin response (25). However, not all sites are needed to be phosphorylated to achieve this quenching. Experiments showed that a minimum of three phosphorylations are required to cause a conformational change in arrestin such that it could bind activated rhodopsin. We suggest that melanopsin may follow a similar pattern of deactivation where multiple phosphorylation sites are available, but only a subset of them are needed at one point of time to achieve complete quenching of the melanopsin response. The purpose of our study was to determine the overall role played by C-terminal melanopsin phosphorylation on whole organism behavior. Further experiments are needed to accurately determine the number and identity of sites phosphorylated *in vivo. In vitro* studies suggest that a region consisting of six serines and threonines (T388, S389, S391, S392, S394, S395) clustered together are necessary for proper deactivation of melanopsin (9). Recent *in vivo* experiments by Mure et al. suggest that a region consisting of nine serines and threonines (S381, S384 and T385 in addition to the ones described by Blasic) are critical for melanopsin deactivation (11). It is however not clear whether these sites are sufficient for wild-type-like melanopsin deactivation.

Detailed mass spectrometric analysis is required to specifically narrow down the sites that are phosphorylated in native conditions. In our study, we have completely eliminated all putative C-terminal phosphorylation sites and demonstrated that C-terminal phosphorylation is essential for the PLR and phase-delay but not masking behavior.

Chapter 4:

Discussion and future directions

Melanopsin is a GPCR expressed in the mammalian retina that was only discovered 19 years ago (18). Although research in the past two decades have helped shed light on various aspects of this visual pigment and its role in non-image forming vision, we still don't understand completely how melanopsin is deactivated once its signaling cascade is initiated, how its activity is regulated, and how it adapts to ambient illumination throughout the day (82). Recent studies using *in vitro* systems have suggested that melanopsin undergoes regulation through phosphorylation by two different kinases - a GPCR kinase acting on the C-terminus (GRK) and a Protein kinase A (PKA) acting on the intracellular loops (34, 35, 66). These phosphorylations were suggested to play a role in deactivation and adaptation of the visual pigment respectively (34, 39). The goal of my study was to investigate these phosphorylations in the context of whole-organism behavior and physiology. In order to achieve this, a viral gene delivery approach was used to generate genetically modified mice that express mutant versions of melanopsin (melanopsin mutants where the GRK or PKA phosphorylation sites were mutated to alanines or glycines). While investigation of PKA-mediated melanopsin phosphorylation in still underway (Appendix A), there has been substantial progress in understanding the role of GRK-mediated C-terminal phosphorylation of melanopsin in non-image forming vision. Recently, Mure et al. demonstrated using a similar viral approach that a series of nine serines and threonines (six of which were earlier described by Blasic et al.) in the proximal part of melanopsin C-terminus (putative GRK phosphorylation sites) are important for melanopsin deactivation *in vivo* (34, 35, 83). They showed that absence of these sites

leads to prolonged constriction of pupils in the virally modified mice and extended the light-evoked response of ipRGCs (34, 35, 83). Similarly, in the present study we focused on all 38 of the C-terminal putative GRK phosphorylation sites, to determine their importance in non-image forming behaviors such as the pupillary light reflex, circadian photoentrainment, masking, and ipRGC physiology.

We found that the absence of all 38 phosphorylation sites causes prolonged pupil constriction in the CPφ mice and speeds up re-entrainment to a 6 hour phase-delay jet lag paradigm. However, the pupils of CPφ mice eventually dilate with a half-time of dilation ~100 times slower than that of wildtype mice. These results indicate that C-terminal phosphorylation is crucial for melanopsin deactivation but only on a short timescale. The eventual dilation of the pupils of CPφ mice suggests that a mechanism independent of C-terminal phosphorylation must also play a role in deactivating melanopsin.

ipRGCs of CPφ mice sustain action potentials for an extended period of time (~15min in single cell recordings and >5 min in MEAs) as compared to wildtype mice where ipRGCs fire action potentials for <1min. This indicates that C-terminal phosphorylation influences the kinetics of the physiology of ipRGCs. However, C-terminal phosphorylation did not seem to be important for masking behavior or phase angle of entrainment. These results taken together indicate that C-terminal phosphorylation of melanopsin is important for some melanopsin-mediated behaviors, but not all of them. These observations lead to two main questions - 1. What explains the differential effects of phosphorylation on melanopsin-mediated

behaviors? 2. What other mechanism is involved in melanopsin deactivation in the absence of C-terminal phosphorylation?

There are multiple possibilities that could explain the differential effects of C-terminal melanopsin phosphorylation. Two of these are - 1. AAV2 may preferentially transduce some ipRGC subtypes, leading to variability in the expression of mutant melanopsin between subtypes. This difference could hide a behavioral phenotype if AAV2 does not transduce a specific ipRGC subtype that may be important for that behavior. 2. Each ipRGC subtype may have a different dependency on GRK-mediated melanopsin phosphorylation. Although we know that generally GRKs 2,3 and 5 are expressed in ipRGCs (34), we don't know if there is a subtype-specific difference in expression of these GRKs. Moreover, it is possible that the melanopsin phototransduction cascade is different between ipRGC subtypes. Some subtypes may use a different mechanism of melanopsin deactivation independent of C-terminal phosphorylation.

Future directions

For the current viral transduction-based approach, one future experiment is to perform western blots on the retinas of the virally modified mice to determine the level of expression of melanopsin protein and compare it to expression levels in wild type animals.

One way to address the problem of preferential transduction of ipRGCs by AAV2 is to use the CRISPR-Cas9 genome editing system to generate genetically modified mice for studying behavior. Using this approach, a subset of six GRK phosphorylation sites (T388, S389, S391, S392, S394, S395) could be mutated to

alanines to study the effect of absence of GRK-mediated phosphorylation on melanopsin-mediated behaviors in a more elaborate and precise manner. This method would provide three main advantages over the viral approach used in the present study- 1. Using CRISPR-Cas9 system would allow us to edit the endogenous melanopsin gene, thereby ensuring better chanves that mutant melanopsin expression levels are comparable to wildtype. 2. Eliminating AAV viral transduction could guarantee the expression of mutant melanopsin in all ipRGC subtypes and in native levels of protein expression. 3. Mutating a subset of phosphorylation sites as against all 38 will help us narrow down the C-terminal phosphorylation sites that are actually crucial *in vivo*.

Another possible future direction is to answer the question, "What is the GRK subtype involved in C-terminal phosphorylation of melanopsin?". Blasic et al. have shown that GRKs 2, 3 and 5 are expressed in ipRGCs, and GRKs 2 and 3 co-localize with melanopsin in the retina (34). Recent work by Sexton et al. has shown that conditionally knocking out GRK2 in mice does not cause a profound influence on ipRGC physiology (81), indicating that GRK2 may not be the kinase involved in this phosphorylation. Conditional knockouts of GRKs 3 and 5 individually, and conditional knockout of all candidates GRKs together, in ipRGCs may be required to identify the GRK subtype that actually phosphorylates melanopsin *in vivo*.

A second important experimental direction to take is to investigate the role of dopamine-dependent PKA-mediated melanopsin phosphorylation in non-image forming vision (Outlined in Appendix A). Studies have pointed towards a role for dopamine via the cAMP-PKA pathway in regulating melanopsin activity (56, 66). To

further probe the role of this regulation, a similar viral transduction approach will be used to that of this study, where a PKA mutant of melanopsin (with all three putative PKA phosphorylation sites mutated to alanines or glycines) will be expressed in melanopsin-knockout mice to determine the effect of absence of PKA-dependent phosphorylation on melanopsin-mediated behaviors. These virally modified mice that express the PKA-Triple Mutant (or PKA-TM) will be assessed for their pupillary light reflex, circadian photoentrainment including phase-delay jet lag, masking, and ipRGC physiology.

Unlike GRK-mediated phosphorylation which is light-dependent, PKA-mediated phosphorylation is complicated by the fact that it is dopamine-dependent (34, 66). Dopamine levels are higher during the subjective day than during subjective night (67). Hence, assessment of behaviors should be conducted both during subjective day and night to determine dopaminergic influence. Since PKA-mediated phosphorylation has been suggested to confer a modulatory effect on melanopsin activity, it is expected that the sensitivity of melanopsin will be higher in PKA-TM mutant mice due to the absence of this phosphorylation. Therefore, for the pupillary light reflex, the intensity response curve (IRC) during the subjective day would be expected to shift to the left, but the same may not be true for a PLR IRC during the subjective night. For circadian behavior experiments, we would not expect to see a phenotype for behaviors that involve introducing light during subjective night such as phase-delay and masking, due to the low levels of dopamine. At the physiological level, the adaptation of ipRGCs would be expected to be affected in the PKA-TM mice. This could be tested in multielectrode or single cell recordings by stimulating

105

the cells with continuous light or repetitive flashes of light. Their adaptation could also be tested with or without external application of a dopamine agonist.

Finally, although melanopsin-mediated PKA phosphorylation in the retina has been suggested through indirect and *in vitro* methods, it is not known whether PKA subunits are expressed in the retina, specifically in ipRGCs. To determine expression of PKA in the retina, I performed RT-PCR to probe for the different PKA subunit subclasses in the retina (see Appendix A). Preliminary experiments indicate that all subclasses of PKA subunits transcripts are present in the retina. However, further experiments are needed to determine if these subunits are present in ipRGCs and if the PKA protein is also present. One way to resolve this is to perform immunohistochemisty on the retina using PKA subunit specific antibodies along with melanopsin antibody to determine colocalization. PKA-mediated melanopsin phosphorylation and PKA expression related experiments are further described in Appendix-A.

Appendices

The following appendices highlight the additional projects that I contributed to during the course of my graduate studies. ***Appendix A*** is a project in progress exploring the behavioral and physiological effects of PKA-mediated melanopsin phosphorylation. ***Appendix B*** is an Elife journal article published by Keenan et al. My contribution to this work involves development of the Cre-loxP dependent viral expression system for expressing wildtype melanopsin in melanopsin knockout mice (described in Chapter 2). The virus prepared using this approach was utilized in this work. This virus was also used for a second project by Rupp et al. (Melanopsin-expressing cells of the retina, not iris, mediate the pupillary light reflex), for which the manuscript is currently in preparation.

Appendix A

Determining the role of dopamine-mediated melanopsin phosphorylation via PKA in non-image forming vision

Part 1- Role of dopamine-mediated melanopsin phosphorylation via PKA in non-image forming vision

Introduction

Dopamine is a widely used neurotransmitter and regulator in the retina. Dopamine's effect extends to ipRGCs, that are a small subset of the ganglion cells in the retina (56). It has been shown in rat ipRGCs that dopamine has a modulatory role in the physiology of these cells. However, the mechanism by which dopamine exerts its effect on these cells has not been established.

Recently, phosphorylation of melanopsin by PKA in a dopamine-dependent manner was demonstrated in HEK293A cells (66). It was shown that this phosphorylation modulates the activity of melanopsin by affecting its overall kinetics. Additionally this modification was also demonstrated in mouse retinal sections by external application of dopamine.

I hypothesize that dopamine-dependent phosphorylation of melanopsin controls adaptation of ipRGCs in mice. The objective of these experiments is to confirm that this PKA-mediated modification occurs *in vivo* in intact retina of mice and to characterize the effect of this modification on the physiological and behavioral state of the mice. I will generate transgenic mice that express a PKA-TM mutant (melanopsin mutant with all three putative PKA phosphorylation sites mutated to alanines or glycines) (See Figure 1.6b and Figure A1). Using adenovirus associated viral vectors I will perform ocular delivery of floxed melanopsin cassettes containing melanopsin PKA-TM tagged with molecular markers into *Opn4$^{cre/cre}$* mice. Cre-loxp recombination will aid in transduction of retinal ganglion cells in the

Opn4^{cre/cre} mice as described in chapter 2. Once the cells have been confirmed to express melanopsin, electrophysiology and behavioral studies will be conducted to assess the physiological and behavioral state of the mice.

Progress

Floxed PKA-TM melanopsin expression cassette with a C-terminal FLAG tag and a N-terminal mRuby-P2A tag was created in a pAAV (adeno associated viral vector) backbone (Figure A1). The viral vector was tested for expression by western blotting and fluorescence microscopy. The PKA-TM-FLAG fusion protein was detected in western blot using a rabbit anti-FLAG antibody (Figure A2). mRuby fluorescence was visualized in HEK293-cre cells transiently transfected with the viral vector construct two days post transfection (Figure A3). After validation that the viral vector is functional is presence of Cre, this construct was packaged into suitable viral capsids. Dr. Zhijian Wu's lab at NIH were kind enough to prepare viral titers for our constructs. Viral titers were then used for ocular delivery into *Opn4^{cre/cre}* mice. Four weeks post injections, animals were single housed in cages with wheels and are currently being monitored for their wheel running activity.
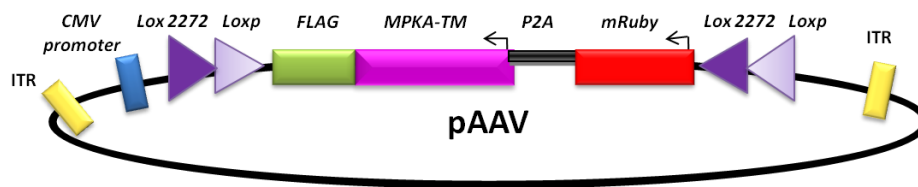
Figure A1: Components of the adeno-associated viral vectors expressing PKA-TM. *PKA-TM coding sequence with C-terminal FLAG tag and N-terminal mRuby-P2A tag in reverse complement orientation flanked by loxp and lox2272 sequences (floxed).*

CMV promoter drives expression of the transgenes in this viral vector in the presence of cre recombinase. Inverted terminal repeats (ITRs) are viral derived sequences that are recognized by viral proteins for packaging into AAV2 capsids.

Probed with Anti-FLAG Ab
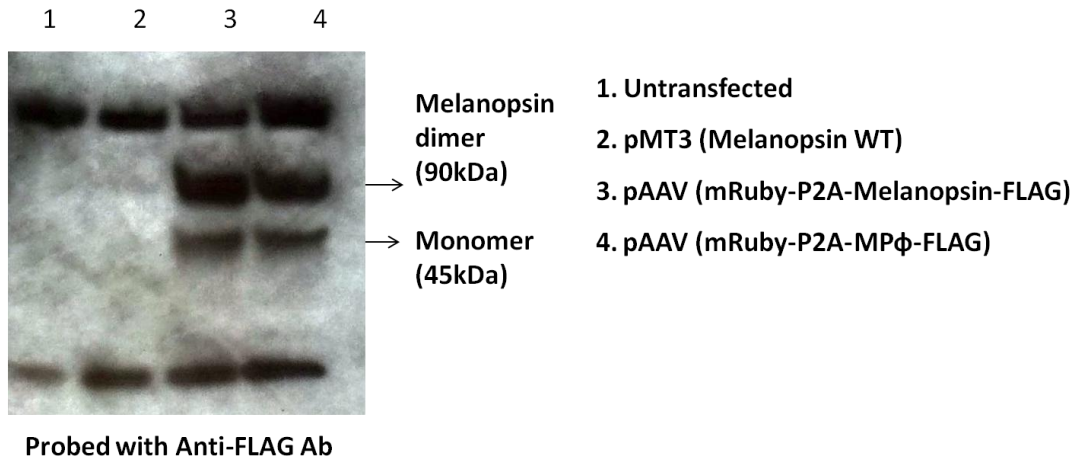
Figure A2: Expression of pAAV/(mRuby-P2A-PKA-TM-FLAG) demonstrated by western blotting. *HEK293A cells were transiently transfected with pAAV/(mRuby-P2A-PKA-TM-FLAG) construct. 48 hours post transfection, total protein was extracted from the cells and separated on a SDS-PAGE gel. Protein was transferred onto a PVDF membrane and probed with a rabbit anti-FLAG primary antibody. Donkey anti-rabbit IgG-HRP conjugate secondary antibody and HyGLO chemiluminescent HRP substrate were used for detection. Expression of MKPA-TM fusion protein can be seen as two bands corresponding in molecular weights to the predicted monomer and dimer of melanopsin.*
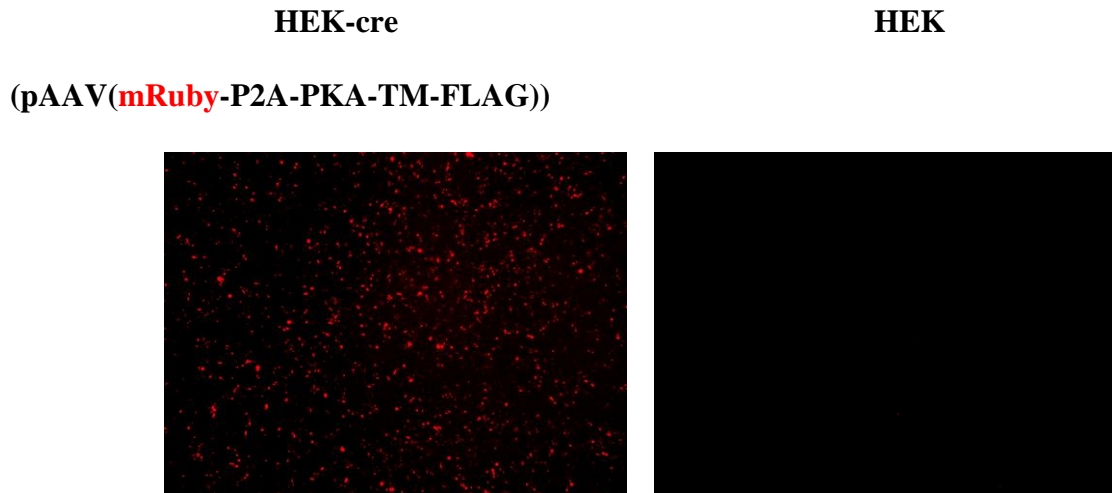
Figure A3: Reporter gene expression from pAAV(mRuby-P2A-PKA-TM-FLAG) viral vector observed in HEK293-cre cells. HEK293-cre and HEK293 cells were transiently transfected with pAAV(mRuby-P2A-PKA-TM-FLAG). mRuby expression was visualized 48 hours post transfection by fluorescence microscopy in HEK293-cre cells. Absence of mRuby fluorescence in transfected HEK293 cells indicates that the transgene is expressed only in the presence of Cre recombinase.

Future directions and expected outcomes

The circadian behavior of the virally modified mice will be assessed by their wheel running activity in light/dark cycles under four different light intensities ranging from 7lux- 500lux. In the circadian photoentrainment experiments, several aspects of the wheel running activity of the animals will be assessed - phase angle of entrainment, period length and days taken to shift activity to phase-delay jet lag. The ability of the PKA-TM mice to align the onset of their activities to the onset of darkness, maintain length of period and shift activity to a phase-delay jet lag paradigm will be determined. PKA-TM mice are expected to photo-entrain owing to the presence of

functional melanopsin and classical photoreceptors. Since PKA phosphorylation of melanopsin is implicated in modulating the activity of melanopsin, the expectation is that eliminating this phosphorylation will render melanopsin hypersensitive.

To assess the effect of dopamine-dependent melanopsin phosphorylation on pupillary light reflex, the pupillary light response will be measured for varying light intensities. Since dopamine is predicted to exert its effect through PKA on melanopsin, and dopamine levels vary between day and night, the PLR experiments will be conducted both during the subjective day and subjective night of the mice. I predict that PKA-TM mice will exhibit increased sensitivity of their pupils during the subjective day but not during the subjective night, owing to increased levels of dopamine during the day.

Following behavioral experiments, retinal explants from the mice will be used to test the melanopsin based light response in these mice by electrophysiological studies (multielectrode array recordings). The prediction is that the intrinsic melanopsin signal in these mice will show no adaptation in response to sustained and/or repetitive light stimuli.

Part 2- Demonstrate expression of PKA in the retina

Overview

Protein kinase A is widely expressed in mammalian cells. However, the holoenzyme structure of the kinase is assembled from multiple subunits each of which differ in their expression levels in a cell type specific manner. Although subunits of PKA are known to be highly expressed in neuronal cells (59), there is no direct evidence

showing expression of PKA in the retina. The objective of these experiments to confirm the expression of PKA in the retina and specifically in ipRGCs at both the mRNA and protein levels. In order to achieve this objective, I will use two specific techniques – reverse transcription PCR to detect PKA mRNA and immunofluorescence to demonstrate protein in the retina.

Progress

PKA subunit mRNA coding sequences were obtained from NCBI nucleotide database. Multiple sequence alignments were performed to identify regions of homology between the subunits. The regulatory subunits of type 1 were 75% identical, regulatory subunits of type 2 were 80% identical and catalytic subunits were 70% identical. Primers that anneal to both members of each subtype and do not cross hybridize with other subtypes were designed. The designed primers were verified for reactivity using RNA isolated from HEK293A cells. Primers specific to bovine rhodopsin were used as control. RNA extracts prepared from mouse retina was used for one step RT-PCR reaction. The results indicated that all classes of PKA subunits were expressed in mouse retina (Figure A4).

R1	R2	C	Rho
700bp	1000bp	700bp	500bp
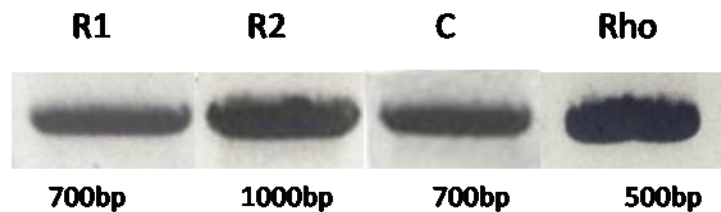
Figure A4: RT-PCR of PKA subunits in total RNA extracted from dissected mouse retinas. Total RNA was extracted from 2 dissected mouse retinas and RT-PCR was

performed for 3 different subtypes of PKA subunits using the designed primers. The product sizes are indicated below the bands. Rhodopsin was used as positive control.

Future directions and expected outcome

In order to confirm expression of PKA in the retina, I will perform immunofluorescence in retinal sections from mice using an antibody specific to the catalytic alpha subunit of the protein. This will help in determining the localization of PKA expression in the retina. More specifically, it will be interesting to see if PKA co-expresses with melanopsin containing ipRGCs. I anticipate that immunofluorescence in ipRGCs will show expression of all PKA subunits, and co-localization of melanopsin with PKA.

x

Appendix B

A visual circuit uses complementary mechanisms to support transient and sustained pupil constriction

William T. Keenan[1†], Alan C. Rupp[1†], Rachel A. Ross[2, 3], Preethi Somasundaram[4], Suja Hiriyanna[5], Zhijian Wu[5], Tudor C. Badea[5], Phyllis R. Robinson[4], Bradford B. Lowell[6,7], and Samer Hattar[1,8]

[1] Department of Biology, Johns Hopkins University, Baltimore, MD, USA

[2] Department of Psychiatry, Beth Israel Deaconess Medical Center, Harvard Medical School

[3] Department of Psychiatry, Massachusetts General Hospital

[4] Department of Biological Sciences, University of Maryland, Baltimore County, Baltimore, MD, USA

[5] National Eye Institute, National Institutes of Health, Bethesda, MD, USA

[6] Division of Endocrinology, Diabetes, and Metabolism, Department of Medicine, Beth Israel Deaconess Medical Center, Harvard Medical School, 3 Blackfan Circle, Boston, MA 02215, USA

[7] Program in Neuroscience, Harvard Medical School, Boston, MA 02115, USA

[8] Department of Neuroscience, Johns Hopkins University, Baltimore, MD, USA

[†] Denotes equal contribution

Abstract

Rapid and stable control of pupil size in response to light is critical for vision, but the neural coding mechanisms remain unclear. Here, we investigated the neural basis of pupil control by monitoring pupil size across time while manipulating each photoreceptor input or neurotransmitter output of intrinsically photosensitive retinal ganglion cells (ipRGCs), a critical relay in the control of pupil size. We show that transient and sustained pupil responses are mediated by distinct photoreceptors and neurotransmitters. Transient responses utilize input from rod photoreceptors and output by the classical neurotransmitter glutamate, but adapt within minutes. In contrast, sustained responses are dominated by non-conventional signaling mechanisms: melanopsin phototransduction in ipRGCs and output by the neuropeptide PACAP, which provide stable pupil maintenance across the day. These results highlight a temporal switch in the coding mechanisms of a neural circuit to support proper behavioral dynamics.

Introduction

Environmental light influences a variety of subconscious physiological functions, including circadian photoentrainment, light modulation of sleep/mood, and the pupillary light response (PLR). These diverse effects of light are all mediated by a small subpopulation of retinal output neurons called intrinsically photosensitive retinal ganglion cells (ipRGCs) (14, 84–89). Even in the vast array of environmental light conditions, subconscious visual behaviors are remarkable for their rapid induction and stable maintenance throughout the day. However, how the ipRGC circuit achieves rapid and stable control of visual behaviors remains uncertain.

117

Multiple photoreceptive systems participate in the ipRGC circuit, including their endogenous melanopsin-based phototransduction and indirect synaptic input from the classical rod and cone photoreceptors (90, 91). Each photoreceptive system presumably encodes a unique aspect of the light environment, but to date no consensus exists on the photoreceptive mechanisms supporting ipRGC-dependent behaviors. Several studies using a variety of methods have proposed competing models arguing for the predominance of cone-based (92–95) or rod-based (96, 97) synaptic input to ipRGCs and their behavioral responses. Additionally, it has been suggested that melanopsin mediates persistent light detection in ipRGCs (84, 88, 98–100) because melanopsin phototransduction is relatively slow to initiate but stable for minutes to hours (79, 99, 101). However, animals lacking melanopsin still retain sustained light responses in ipRGCs and their central targets (101–103) and relatively normal circadian photoentrainment (104, 105) and PLR (25, 106). In total, it remains unclear how ipRGCs utilize each distinct photoreceptive input, especially across the environmental range of light intensities and durations.

ipRGCs must faithfully relay information about the light environment to the brain. Many neurons, including ipRGCs, release multiple neurotransmitters, a classical neurotransmitter and one or more neuropeptides (107). However, systems to evaluate mammalian cotransmitter systems *in vivo* in real time are lacking. ipRGCs contain the principal excitatory neurotransmitter glutamate and the neuropeptide PACAP (pituitary adenylyl cyclase-activating polypeptide) (108, 109). Recent studies have suggested that glutamate is the predominant regulator of ipRGC-dependent behaviors, including circadian photoentrainment and the PLR (110–112). By

comparison, animals lacking PACAP or its receptors show at best minor deficits in circadian photoentrainment and the PLR (113–117). This difference in outcomes between glutamate and PACAP has led to the conclusion that PACAP is dispensable and serves primarily as a modulator of glutamatergic signaling (118). It remains puzzling why ipRGCs, like many other neuronal cell types, would possess two distinct neurotransmitters.

To date, the precise behavioral contributions of rod, cone, and melanopsin input or their output neurotransmitters glutamate and PACAP to visual behaviors across time are essentially unknown. Here, we have systematically addressed the behavioral contributions of all three photoreceptive inputs and both neurotransmitter outputs of ipRGCs, and how these change with time. To do so, we have silenced each individual photoreceptor or neurotransmitter component of ipRGCs, and in multiple combinations, while measuring pupil size across environmental light intensities and time domains. We have taken advantage of the fact that the PLR provides the unique opportunity to dissect the precise temporal dynamics of inputs and outputs of the ipRGC circuit in a behaving animal. This study reveals how ipRGC circuit dynamics *in vivo* support pupil regulation across time and provides insights into ipRGC regulation of other subconscious visual behaviors.

Results

ipRGC behavioral responses are composed of both transient and sustained phases

To measure ipRGC responses in real time, we measured the pupillary light response (PLR). Importantly, we used a novel experimental setup that mimics environmental light using overhead light with spectral composition similar to daylight

in an unanesthetized mouse (**Figure 1A** and **Figure 1—figure supplement 1**), unlike previous studies that used monochromatic light delivered to a single eye (85, 93, 99, 106, 112, 114).

Following light onset, we observed rapid pupil constriction that is maintained for the duration of the 30-second recording (**Figure 1B**), with greater constriction under higher light intensities (**Figure 1D**). Previous studies have noted a PLR decay during a sustained light stimulus lasting minutes (96, 99, 119), prompting us to systematically monitor the pupil across a range of times and light intensities. We observed a decay in pupil constriction over time that reached a new steady state (**Figure 1C**), resulting in two phases in the PLR: transient and sustained (mean intensity to reach 50% constriction (EC_{50}) for transient PLR = 0.53 lux, sustained PLR = 7.9 lux)(**Figure 1D,E**). Because pupil constriction itself lowers the amount of light reaching the retina and therefore limits the drive to continued pupil constriction, the PLR is a form of negative feedback. To test if PLR decay is a consequence of negative feedback, we measured the effect of negative feedback both computationally and experimentally, and found that it has little role in PLR decay (**Figure 1—figure supplement 2**). Furthermore, we observed full PLR decay at dim light intensities ($\leq$1 lux) within the first 5 minutes of light stimulation (**Figure 1C,F**), but full maintenance of pupil constriction at high light intensities ($\geq$1000 lux), with apparently slower decay rates at higher light intensities (half-time: ~2–5 minutes, **Figure 1F**). These results suggest that ipRGCs possess temporally distinct inputs and/or outputs for transient and sustained signaling.

Transient input to ipRGCs is mediated by rods

To identify the photoreceptor(s) inputs that contribute to transient ipRGC responses (**Figure 2A**), we tested the PLR in mutant mouse lines that lack the function of a single photoreceptor type, leaving the function of the other photoreceptors intact (**Table 1**, for references on production and initial characterization of each line); we refer to these lines as cone knockout, rod knockout, and melanopsin knockout mice. To corroborate our findings, we tested a variety of mutant mouse lines that silence each photoreceptor type in unique ways (**Table 1**).

Importantly, these mutant mouse lines have been extensively tested for visual function (97, 120–126). Rod sensitivity and function is unchanged in cone mutant animals and cone sensitivity and function is unchanged in rod mutant animals (97, 120–125). Electrophysiological recordings of ipRGCs show functional rod input in cone mutants and functional cone input in rod mutants (126). Additionally, all of the photoreceptor mutant lines we used have similar pupil sizes in darkness (**Figure 2— figure supplement 1**). Therefore, these mouse lines allow precise separation of rod, cone, and melanopsin activation while leaving the function of the other photoreceptors intact.

When we tested the transient PLR of rod, cone, and melanopsin mutant mice, we found that both cone and melanopsin knockout mice were identical to wildtype in both sensitivity and kinetics (**Figure 2B** and **Figure 2—figure supplement 2B**). Despite previous reports of melanopsin requirement for the transient PLR (106), we find that melanopsin is dispensable for the PLR when using more environmentally relevant stimuli (**Figure 2—figure supplement 3**). In contrast, rod knockout mice displayed no pupil constriction until the light intensity becomes relatively bright (i.e.

>10 lux, **Figure 2B**), despite the normal spatial vision in rod knockout mice at these moderate light intensities (120). To corroborate these results, we tested three different cone mutant lines and two different rod mutant lines with distinct mutations and observed virtually identical results: cone mutants are similar to wildtype and rod mutants have severe transient sensitivity deficits (**Figure 2—figure supplement 2C,D**).

These results are surprising given previous proposals that cones are important for transient ipRGC responses, including acute changes in pupil size (92–94, 99, 127–132). Therefore, we sought to acutely modulate cone activity using a previously characterized mouse line that expresses the human 'red' opsin (*OPN1LW*) in place of the mouse 'green' opsin (*Opn1mw*) (Red cone KI), making cones the only photoreceptors with enhanced sensitivity to red light (93) (**Figure 2C**). We found that these mice have identical transient PLR in response to red light as wildtype (**Figure 2D**), indicating that acute cone modulation does not affect the overall magnitude of the PLR. Furthermore, crossing this line to a rod knockout line abolishes the PLR in response to red light (**Figure 2E**). These results show that rods are the predominant photoreceptor inputs for transient PLR at low to moderate light intensities, even in a mouse line with sensitized cones.

To evaluate the inputs contributed by each photoreceptor in isolation to the PLR, we generated double mutants lacking the function of two photoreceptor types, resulting in mice with only rods (Rods alone), only cones (Cones alone) or only melanopsin (Melanopsin alone) (**Table 1**). We found that the only photoreceptors capable of recapitulating the wildtype PLR are rods. Mice with only rod function had

identical light sensitivity as wildtype and a similar rapid induction of pupil constriction (**Figure 2F,G**), though their ability to maintain stable pupil sizes in bright light was slightly diminished (**Figure 2G**). We corroborated the sufficiency of rods using three different mouse lines (**Figure 2—figure supplement 4**). Interestingly, while two of the lines were nearly identical to wildtype, one line had similar sensitivity, but altered kinetics, suggesting that cones might regulate rod signaling dynamics.

In marked contrast to rod input, cone and melanopsin inputs were severely deficient in mediating the transient PLR (**Figure 2F,G**). Animals with melanopsin alone retained a normal PLR at bright light intensities (**Figure 2F**), as seen previously (25, 99, 133), with sensitivity that is indistinguishable from rod knockouts (**Figure 2—figure supplement 5**), though they had relatively sluggish kinetics (**Figure 2G**). In contrast, cone-only animals had minimal PLR (**Figure 2F**), resulting in a further sensitivity deficit compared to rod knockout and melanopsin-only animals (**Figure 2—figure supplement 5**). Additionally, cone input decayed rapidly (**Figure 2G**), presumably due their robust light adaptation properties.

Collectively, these results show that rods serve as the primary input to ipRGCs for transient PLR responses, especially at low to moderate light intensities. At bright light intensities, additional input originates predominantly from melanopsin phototransduction.

Glutamaterigic output provides precise and rapid transient signaling

To investigate how ipRGCs relay transient light detection to the brain, we tested the transient PLR in mice lacking glutamatergic neurotransmission in ipRGCs

($Opn4^{Cre/+}$; $Slc17a6^{fl/fl}$, also known as $Vglut2^{fl/fl}$) or mice lacking PACAP in ipRGCs ($Opn4^{Cre/+}$; $Adcyap1^{fl/-}$) (**Figure 3A** and **Table 2**). See **Figure 3—figure supplement 2** for details on design of the conditional PACAP allele ($Adcyap1^{fl}$).

Though ipRGC glutamate knockout mice ($Opn4^{Cre/+}$; $Slc17a6^{fl/fl}$) exhibited a small decrease in resting pupil size (**Figure 3—figure supplement 1**) (112), we observed that they had minimal transient PLR at all light intensities (**Figure 3B-E**), with more robust PLR at very bright light intensities (**Figure 3—figure supplement 3**), in agreement with previous studies (111, 112). This indicates that ipRGC glutamatergic neurotransmission is a critical transient signal for the PLR. Presumably, the residual transient response is PACAPergic.

In contrast to ipRGC glutamate knockout mice, ipRGC PACAP knockout mice had no deficits in transient PLR sensitivity or kinetics (**Figure 3B-E**), as observed previously (114), suggesting that glutamate is sufficient for the entirety of the transient PLR. Additionally, these results show that any potential modulation of glutamatergic signaling by PACAP (118, 134) is dispensable for the transient PLR. Together, these data derived from retinal mutants for photoreceptors and neurotransmitters identify rods as the principal input and glutamate as the principal output of ipRGC-mediated transient PLR signaling.

Melanopsin/rod synergy supports PLR under sustained conditions

Since wildtype responses decay over time (**Figure 1**), we next asked how ipRGC inputs and outputs drive the PLR across longer times (**Figure 4A**). Strikingly, when we measured the sustained PLR in melanopsin knockout mice, which have a normal transient PLR (**Figure 2B**), there was virtually no pupil constriction (**Figure**

4B), even at bright light intensities (up to 10,000 lux, **Figure 4—figure supplement 1A**). We observed that melanopsin knockout mice lose pupil constriction in minutes (half-time: ~4 minutes, **Figure 4C**), similar to the wildtype PLR decay rate at lower light intensities (WT half-time range: ~2–4 minutes at 1–100 lux, **Fig. 1F**). This suggests that melanopsin phototransduction maintains robust light input in ipRGCs during the day (**Figure 4—figure supplement 1B**), after rods adapt to background light.

The severe deficits we observed in the sustained PLR in melanopsin knockout mice raised the possibility that these animals may have developmental deficits that affect their signaling (135, 136). To directly address this issue, we rescued ipRGC function in adult melanopsin knockout mice using either chemogenetics or restoration of melanopsin expression. Using our mouse line with Cre introduced into the melanopsin locus ($Opn4^{Cre/Cre}$) and a Cre-dependent chemogenetic DREADD virus (AAV2-hSyn-DIO-hM3D(G$_q$)-mCherry) (**Figure 4—figure supplement 2**), we administered the selective DREADD agonist CNO (137) and observed robust and sustained pupil constriction for at least one hour (**Figure 4D**). This result demonstrates that ipRGCs and their downstream circuits remain competent for sustained signaling in melanopsin knockout mice. Furthermore, we acutely restored melanopsin in the majority of ipRGCs of melanopsin-Cre knockout mice ($Opn4^{Cre/Cre}$) using a virus that expresses melanopsin in a Cre-dependent manner (**Figure 4E** and **Figure 4—figure supplement 2C-E**, AAV2-CMV-DIO-mRuby-P2A-Melanopsin-FLAG). Following melanopsin restoration, we observed a rescue of the sustained PLR (**Figure 4F**). These results demonstrate for the first time that the

effect of melanopsin loss can be rescued in adulthood, indicating that melanopsin-based light detection is directly required for ipRGCs to signal sustained PLR.

Surprisingly, although melanopsin is required for sustained signaling, we found that melanopsin signaling could not fully recapitulate the sustained PLR. Despite the observation that the sustained PLR is normal at bright light intensities in melanopsin-only mice, these mice had a sensitivity deficit compared to wildtype (**Figure 4G**). Notably, we observed that rod knockout mice display an identical sensitivity deficit as melanopsin-only (**Figure 4G** and **Figure 4—figure supplement 3**), indicating that rods contribute to sustained ipRGC signaling. This indicates that at intermediate intensities, both rod and melanopsin signaling cooperate to sustain the PLR.

As with the transient PLR, we found that cone knockout mice had no deficit in sustained PLR (**Figure 4G**). Again, multiple independent mouse lines corroborate these conclusions (**Figure 4—figure supplement 3**). Furthermore, we found that rods alone could drive the remainder of the sustained PLR in melanopsin knockout mice (**Figure 4—figure supplement 4A**), whereas cone-only mice had no sustained PLR (**Figure 4—figure supplement 4B**).

These results show that melanopsin signaling dominates sustained light input to ipRGCs, but rods, which are thought to be nonfunctional under continuous bright light, are intimately involved in supporting the sustained PLR. Notably, rod contributions to the sustained PLR occur predominantly at light intensities above their presumed saturation (~40 lux), showing that rods are indeed capable of contributing to visual function above previously defined limits (97, 120, 124). Therefore, sustained

126

ipRGC responses are not a simple consequence of a single photoreceptive system, but instead require rod/melanopsin synergy for highest sensitivity.

PACAP is essential for the sustained PLR

Studies of ipRGC neurotransmitters, in combination with our transient PLR results presented here, suggest that glutamate is the primary ipRGC neurotransmitter, and that PACAP plays a minor, or modulatory, role (111, 112, 114–117, 138). However, when we tested the sustained PLR in ipRGC glutamate knockout mice, we found that their pupil constriction improved over time compared to their transient PLR sensitivity (**Figure 5B,C**). In contrast, PLR sensitivity either stays the same or declines in all other mutant lines, suggesting that the remaining signal in glutamate knockout mice, presumably PACAP, becomes more effective with longer stimulus duration. Intriguingly, ipRGC glutamate knockout mice showed pulsatile or periodic pupil constriction over time, potentially due to waves of neuropeptide vesicle delivery and release from ipRGC axons (**Video 1**).

Neuropeptides have been shown to require high frequency neuronal activity for release and have relatively slow signaling kinetics compared to classical neurotransmitters (107), suggesting that PACAP may be involved in sustained ipRGC signaling at bright light intensities. In support of a role for PACAP in sustained PLR signaling, we find that even though ipRGC PACAP knockout mice show normal transient PLR, they have an attenuated sustained PLR (**Figure 5B-E**). This deficit in ipRGC PACAP knockout mice occurs even at moderate light intensities (10 and 100 lux). ipRGC PACAP KO mice display decaying constriction over time at 1000 lux as opposed to maintained constriction in wildtype mice and enhanced constriction in

ipRGC glutamate KOs (**Figure 5D**). At the brightest light intensity tested, 5000 lux, ipRGC PACAP KO mice display present significantly worse sustained constriction than ipRGC glutamate KO mice (**Figure 5E**), suggesting that PACAP is more important than glutamate for maintained responses under daylight conditions (1,000-100,000+ lux).

Additionally, we observed similar yet more pronounced deficits in full body PACAP KO mice (*Adcyap1*^{-/-} ; **Figure 5—figure supplement 1**). They display wildtype transient responses (**Figure 5—figure supplement 1A,B**) and severely attenuated sustained responses (**Figure 5—figure supplement 1C-E**). Interestingly, these PACAP knockout mice exhibit PLR decay on a similar timescale as melanopsin knockout mice (half-time: ~5 minutes, **Figure 4C** and **Figure 5—figure supplement 1F**). These results provide evidence that PACAP allows ipRGCs to communicate sustained input to downstream neurons. As observed with the photoreceptor contributions, the highest sensitivity of sustained PLR requires PACAP/glutamate synergy.

Model of ipRGC circuit transitions

Based on our results, we generated a quantitative representation of the distinct roles played by each photoreceptor input and neurotransmitter output of ipRGCs for the PLR over a range of light intensities and light stimulus durations (**Figure 6,** see Methods for detailed explanation). We integrated individual necessity (i.e. from knockout lines) and sufficiency (i.e. from '–only' lines) of rods, cones, and melanopsin in driving the PLR (**Figure 6—figure supplement 1**) to generate a merged heat map representing each photoreceptor's input to the PLR (**Figure 6A,B**).

We then performed the same technique to represent the neurotransmitter outputs of ipRGCs for the PLR (**Figure 6C,D** and **Figure 6—figure supplement 1**) using only the necessity heat maps because we cannot rule out the possibility that other neurotransmitters contribute to ipRGC function. These heat maps provide a comprehensive visualization of the contribution made by each photoreceptor's input and each neurotransmitter's output for ipRGC signaling at any particular time or environmental light intensity. ipRGC transient signaling for the PLR is dominated by input from rods (**Figure 6A**, red) and output by glutamate (**Figure 6C**, green). In contrast, sustained PLR signaling is dominated by melanopsin (**Figure 6B**, blue) and PACAP (**Figure 6D**, blue). Together, these experiments and our model highlight a mechanistic transition in the ipRGC circuit supporting transient and sustained behavioral outputs.

Discussion

We show here how inputs and outputs for a specific circuit change across time to support a behavioral response. Remarkably, the mechanisms supporting transient and sustained responses are distinct, suggesting stimulus duration as a critical determinant of circuit state. Transient PLR responses predominantly utilize classical, well-characterized visual system synaptic mechanisms: rod phototransduction and signal relay to ipRGCs, followed by ipRGC glutamatergic output. However, as conventional signaling mechanisms adapt, non-conventional mechanisms are recruited to maintain persistent signaling, including endogenous melanopsin phototransduction and peptidergic neurotransmission through PACAP. Our findings

highlight fundamental circuit changes in the light-adapted retina that are relatively unexplored (139).

Our results reveal the roles of distinct photoreceptors and neurotransmitters in the PLR and probably other ipRGC-dependent behaviors. We show how ipRGC inputs and outputs can contribute to the PLR through changes in their relative contribution across stimulus intensity and duration. Our ability to decipher these elaborate dynamic changes stems from the fact that we used a large array of environmental light intensities and durations, coupled with genetic means to silence individual circuit components. Ultimately, our quantitative model makes testable predictions about the role of each photoreceptor and neurotransmitter for other ipRGC-dependent behaviors.

We show that in contrast to many proposed models, rods provide the exclusive transient input to ipRGCs for the PLR at dim (scotopic) and moderate (mesopic) light intensities. That rods are capable of rapid and sensitive input to ipRGCs is not surprising given electrophysiological evidence of sensitive rod input to ipRGCs (126, 140) and the fact that rods are widely appreciated as the mediators of dim light vision. However, their exclusive input at mesopic light intensities suggests that cone input to ipRGCs is relatively weak, consistent with the inability of cones to drive circadian photoentrainment (93, 141). Furthermore, we report here that in addition to their role in high-sensitivity transient signaling, rods are capable of driving sustained signaling at bright light intensities well above their saturation level (~40 lux, **Figure 4—figure supplement 4**). This agrees with previous findings that rods are capable of supporting circadian photoentrainment at bright light intensities

(97) but also provides more precise temporal kinetics of rod input to subconscious behaviors. It has been proposed that rods never fully saturate (142), and here we provide a physiological role for rod activity at daylight intensities.

In contrast to previous data that melanopsin is largely dispensable for the PLR (106), we find that it is the dominant determinant of pupil size during the day. This is likely due to the fact that rod and cone inputs adapt to background light, while we find no evidence of behavioral light adaptation in melanopsin phototransduction (i.e. identical sensitivity of melanopsin-only mice in transient and sustained PLR). While melanopsin phototransduction adapts *in vitro* (143, 144), it has been proposed that only the adapted state is able to influence downstream behaviors (144). We predict that melanopsin will be required in other visual functions throughout the day, for example as in more natural photoentrainment conditions that need to precisely measure changing light intensity under bright conditions or measuring day length (100, 132, 145). This requirement for melanopsin in sustained light detection is likely the main reason melanopsin has been conserved in vertebrates.

To date, glutamatergic neurotransmission is the only retina-brain signaling mechanism that has been robustly characterized. We confirm previous data that ipRGCs predominantly rely on glutamatergic output for the transient PLR (110–112). However, we show that the stimulus durations in which glutamate predominates over PACAP is relatively restricted (<5 min), revealing the first critical role for a neuropeptide in retinal signaling to the brain. Further, we find that PACAP appears sufficient to drive the PLR independent of its potential to modulate glutamate. There have been discrepancies in the literature about the role of PACAP in the PLR (113,

131

114), which we believe is likely due to differences in light stimulus duration. Intriguingly, PACAPergic neurotransmission appears to be pulsatile, potentially reflecting the imprecision of slow vesicle delivery from the soma and suggesting why ipRGCs also require a fast and reliable glutamatergic signal. Glutamate and PACAP are the only known ipRGC neurotransmitters, but it remains possible there are neurotransmitters which remain undiscovered. An ipRGC-specific glutamate/PACAP double knockout is a crucial next step in understanding ipRGC neurotransmission. Given the expression of other neuropeptides in many RGCs, including ipRGCs (146– 149), it remains possible that neuropeptides have a broader role in visual function than previously appreciated.

The complementary arrangement of inputs and outputs for the PLR we describe here demonstrates how the visual system accomplishes high sensitivity, transient responses as well as integrative, long-term responses. Many other signaling systems may employ discrete methods for signaling robustly through time. While melanopsin is specific to the ipRGC circuit, PACAP and other neuropeptides may play similar roles in long-term signaling in other circuits, such as hypothalamic feeding circuits (150). Expanding the timescales over which we investigate these systems is likely to reveal entirely new aspects of cell signaling.

Materials and Methods

Animal husbandry

C57Bl/6 × Sv129 hybrid mice were used in all experiments except PACAP KO mice which were C57Bl/6. All mice were housed according to guidelines from the Animal Care and Use Committee of Johns Hopkins University. Male and female

mice age 2–8 months were housed in plastic translucent cages with steel-lined lids in an open room. Ambient room temperature and humidity were monitored daily and tightly controlled. Food and water were available *ad libitum.* All mice were maintained in a 12hr:12hr light-dark cycle with light intensity around 100 lux for the entirety of their lives.

Pupillometry

All mice were dark-adapted for at least 30 minutes prior to any experiments and all PLR experiments were performed between Zeitgeber times (ZT) 2 and 10. For all experiments, mice were unanesthetized and restrained by hand. Because stress can affect pupil size, we ensured that the mice were not stressed during these experiments. To do so, we handled the mice for several days prior to the experiments to get them accustomed to the researchers and to being scruffed. Any mice that showed signs of stress, including vocalizations and wriggling during the experiments, were not used and were subjected to more handling sessions before use in experiments.

Mice were restrained manually under a 10-, 13-, or 23-Watt compact fluorescent light bulb (GE Daylight FLE10HT3/2/D or Sylvania Daylight CF13EL and CF23EL) with a color temperature of 6500 K to simulate natural sunlight. The light intensity was measured using a light meter (EXTECH Foot Candle/Lux Light Meter, 401025) at the surface on which the mouse was held. The light meter was initially calibrated by EXTECH using a Tungsten 2856 K light source; because our experiments used a fluorescent bulb of 6500 K, all measured light intensities reported here may vary by 0.92–1.12 times the actual light intensity. Light intensity was

adjusted by a combination of altering the distance of the light bulb(s) from the mouse and/or applying neutral density filters (Roscolux). The light meter is incapable of detecting light intensities below 1 lux, so one neutral density filter cutting the light intensity by 12.5% was applied to the bulb to estimate 1-log unit decreases in illumination below 1 lux. Light intensities above 500 lux required the use of multiple light bulbs.

For the monochromatic light PLR experiments, an LED light (SuperBrightLEDs) was housed in a microscope light source with fiber optic gooseneck arms to direct the light source to the mouse eye. For the experiments involving the $Opn1mw^{red}$ mice, we used a 626-nm LED in this setup and directed light to both eyes simultaneously or to just one eye and measured the PLR in the illuminated eye (see figure legends). The photon flux was measured using a luminometer (SolarLight) and converted from W/m^2 to photons/cm^2/sec. The light intensity was decreased by 12.5% using neutral density filters (Rosco).

Videos of the eye were taken using a Sony Handycam (DCR-HC96) mounted on a tripod a fixed distance from the mouse. Manual focus was maintained on the camera to ensure that only one focal plane existed for each mouse and that therefore variable distance from the camera should not contribute to differences in relative pupil area throughout the video. Pupil size was first recorded under dim red light and the endogenous infrared light source of the camera to capture the dark-adapted pupil size. Following at least 5 seconds of recording in dark, the pupil was continuously recorded for at least 30 seconds of a light step stimulus. For all sustained PLR, animals were kept in a cage for 60 minutes under the light stimulus. Animals were

removed from the cage after 60 minutes and held in front of the camera for 30 seconds as for the transient PLR. All pupil images presented in the paper were cropped to a fixed square area (generally 100×100 pixels) surrounding the eye using GNU Image Manipulation Program (GIMP). The images were made grayscale and then brightness and contrast were adjusted to enhance visibility of the pupil and exported as PNG files.

Data analysis

Videos were transferred from the camera to a computer as Audio Video Interleave (AVI) files and individual frames were taken using VLC media player (www.videolan.org/vlc/) and saved in portable network graphics format (PNG). Images were taken in the dark, at 5 seconds, and 30 seconds following stimulus onset. Pupil area was then quantified manually in ImageJ (http://rsbweb.nih.gov/ij/) software. The pupil area was measured in pixels using the oval tool in which the 4 cardinal points of the oval were touching their respective edges of the pupil. The relative pupil area was calculated using LibreOffice Calc or Microsoft Excel in which the area during the light stimulus was divided by the area prior to lights onset. For the transient PLR, the minimum relative pupil size of either 5 seconds or 30 seconds after stimulus was used for all genotypes.

The intensity-response curve was fit using a variable slope sigmoidal dose-response curve in Graphpad Prism 6. The top and bottom of the fit were constrained to 1.0 and between 0 and 0.10, respectively, to ensure the EC_{50} for each genotype was represented by similar curves. For genotypes that never showed evidence of reaching between 0 and 0.10 relative pupil size, the bottom was not constrained. The

135

sensitivity for each genotype was calculated using the same process of fitting each individual animal's data points with a sigmoidal dose-response curve to generate EC_{50}.

Conditional PACAP allele

The lox-modified *PACAP* (*Adcyap1*) targeting construct was made by recombineering technology. To engineer the targeting vector, 5' homology arm, 3' homology arm and CKO region were amplified from mouse Sv129 BAC genomic DNA and confirmed by end sequencing (Cyagen biosciences, Santa Clara, CA). The two *loxP* sites flank the second exon and when recombined, create a frameshift mutation and truncated protein. The plasmid was electroporated into W4 ES cells and cells expanded from targeted ES clones were injected into C57BL6 blastocysts. Germline transmitting chimeric animals were obtained and then mated with flpE mice to delete the *frt*-site flanked neomycin selection cassette. The resulting heterozygous offspring were crossed to generate homozygous PACAP$^{lox/lox}$ study subjects. All mice are thus on a mixed C57Bl6/J and 129Sv background. Offspring were genotyped by PCR using 2 primers (F: CCGATTGATTGACTACAGGCTCC and R: GTGTTAAACACCAGTTAGCCACGC) which detect the presence or absence of the 5' loxP site and a 3rd primer was used in conjunction with the forward primer (CKO-R GGGCTTTGATCTGGGAACTGAAG) to detect the recombination event. By generating mice homozygous for a germline deleted cre-deleted allele, we have established that the cre-deleted allele does not express intact *PACAP* mRNA (by PCR and by ISH). A more detailed description of the generation and use of the allele will appear in a manuscript that is in preparation (Ross RA…Lowell BB *in preparation*).

Viral infection

Mice were anesthetized by intraperitoneal injection of avertin (2, 2, 2-Tribromoethanol) and placed under a stereo microscope. 1 µl of AAV2-hSyn-DIO-hM3DG$_q$-mCherry (4.6 × 10^{12} viral particles/ml, Roth lab, UNC Vector Core) or AAV2-CMV-DIO-mRuby-P2A-Melanopsin-FLAG (Robinson lab, UMBC) was placed on a piece of Parafilm and drawn into a 10-µl microcapillary tube (Sigma P0674) that had been pulled to a needle (Sutter Instruments, Model P-2000). The loaded needle was then placed in the holster of a pico-injector (Harvard Apparatus PLI-90). The needle punctured the eye posterior to the ora serrata and air pressure was used to drive the viral solution into the vitreous chamber of the eye to ensure delivery specifically to the retina. Mice recovered from surgery on a heating pad until they woke from anesthesia. All PLR experiments and confocal imaging were done at least 3 weeks following viral injection.

Immunofluorescence and confocal microscopy

Mice that had been infected with the AAVs were anesthetized with avertin and then euthanized using cervical dislocation. The eyes were removed and the retinas were dissected in PBS and then fixed in 4% paraformaldehyde for 1–2 hours on ice. The retinas were then washed in PBS at least three times before mounting on a microscope slide (Fisher) in Fluoromount (Sigma) with DAPI (2-(4-amidinophenyl)-1H -indole-6-carboxamidine). Some retinas were co-stained for melanopsin using rabbit anti-OPN4 (Advanced Targeting Systems, AB-N38, 1:1000) in 4% goat serum with secondary antibody Alexa Fluor 488 goat anti-rabbit (Life Technologies

A11008, 1:1000). Images were taken on a Zeiss LSM 710 confocal microscope using a 20× objective. After imaging, images were made grayscale, background subtracted, and brightness and contrast were adjusted in FIJI (http://fiji.sc) for the image presented in the paper.

Statistical analysis

All statistical tests were performed in Graphpad Prism 6. Specific statistical comparisons are listed in the figure captions. Because the EC_{50} data appears to be a normal distribution on a log scale (log-normal distribution), all statistical tests and data analysis involving EC_{50} were performed on the log transformed data set.

Heat map generation

The photoreceptor contribution heat map was generated by first creating estimated pupil size matrices for the both the rapid and sustained PLR at every light intensity and time for wildtype mice (x axis = time, y axis = intensity). To do so, we applied the equation for a one-phase association:

$$(1) \quad Y = Y0 + (Plataeu - Y0) * (1 - e^{(-K*x)})$$

In our case, Y is the **relative pupil area** generated at **time**, x. For the WT rapid PLR heat map, $Y0_{rapid}$ is set to 1 for every light intensity and the K_{rapid} was extracted from the wildtype rapid constriction kinetics curve at 100 lux. The *Plateau$_{rapid}$* value at each light intensity is the rapid PLR value extracted from the WT rapid intensity-response curve fit. This allows us to generate a full matrix of WT pupil sizes at every intensity and time by knowing the final pupil size (Plateau) and the rate of constriction (K). This then generates a full matrix of values for every time and intensity for WT mice.

The same method was applied to make the sustained PLR heat map. However, in this case, $Y0_{sustained}$ was set to the value of the rapid PLR at each light intensity (e.g. the same value as $Plateau_{rapid}$). The $Plateau_{sustained}$ value is extracted from the sustained intensity-response curve fit at each intensity. The $K_{sustained}$ was extracted from our wildtype sustained time courses (**Fig. 1c**). Because the decay rate for sustained constriction appeared to change with intensity (**Fig. 1f**) we used a sigmoidal curve fit to our experimentally determined decay rates (1, 10, 100 lux) to generate decay rates for a range of light intensities. We constrained the top and bottom of this curve to the decay rates determined for 1 and 100 lux respectively.

This process was used to generate two matrices of relative pupil areas with the y-axis being light intensity varying logarithmically (0.001-100,000 lux) and the x-axis being time varying linearly from 0 to 30 seconds for the rapid and 30 seconds to 60 minutes for the sustained. This was done using a custom MATLAB script.

The matrices generated for the wildtype mice were also done to the photoreceptor mutants. In order to determine necessity of a photoreceptor we subtracted rod (average of $Gnat1^{-/-}$ and Rod-DTA), cone (average of $Cnga3^{-/-}$, $Gnat2^{-/-}$ and Cone-DTA), or melanopsin ($Opn4^{-/-}$) knockout matrices from the wildtype matrix. This yields larger values for genotypes that are more required and also normalizes for the overall constriction in wildtype mice at that intensity (i.e. because rods are fully necessary at some dim intensities at which WT mice have minimal constriction, the necessity value attributed to rods is small despite their absolute necessity at that intensity). To determine sufficiency we used 'rod-only' ($Cnga3^{-/-}$; $Opn4^{-/-}$), 'cone-only' ($Gnat1^{-/-}$;$Opn4^{-/-}$) and 'melanopsin-only' (average of $Gnat1^{-/-}$

;*Gnat2^{-/-}*, *Gnat1^{-/-}*; *Cnga3^{-/-}* and Rod-DTA;Cone-DTA) matrices. Additionally, we applied the decay rate of pupil constriction from the 'cone-only' mouse line transient PLR at 100 lux for all light intensities.

Finally, matrices generated above were exported as heat map images with MATLAB.

Negative feedback modeling

In order to isolate negative feedback's impact on the PLR, we generated a computational model. Computational modeling was performed with MATLAB using two experimentally determined parameters. First, the relative pupil area (RPA) values for the wildtype intensity-response curve (**Fig. 1d**). These values give us the response driven when the pupil starts fully open. We will later multiply the environmental intensity by the new relative pupil area to determine the new retinal intensity. We will use this new retinal intensity to extract the pupil size from the rapid intensity-response curve to find the constriction driven by that new intensity under baseline conditions. The model does this recalculation of retinal intensity and the PLR driven by it every second for 956 seconds.

The second experiment integrated into the model is a 1s light pulse-chase experiment. Here, we dark-adapted the mouse, gave a single second of light and then followed subsequent constriction for 30 sec. These constriction values were normalized to the maximum constriction achieved, in this case the 6-sec time point. This gives us the ability to weight the contribution of light at a particular time to constriction at subsequent times. As you can see, light does not instantly constrict the pupil. It takes several seconds for the signal to maximally impact pupil size, which is

then followed by signal decay. Importantly, this temporal weighting, while not required for the model, does give us a rough estimate of the potential kinetics of feedback's impact on PLR decay.

With these pieces of experimental data in hand, the model does the following at every light intensity (0.0001-100,000 lux): (1) it extracts the RPA in response to a particular light intensity from the wildtype intensity-response curve. (2) The model uses the temporal weighting values from the pulse-chase experiment to weight that RPA across subsequent times (0-30s). This gives us a 30-sec constriction time course for the light detected at time zero. (3) The model next moves to time 1 sec. Now it takes into account the maximum constriction caused by light at previous times (time 0 in this case). The model uses that constriction to reduce the light intensity and calculate a new retinal light intensity: RPA * Light intensity = Retinal intensity. (4) Next, it determines the RPA driven by this new retinal intensity using the DRC once again. (5) Repeats step (2) for this RPA giving another time course of constriction (1-31s). (6) The model repeats steps (3-5) moving up in 1s increments each time. Importantly, at each new time point it finds the maximum constriction value in response to all previous time points in order to calculate the new retinal intensity. (7) Finally, it finds the maximum constriction at each time point in order to produce a negative feedback PLR decay time course. See graphical representation of the negative feedback model (**Figure 1—figure supplement 2A**)

*The primary assumption the model makes is that the PLR system has zero summation of signal. This is probably unlikely. However, this assumption was made

to maximize the impact of feedback on pupil constriction. This model provides us with an <u>upper bound</u> on negative feedback's contribution to PLR decay.

*Source code and materials used are available on Github (<u>https://github.com/keenanw27/PLR-Decay-Model</u>).

Mathematical description of the negative-feedback model of PLR decay

At a given environmental light intensity: lux_o. The effect of pupillary negative-feedback during a 956s stimulation is modeled as follows:

$$for\ time\ t = 1, 2, 3 \ldots 956$$

$$max\left(\overrightarrow{RPA}(:, t)\right) \times lux_o$$
$$= lux_t \qquad (1)$$

In equation (1) above, we determine the retinal light intensity, lux_t , that is, the intensity of light after modulation by pupil size at time t. At $t = 1$ there is no pupil constriction and therefore no light intensity modulation $(lux_o = lux_t)$. $\overrightarrow{RPA}$ is a 956×956 matrix which stores subsequent pupil constriction values. With lux_t we determine the constriction driven by light sensed at time, t :

$$\vec{a}(lux_t) \times \vec{\omega} = \overrightarrow{RPA}(t, t:t + 30) \qquad (2)$$

In equation (2), we calculate the amount of constriction driven by lux_t , $\vec{a}(lux_t)$, and approximate the temporal characteristics of that constriction with $\vec{\omega}$. $\vec{\omega}$ is based on a <u>1s light pulse-chase experiment</u> where we followed the constriction driven by 1s of light for 30s. Again, we store calculated constriction values: $\overrightarrow{RPA}(t, t:t + 30)$. Finally, we extract the highest constriction value at t :

$$\overline{max\left(\overrightarrow{RPA}(:,t)\right)} = \overrightarrow{Model}_{lux_0}(1,t) \qquad (3)$$

After completing $t = 956$, $\overrightarrow{Model}_{lux_0}$ is a vector containing the model-predicted timecourse of pupil constriction when negative-feedback is the only source of PLR decay.

Bibliography

1. Arshavsky VY, Lamb TD, Pugh EN (2002) G proteins and phototransduction. *Annu Rev Physiol* 64:153–187.
2. Arshavsky VY, Burns ME (2012) Photoreceptor signaling: supporting vision across a wide range of light intensities. *J Biol Chem* 287(3):1620–1626.
3. Winslow BD, Shao H, Stewart RJ, Tresco PA (2010) Biocompatibility of adhesive complex coacervates modeled after the sandcastle glue of Phragmatopoma californica for craniofacial reconstruction. *Biomaterials* 31(36):9373–9381.
4. Purves Dale AG ed. *Neuroscience* (Sinauer Associates, Inc.). 3rd Ed.
5. Reppert SM, Weaver DR (2002) Coordination of circadian timing in mammals. *Nature* 418(6901):935–941.
6. Zylka MJ, Shearman LP, Weaver DR, Reppert SM (1998) Three period homologs in mammals: differential light responses in the suprachiasmatic circadian clock and oscillating transcripts outside of brain. *Neuron* 20(6):1103–10.
7. Balsalobre A, Damiola F, Schibler U (1998) A Serum Shock Induces Circadian Gene Expression in Mammalian Tissue Culture Cells. *Cell* 93(6):929–937.
8. Ko CH, Takahashi JS (2006) Molecular components of the mammalian circadian clock. *Hum Mol Genet* 15(Review Issue 2):R271–R277.
9. Shigeyoshi Y, et al. (1997) Light-Induced Resetting of a Mammalian Circadian Clock Is Associated with Rapid Induction of the mPer1 Transcript. *Cell* 91(7):1043–1053.
10. Cao R, et al. (2015) Light-regulated translational control of circadian behavior by eIF4E phosphorylation. *Nat Neurosci* 18(6):855–862.
11. LeGates TA, Fernandez DC, Hattar S (2014) Light as a central modulator of circadian rhythms, sleep and affect. *Nat Rev Neurosci* 15(7):443–454.
12. Borbély AA (1982) A two process model of sleep regulation. *Hum Neurobiol* 1(3):195–204.
13. TUREK F, GILLETTE M (2004) Melatonin, sleep, and circadian rhythms: rationale for development of specific melatonin agonists. *Sleep Med* 5(6):523–532.
14. Legates TA, et al. (2012) Aberrant light directly impairs mood and learning through melanonopsin-expression neurons. *Nature* 491(7425):594–598.
15. Purnyn H (2013) The Mammalian Retina: Structure and Blood Supply. *Neurophysiology* 45(3):266–276.
16. Bok D (1993) The retinal pigment epithelium: a versatile partner in vision. *J Cell Sci Suppl* 17:189–95.
17. Swaroop A, Kim D, Forrest D (2010) Transcriptional regulation of photoreceptor development and homeostasis in the mammalian retina. *Nat Rev Neurosci* 11(8):563–576.
18. Provencio I, Jiang G, De Grip WJ, Hayes WP, Rollag MD (1998) Melanopsin: An opsin in melanophores, brain, and eye. *Proc Natl Acad Sci U S A* 95(1):340–345.
19. Provencio I, et al. (2000) A novel human opsin in the inner retina. *J Neurosci*

20(2):600–605.

20. Bellingham J, et al. (2006) Evolution of melanopsin photoreceptors: discovery and characterization of a new melanopsin in nonmammalian vertebrates. *PLoS Biol* 4(8):e254.

21. Hattar S, Liao HW, Takao M, Berson DM, Yau KW (2002) Melanopsin-containing retinal ganglion cells: architecture, projections, and intrinsic photosensitivity. *Science (80-)* 295(5557):1065–1070.

22. Schmidt TM, Chen SK, Hattar S (2011) Intrinsically photosensitive retinal ganglion cells: many subtypes, diverse functions. *Trends Neurosci* 34(11):572–580.

23. Hattar S, et al. (2003) Melanopsin and rod-cone photoreceptive systems account for all major accessory visual functions in mice. *Nature* 424(6944):76–81.

24. Panda S, et al. (2003) Melanopsin is required for non-image-forming photic responses in blind mice. *Science (80-)* 301(5632):525–527.

25. Xue T, et al. (2011) Melanopsin signalling in mammalian iris and retina. *Nature* 479(7371):67–73.

26. Graham DM, et al. (2008) Melanopsin ganglion cells use a membrane-associated rhabdomeric phototransduction cascade. *J Neurophysiol* 99(5):2522–2532.

27. Perez-Leighton CE, Schmidt TM, Abramowitz J, Birnbaumer L, Kofuji P (2011) Intrinsic phototransduction persists in melanopsin-expressing ganglion cells lacking diacylglycerol-sensitive TRPC subunits. *Eur J Neurosci* 33(5):856–867.

28. Baver SB, Pickard GE, Sollars PJ (2008) Two types of melanopsin retinal ganglion cell differentially innervate the hypothalamic suprachiasmatic nucleus and the olivary pretectal nucleus. *Eur J Neurosci* 27(7):1763–1770.

29. Berson DM, Castrucci AM, Provencio I (2010) Morphology and mosaics of melanopsin-expressing retinal ganglion cell types in mice. *J Comp Neurol* 518(13):NA-NA.

30. Schmidt TM, Kofuji P (2009) Functional and morphological differences among intrinsically photosensitive retinal ganglion cells. *J Neurosci* 29(2):476–482.

31. Hu C, Hill DD, Wong KY (2013) Intrinsic physiological properties of the five types of mouse ganglion-cell photoreceptors. *J Neurophysiol* 109(7):1876–1889.

32. Ecker JL, et al. (2010) Melanopsin-expressing retinal ganglion-cell photoreceptors: cellular diversity and role in pattern vision. *Neuron* 67(1):49–60.

33. Chen S-K, Badea TC, Hattar S (2011) Photoentrainment and pupillary light reflex are mediated by distinct populations of ipRGCs. *Nature* 476(7358):92–5.

34. Blasic JR, Lane Brown R, Robinson PR (2012) Light-dependent phosphorylation of the carboxy tail of mouse melanopsin. *Cell Mol Life Sci* 69(9):1551–1562.

35. Blasic JR, et al. (2014) Identification of critical phosphorylation sites on the

carboxy tail of melanopsin. *Biochemistry* 53(16):2644–2649.

36.   Walker MT, Brown RL, Cronin TW, Robinson PR (2008) Photochemistry of retinal chromophore in mouse melanopsin. *Proc Natl Acad Sci U S A* 105(26):8861–8865.

37.   Isoldi MC, et al. (2004) Mechanisms of action of melanin-concentrating hormone in the teleost fish erythrophoroma cell line (GEM-81). *Gen Comp Endocrinol* 136(2):270–275.

38.   Cameron EG, Robinson PR (2014) β-Arrestin-dependent deactivation of mouse melanopsin. *PLoS One* 9(11):e113138.

39.   Blasic JR, Brown RL, Robinson PR (2012) Phosphorylation of mouse melanopsin by protein kinase A. *PLoS One* 7(9):e45387.

40.   Somers RL, Klein DC (1984) Rhodopsin kinase activity in the mammalian pineal gland and other tissues. *Science* 226(4671):182–4.

41.   Gruber CW, Muttenthaler M, Freissmuth M (2010) Ligand-based peptide design and combinatorial peptide libraries to target G protein-coupled receptors. *Curr Pharm Des* 16(28):3071–3088.

42.   Pitcher JA, et al. (1996) Phosphatidylinositol 4,5-bisphosphate (PIP2)-enhanced G protein-coupled receptor kinase (GRK) activity. Location, structure, and regulation of the PIP2 binding site distinguishes the GRK subfamilies. *J Biol Chem* 271(40):24907–24913.

43.   Siderovski DP, Hessel A, Chung S, Mak TW, Tyers M (1996) A new family of regulators of G-protein-coupled receptors? *Curr Biol* 6(2):211–212.

44.   Lodowski DT, Tesmer VM, Benovic JL, Tesmer JJ (2006) The structure of G protein-coupled receptor kinase (GRK)-6 defines a second lineage of GRKs. *J Biol Chem* 281(24):16785–16793.

45.   Gurevich E V, Tesmer JJ, Mushegian A, Gurevich V V (2012) G protein-coupled receptor kinases: more than just kinases and not only for GPCRs. *Pharmacol Ther* 133(1):40–69.

46.   Bownds D, Dawes J, Miller J, Stahlman M (1972) Phosphorylation of frog photoreceptor membranes induced by light. *Nat New Biol* 237(73):125–127.

47.   Kennedy MJ, et al. (2001) Multiple phosphorylation of rhodopsin and the *in vivo* chemistry underlying rod photoreceptor dark adaptation. *Neuron* 31(1):87–101.

48.   Horner TJ, Osawa S, Schaller MD, Weiss ER (2005) Phosphorylation of GRK1 and GRK7 by cAMP-dependent protein kinase attenuates their enzymatic activities. *J Biol Chem* 280(31):28241–28250.

49.   Osawa S, et al. (2011) Phosphorylation of G protein-coupled receptor kinase 1 (GRK1) is regulated by light but independent of phototransduction in rod photoreceptors. *J Biol Chem* 286(23):20923–20929.

50.   Trifilieff P, et al. (2011) Detection of antigen interactions ex vivo by proximity ligation assay: endogenous dopamine D2-adenosine A2A receptor complexes in the striatum. *Biotechniques* 51(2):111–118.

51.   Mure LSS, et al. (2016) Melanopsin-Encoded Response Properties of Intrinsically Photosensitive Retinal Ganglion Cells. *Neuron* 90(5):1016–1027.

52.   Mendez A, et al. (2000) Rapid and reproducible deactivation of rhodopsin requires multiple phosphorylation sites. *Neuron* 28(1):153–164.

53. Piccolino M, Neyton J, Gerschenfeld HM (1984) Decrease of gap junction permeability induced by dopamine and cyclic adenosine 3':5'-monophosphate in horizontal cells of turtle retina. *J Neurosci* 4(10):2477–2488.

54. Dyer MA, Cepko CL (2001) Regulating proliferation during retinal development. *Nat Rev Neurosci* 2(5):333–342.

55. Lasater EM (1987) Retinal horizontal cell gap junctional conductance is modulated by dopamine through a cyclic AMP-dependent protein kinase. *Proc Natl Acad Sci U S A* 84(20):7319–7323.

56. Van Hook MJ, Wong KY, Berson DM (2012) Dopaminergic modulation of ganglion-cell photoreceptors in rat. *Eur J Neurosci* 35(4):507–518.

57. Zhang DQ, et al. (2008) Intraretinal signaling by ganglion cell photoreceptors to dopaminergic amacrine neurons. *Proc Natl Acad Sci U S A* 105(37):14181–14186.

58. Kirschner LS, Yin Z, Jones GN, Mahoney E (2009) Mouse models of altered protein kinase A signaling. *Endocr Relat Cancer* 16(3):773–793.

59. Brandon EP, Idzerda RL, McKnight GS (1997) PKA isoforms, neural pathways, and behaviour: making the connection. *Curr Opin Neurobiol* 7(3):397–403.

60. Beebe SJ, Salomonsky P, Jahnsen T, Li Y (1992) The C gamma subunit is a unique isozyme of the cAMP-dependent protein kinase. *J Biol Chem* 267(35):25505–25512.

61. Cadd G, McKnight GS (1989) Distinct patterns of cAMP-dependent protein kinase gene expression in mouse brain. *Neuron* 3(1):71–79.

62. Vitalis EA, et al. (2000) Role of the cAMP signaling pathway in the regulation of gonadotropin-releasing hormone secretion in GT1 cells. *Proc Natl Acad Sci U S A* 97(4):1861–1866.

63. Akamine P, et al. (2003) Dynamic features of cAMP-dependent protein kinase revealed by apoenzyme crystal structure. *J Mol Biol* 327(1):159–171.

64. Ventra C, et al. (1996) The differential response of protein kinase A to cyclic AMP in discrete brain areas correlates with the abundance of regulatory subunit II. *J Neurochem* 66(4):1752–1761.

65. Dunn TA, Storm DR, Feller MB (2009) Calcium-dependent increases in protein kinase-A activity in mouse retinal ganglion cells are mediated by multiple adenylate cyclases. *PLoS One* 4(11):e7877.

66. Blasic JR, Brown RL, Robinson PR (2012) Phosphorylation of mouse melanopsin by protein kinase a. *PLoS One* 7(9):e45387.

67. Doyle SE, Grace MS, McIvor W, Menaker M (2002) Circadian rhythms of dopamine in mouse retina: the role of melatonin. *Vis Neurosci* 19(5):593–601.

68. Brown TM, Wynne J, Piggins HD, Lucas RJ (2011) Multiple hypothalamic cell populations encoding distinct visual information. *J Physiol* 589(Pt 5):1173–1194.

69. Haruyama N, Cho A, Kulkarni AB Overview: Engineering transgenic constructs and mice. doi:10.1002/0471143030.cb1910s42.

70. Gordon JW, Scangos GA, Plotkin DJ, Barbosa JA, Ruddle FH (1980) Genetic transformation of mouse embryos by microinjection of purified DNA. *Proc Natl Acad Sci U S A* 77(12):7380–4.

71.   Smithies O, Gregg RG, Boggs SS, Koralewski MA, Kucherlapati RS Insertion of DNA sequences into the human chromosomal beta-globin locus by homologous recombination. *Nature* 317(6034):230–4.

72.   Robertson E, Bradley A, Kuehn M, Evans M (1986) Germ-line transmission of genes introduced into cultured pluripotential cells by retroviral vector. *Nature* 323(6087):445–448.

73.   Thomas KR, Folger KR, Capecchi MR (1986) High frequency targeting of genes to specific sites in the mammalian genome. *Cell* 44(3):419–28.

74.   Sternberg N, Hamilton D (1981) Bacteriophage P1 site-specific recombination. I. Recombination between loxP sites. *J Mol Biol* 150(4):467–86.

75.   Lin B, Koizumi A, Tanaka N, Panda S, Masland RH (2008) Restoration of visual function in retinal degeneration mice by ectopic expression of melanopsin. *Proc Natl Acad Sci U S A* 105(41):16009–16014.

76.   Lucas RJ, Douglas RH, Foster RG (2001) Characterization of an ocular photopigment capable of driving pupillary constriction in mice. *Nat Neurosci* 4(6):621–626.

77.   Lucas RJ, et al. (2003) Diminished pupillary light reflex at high irradiances in melanopsin-knockout mice. *Science (80-)* 299(5604):245–247.

78.   Do MT, et al. (2009) Photon capture and signalling by melanopsin retinal ganglion cells. *Nature* 457(7227):281–287.

79.   Berson DM, Dunn FA, Takao M (2002) Phototransduction by retinal ganglion cells that set the circadian clock. *Science (80-)* 295(5557):1070–3.

80.   Daan S, Pittendrigh CS (1976) A Functional analysis of circadian pacemakers in nocturnal rodents. *J Comp Physiol ? A* 106(3):253–266.

81.   Sexton TJ, Van Gelder RN (2015) G-Protein Coupled Receptor Kinase 2 Minimally Regulates Melanopsin Activity in Intrinsically Photosensitive Retinal Ganglion Cells. *PLoS One* 10(6):e0128690.

82.   Sand A, Schmidt TM, Kofuji P (2012) Diverse types of ganglion cell photoreceptors in the mammalian retina. *Prog Retin Eye Res* 31(4):287–302.

83.   Mure LS, et al. (2016) Melanopsin-Encoded Response Properties of Intrinsically Photosensitive Retinal Ganglion Cells. *Neuron* 90(5):1016–1027.

84.   Altimus CM, et al. (2008) Rods-cones and melanopsin detect light and dark to modulate sleep independent of image formation. *Proc Natl Acad Sci USA* 105(50):19998–20003.

85.   Güler AD, et al. (2008) Melanopsin cells are the principal conduits for rod–cone input to non-image-forming vision. *Nature* 453(7191):102–5.

86.   Göz D, et al. (2008) Targeted destruction of photosensitive retinal ganglion cells with a saporin conjugate alters the effects of light on mouse circadian rhythms. *PLoS One* 3(9):e3153.

87.   Hatori M, et al. (2008) Inducible ablation of melanopsin-expressing retinal ganglion cells reveals their central role in non-image forming visual responses. *PLoS One* 3(6):e2451.

88.   Lupi D, Oster H, Thompson S, Foster RG (2008) The acute light-induction of sleep is mediated by OPN4-based photoreception. *Nat Neurosci* 11(9):1068–73.

89.   Tsai JW, et al. (2009) Melanopsin as a sleep modulator: circadian gating of the

direct effects of light on sleep and altered sleep homeostasis in Opn4-/- mice. *PLoS Biol* 7(6):e1000125.

90. Hattar S, et al. (2003) Melanopsin and rod–cone photoreceptive systems account for all major accessory visual functions in mice. *Nature* 424:76–81.

91. Panda S, et al. (2003) Melanopsin is required for non-image-forming photic responses in blind mice. *Science* 301(5632):525–7.

92. Dkhissi-Benyahya O, Gronfier C, De Vanssay W, Flamant F, Cooper HM (2007) Modeling the role of mid-wavelength cones in circadian responses to light. *Neuron* 53(5):677–687.

93. Lall GS, et al. (2010) Distinct contributions of rod, cone, and melanopsin photoreceptors to encoding irradiance. *Neuron* 66:417–28.

94. Allen AE, Brown TM, Lucas RJ (2011) A distinct contribution of short-wavelength-sensitive cones to light-evoked activity in the mouse pretectal olivary nucleus. *J Neurosci* 31(46):16833–16843.

95. Butler MP, Silver R (2011) Divergent photic thresholds in the non-image-forming visual system: entrainment, masking and pupillary light reflex. *Proc Biol Sci* 278(1706):745–50.

96. McDougal DH, Gamlin PD (2010) The influence of intrinsically-photosensitive retinal ganglion cells on the spectral sensitivity and response dynamics of the human pupillary light reflex. *Vision Res* 50(1):72–87.

97. Altimus CM, et al. (2010) Rod photoreceptors drive circadian photoentrainment across a wide range of light intensities. *Nat Neurosci* 13(9):1107–12.

98. Zhu Y, et al. (2007) Melanopsin-dependent persistence and photopotentiation of murine pupillary light responses. *Invest Ophthalmol Vis Sci* 48(3):1268–75.

99. Gooley JJ, et al. (2012) Melanopsin and rod-cone photoreceptors play different roles in mediating pupillary light responses during exposure to continuous light in humans. *J Neurosci* 32(41):14242–14253.

100. Mrosovsky N, Hattar S (2003) Impaired masking responses to light in melanopsin-knockout mice. *Chronobiol Int* 20(6):989–99.

101. Wong KY (2012) A retinal ganglion cell that can signal irradiance continuously for 10 hours. *J Neurosci* 32(33):11478–11485.

102. van Diepen HC, Ramkisoensing A, Peirson SN, Foster RG, Meijer JH (2013) Irradiance encoding in the suprachiasmatic nuclei by rod and cone photoreceptors. *FASEB J* 27(10):4204–12.

103. Schmidt TM, et al. (2014) A role for melanopsin in alpha retinal ganglion cells and contrast detection. *Neuron* 82(4):781–8.

104. Ruby NF, et al. (2002) Role of melanopsin in circadian responses to light. *Science (80-)* 298(5601):2211–3.

105. Panda S, et al. (2002) Melanopsin (Opn4) requirement for normal light-induced circadian phase shifting. *Science (80-)* 298(5601):2213–6.

106. Lucas RJ, et al. (2003) Diminished pupillary light reflex at high irradiances in melanopsin-knockout mice. *Science (80-)* 299:245–7.

107. Vaaga CE, Borisovska M, Westbrook GL (2014) Dual-transmitter neurons: functional implications of co-release and co-transmission. *Curr Opin Neurobiol* 29:25–32.

108. Hannibal J, Hindersson P, Knudsen SM, Georg B, Fahrenkrug J (2002) The photopigment melanopsin is exclusively present in pituitary adenylate cyclase-activating polypeptide-containing retinal ganglion cells of the retinohypothalamic tract. *J Neurosci* 22(1):RC191.
109. Engelund A, Fahrenkrug J, Harrison A, Hannibal J (2010) Vesicular glutamate transporter 2 (VGLUT2) is co-stored with PACAP in projections from the rat melanopsin-containing retinal ganglion cells. *Cell Tissue Res* 340(2):243–55.
110. Gompf HS, Fuller PM, Hattar S, Saper CB, Lu J (2015) Impaired circadian photosensitivity in mice lacking glutamate transmission from retinal melanopsin cells. *J Biol Rhythm* 30(1):35–41.
111. Purrier N, Engeland WC, Kofuji P (2014) Mice deficient of glutamatergic signaling from intrinsically photosensitive retinal ganglion cells exhibit abnormal circadian photoentrainment. *PLoS One* 9(10):e111449.
112. Delwig A, et al. (2013) Glutamatergic neurotransmission from melanopsin retinal ganglion cells is required for neonatal photoaversion but not adult pupillary light reflex. *PLoS One* 8(12):e83974.
113. Engelund A, Fahrenkrug J, Harrison A, Luuk H, Hannibal J (2012) Altered pupillary light reflex in PACAP receptor 1-deficient mice. *Brain Res* 1453:17–25.
114. Kawaguchi C, et al. (2010) PACAP-deficient mice exhibit light parameter-dependent abnormalities on nonvisual photoreception and early activity onset. *PLoS One* 5(2):e9286.
115. Beaulé C, et al. (2009) Temporally restricted role of retinal PACAP: Integration of the phase-advancing light signal to the SCN. *J Biol Rhythm* 24(2):126–34.
116. Kawaguchi C, et al. (2003) Changes in light-induced phase shift of circadian rhythm in mice lacking PACAP. *Biochem Biophys Res Commun* 310(1):169–175.
117. Colwell CS, et al. (2004) Selective deficits in the circadian light response in mice lacking PACAP. *Am J Physiol Regul Integr Comp Physiol* 287(5):R1194–R1201.
118. Chen D, Buchanan GF, Ding JM, Hannibal J, Gillette MU (1999) Pituitary adenylyl cyclase-activating peptide: a pivotal modulator of glutamatergic regulation of the suprachiasmatic circadian clock. *Proc Natl Acad Sci USA* 96(23):13468–73.
119. Loewenfeld IE (1993) The Pupil: Anatomy, Physiology, and Clinical Applications. 1:86–88.
120. Alam NM, Altimus CM, Douglas RM, Hattar S, Prusky GT (2015) Photoreceptor regulation of spatial visual behavior. *Invest Ophthalmol Vis Sci* 56(3):1842–9.
121. Biel M, et al. (1999) Selective loss of cone function in mice lacking the cyclic nucleotide-gated channel CNG3. *Proc Natl Acad Sci USA* 96:7553–7.
122. Cahill H, Nathans J (2008) The optokinetic reflex as a tool for quantitative analyses of nervous system function in mice: application to genetic and drug-induced variation. *PLoS One* 3(4):e2055.
123. Calvert PD, et al. (2000) Phototransduction in transgenic mice after targeted

deletion of the rod transducin □-subunit. *Proc Natl Acad Sci USA* 97(25):13913–8.

124. Naarendorp F, et al. (2010) Dark light, rod saturation, and the absolute and incremental sensitivity of mouse cone vision. *J Neurosci* 30(37):12495–507.

125. Nathan J, et al. (2006) Scotopic and photopic visual thresholds and spatial and temporal discrimination evaluated by behavior of mice in a water maze. *Photochem Photobiol* 82(6):1489–94.

126. Zhao X, Stafford BK, Godin AL, King WM, Wong KY (2014) Photoresponse diversity among the five types of intrinsically photosensitive retinal ganglion cells. *J Physiol* 592(Pt 7):1619–36.

127. van Oosterhout F, et al. (2012) Ultraviolet light provides a major input to non-image-forming light detection in mice. *Curr Biol* 22(15):1397–402.

128. Ho Mien I, et al. (2014) Effects of Exposure to Intermittent versus Continuous Red Light on Human Circadian Rhythms, Melatonin Suppression, and Pupillary Constriction. *PLoS One* 9(5):e96532.

129. Spitschan M, Jain S, Brainard DH, Aguirre GK (2014) Opponent melanopsin and S-cone signals in the human pupillary light response. *Proc Natl Acad Sci USA* 111(43):15568–72.

130. Kimura E, Young RSL (2010) Sustained pupillary constrictions mediated by an L- and M-cone opponent process. *Vis Res* 50(5):489–96.

131. Kimura E, Young RSL (1999) S-cone contribution to pupillary responses evoked by chromatic flash offset. *Vis Res* 39(6):1189–1197.

132. Gooley JJ, et al. (2010) Spectral responses of the human circadian system depend on the irradiance and duration of exposure to light. *Sci Transl Med* 2(31):31ra33.

133. Lucas RJ, Douglas RH, Foster RG (2001) Characterization of an ocular photopigment capable of driving pupillary constriction in mice. *Nat Neurosci* 4(6):621–6.

134. Toda AMA, Huganir RL (2015) Regulation of AMPA receptor phosphorylation by the neuropeptide PACAP38. *Proc Natl Acad Sci* 112(21):6712–6717.

135. Rao S, et al. (2013) A direct and melanopsin-dependent fetal light response regulates mouse eye development. *Nature* 494(7436):243–246.

136. Renna JM, Weng S, Berson DM (2011) Light acts through melanopsin to alter retinal waves and segregation of retinogeniculate afferents. *Nat Neurosci* 14(7):827–829.

137. Armbruster BN, Li X, Pausch MH, Herlitze S, Roth BL (2007) Evolving the lock to fit the key to create a family of G protein-coupled receptors potently activated by an inert ligand. *Proc Natl Acad Sci U S A* 104(12):5163–8.

138. Gompf HS, Fuller PM, Hattar S, Saper CB, Lu J (2015) Impaired Circadian Photosensitivity in Mice Lacking Glutamate Transmission from Retinal Melanopsin Cells. *J Biol Rhythms* 30(1):35–41.

139. Tikidji-Hamburyan A, et al. (2015) Retinal output changes qualitatively with every change in ambient illuminance. *Nat Neurosci* 18(1):66–74.

140. Weng S, Estevez ME, Berson DM (2013) Mouse Ganglion-Cell Photoreceptors Are Driven by the Most Sensitive Rod Pathway and by Both

Types of Cones. *PLoS One* 8(6):e66480.

141. Mrosovsky N, Hattar S (2005) Diurnal mice (Mus musculus) and other examples of temporal niche switching. *J Comp Physiol A Neuroethol Sens Neural Behav Physiol* 191:1011–1024.

142. Blakemore CB, Rushton WAH (1965) The rod increment threshold during dark adaptation in normal and rod monochromat. *J Physiol* 181(3):629–640.

143. Wong KY, Dunn F a, Berson DM (2005) Photoreceptor adaptation in intrinsically photosensitive retinal ganglion cells. *Neuron* 48(6):1001–10.

144. Do MTH, Yau K (2013) Adaptation to steady light by intrinsically photosensitive retinal ganglion cells. *Proc Natl Acad Sci U S A* 2013:1–6.

145. VanderLeest HT, et al. (2007) Seasonal encoding by the circadian pacemaker of the SCN. *Curr Biol* 17(5):468–73.

146. Kay JN, et al. (2011) Retinal Ganglion Cells with Distinct Directional Preferences Differ in Molecular Identity, Structure, and Central Projections. *J Neurosci* 31(21):7753–7762.

147. Liu F, et al. (2011) Gene expression and protein distribution of orexins and orexin receptors in rat retina. *Neuroscience* 189:146–55.

148. Brecha NC, et al. (1987) Substance P-immunoreactive retinal ganglion cells and their central axon terminals in the rabbit. *Nature* 327(6118):155–158.

149. Djeridane Y (1994) Immunohistochemical evidence for the presence of vasopressin in the rat Harderian gland, retina, and lacrimal gland. *Exp Eye Res* 59:117–120.

150. Krashes MJ, Shah BP, Koda S, Lowell BB (2013) Rapid versus delayed stimulation of feeding by the endogenously released agRP neuron mediators GABA, NPY, and AgRP. *Cell Metab* 18(4):588–595.